AN EXPERIMENTAL STUDY ON THE BEHAVIOR OF BOX-SHAPED CULVERTS
BURIED IN SAND UNDER DYNAMIC EXCITATIONS

A THESIS SUBMITTED TO
THE GRADUATE SCHOOL OF NATURAL AND APPLIED SCIENCES
OF
MIDDLE EAST TECHNICAL UNIVERSITY

BY

DENİZ ÜLGEN

IN PARTIAL FULFILLMENT OF THE REQUIREMENTS
FOR
THE DEGREE OF DOCTOR OF PHILOSOPHY
IN
CIVIL ENGINEERING

SEPTEMBER 2011

Approval of the thesis:

AN EXPERIMENTAL STUDY ON THE BEHAVIOR OF BOX-SHAPED CULVERTS BURIED IN SAND UNDER DYNAMIC EXCITATIONS

submitted by **DENİZ ÜLGEN** in partial fulfillment of the requirements for the degree of **Doctor of Philosophy in Civil Engineering Department, Middle East Technical University** by,

Prof. Dr. Canan ÖZGEN   _____
Dean, Graduate School of **Natural and Applied Sciences**

Prof. Dr. Güney ÖZCEBE   _____
Head of Department, **Civil Engineering**

Prof. Dr. M. Yener ÖZKAN   _____
Supervisor, **Civil Engineering Dept., METU**

Prof. Dr. K. Önder ÇETİN   _____
Co-Supervisor, **Civil Engineering Dept., METU**

Examining Committee Members:

Prof. Dr. Orhan EROL   _____
Civil Engineering Dept., METU

Prof. Dr. M. Yener ÖZKAN   _____
Civil Engineering Dept., METU

Prof. Dr. Naci BÖLÜKBAŞI   _____
Mining Engineering Dept., METU

Asst. Prof. Dr. Mehmet ÖZYAZICIOĞLU   _____
Civil Engineering Dept., Atatürk Üniversity

Asst. Prof. Dr. Nejan Huvaj SARIHAN   _____
Civil Engineering Dept., METU

Date: _____15.09.2011_____

I hereby declare that all information in this document has been obtained and presented in accordance with academic rules and ethical conduct. I also declare that, as required by these rules and conduct, I have fully cited and referenced all material and results that are not original to this work.

Name, Last name : Deniz ÜLGEN

Signature   :

ABSTRACT

AN EXPERIMENTAL STUDY ON THE BEHAVIOR OF BOX-SHAPED CULVERTS BURIED IN SAND UNDER DYNAMIC EXCITATIONS

Ülgen, Deniz

Ph.D., Department of Civil Engineering
Supervisor   : Prof. Dr. M. Yener ÖZKAN
Co-Supervisor : Prof. Dr. K. Önder ÇETİN

September 2011, 182 pages

Seismic safety of underground structures (culvert, subway, natural gas and water sewage systems) plays a major role in sustainable public safety and urban development. Very few experimental data are currently available and there is not generally accepted procedure to estimate the dynamic pressures acting on underground structures. This study aims to enhance the state of prevalent information necessary in understanding the dynamic behavior of box culverts and the stresses acting under dynamic excitations through experimental analyses. For this purpose, a series of shaking table tests were conducted on box-type culverts buried in dry sand. To simulate the free-field boundary conditions, a laminar box was designed and manufactured for use in a 1-g shake table. Four culvert models having different rigidities were tested under various harmonic motions in order to examine the effect of flexibility ratio on dynamic lateral soil pressures. Based on the tests results, a simplified dynamic pressure distribution acting on sidewalls of the culvert model was suggested. Then, a dynamic lateral coefficient was defined for the

proposed peak pressure value in the distribution. The values of this coefficient were obtained as a function of shear strain and relative stiffness between the soil and underground structure. Finally, a simplified frame analysis approach was suggested for the assessment of the forces on the structure, to help to carry out a preliminary design of box-type culverts. In this approach, it was assumed that the culvert was fixed at bottom and subjected to lateral stresses on sidewalls and shear stresses on the upper face. For the confirmation of the method, centrifuge tests were conducted on a box-type culvert model under the Seventh Framework Programme of European Union with Grant Agreement No.227887. Results show that the proposed simplified procedure can be used in reasonable accuracy as a practical approach for the preliminary assessment of box-type culverts buried in dry sand under seismic action.

Keywords: Box-type Culvert, Dynamic Soil Pressure, Shaking Table Test, Centrifuge Test, Dynamic Soil-Structure Interaction

ÖZ

KUM İÇİNDE GÖMÜLÜ KUTU TİPİ MENFEZLERİN DİNAMİK HAREKETLER ALTINDAKİ DAVRANIŞI ÜZERİNE DENEYSEL BİR ÇALIŞMA

Ülgen, Deniz

Doktora, İnşaat Mühendisliği Bölümü
Tez Yöneticisi   : Prof. Dr. M. Yener ÖZKAN
Ortak Tez Yöneticisi : Prof. Dr. K. Önder ÇETİN

Eylül 2011, 182 sayfa

Yeraltı yapılarının sismik güvenliği (menfez, metro, doğal gaz ve atık su sistemleri) kamu güvenliği ve kentsel gelişimin sürekliliği açısından önemli rol oynamaktadır. Mevcut deneysel veriler çok az olduğu gibi, yeraltı yapılarına etkiyen dinamik basınçları öngörebilecek genel olarak kabul görmüş bir prosedür bulunmamaktadır. Bu çalışma kutu menfezlerin dinamik davranışını ve dinamik hareketler altında etki eden basınçları anlamak için gerekli olan mevcut yaygın bilgiyi deneysel analizlerle geliştirmeyi amaçlamaktadır. Bu amaçla, kuru kuma gömülü kutu menfezlerin üzerinde bir dizi sarsma tablası deneyleri yapılmıştır. Saha sınır koşullarını temsil etmek amacıyla 1-g sarsma tablasında kullanılmak üzere bir laminar kutu tasarlanıp imal edilmiştir. Esneklik oranının yanal dinamik zemin basıncı üzerindeki etkisini incelemek için farklı rijitlikteki dört menfez modeli çeşitli harmonik hareketler altında test edilmiştir. Deney sonuçlarına dayanarak, menfez modelinin yan duvarlarına etkiyen basitleştirilmiş dinamik basınç dağılımı önerilmiştir. Daha sonra, dağılımda önerilen maksimum basınç değerini hesaplamak için dinamik yanal basınç katsayısı

tanımlanmıştır. Bu katsayının değerleri, kayma birim deformasyonu ve zeminle yeraltı yapısı arasındaki rölatif rijitliğin fonksiyonu olarak elde edilmiştir. Son olarak, kutu menfezlerin ön tasarımının gerçektirilmesinde yardımcı olmak üzere, yapının üzerine gelen kuvvetleri değerlendiren basitleştirilmiş bir çerçeve analizi yaklaşımı önerilmiştir. Bu yaklaşımda, menfezin alt bölümden sabitlenmiş olduğu, yan duvarlarından yanal gerilmelere, üstten de kayma gerilmesine maruz kaldığı varsayılmıştır. Metodu doğrulamak için, Avrupa Birliği 7. Çervevi Programı, 227887 no'lu Proje kapsamında kutu tipi menfez üzerinde santrifüj testleri yapılmıştır. Elde edilen sonuçlar, kuru kuma gömülü kutu menfezlerin sismik ön değerlendirilmesinin yapılması için önerilen basitleştirilmiş prosedürün, makul doğrulukta pratik bir yaklaşım olarak kullanılabileceğini göstermiştir.

Anahtar kelimeler: Kutu Tipi Menfez, Dinamik Zemin Basıncı, Sarsma Tablası Deneyi, Santrifüj Deneyi, Dinamik Yapı-Zemin Etkileşimi

To My Family

ACKNOWLEDGMENTS

TABLE OF CONTENTS

LIST OF TABLES

LIST OF FIGURES

FIGURES

xvii

xviii

CHAPTER 1

INTRODUCTION

1.1 General

Seismic design and safety of buried structures including pipelines, culverts, subways and tunnels are crucial requirements for economic and infrastructure development. In the past, the common belief among the geotechnical engineers was that the underground structures had been adequately resistant to the seismic forces. For this reason, in earlier projects, underground structures were not designed in detail to withstand earthquakes. However, seismic assessment of underground structures gained more importance after suffering heavy damage from large earthquakes such as 1995 Kobe, Japan, 1999 Kocaeli, Turkey and 1999 Chi Chi, Taiwan earthquakes.

The 1995 Hyogo-ken Nanbu (Kobe) Earthquake of magnitude M_w=6.9 occurred at the northern part of Awaji island near Kobe, Japan. It was one of the most destructive earthquakes that caused significant damage to Kobe's underground rapid transit system (Figure 1.1) (Sitar et al. 1995). The extensive damage occurred in Daikai Subway station built by cut and cover technique. It was mentioned that collapse of the subway and the intense damage was caused by the earthquake forces. Besides, it was emphasized that no permanent ground deformation or fault displacement was observed near the station.

Iida et al. (1996) presented the observations from Daikai Station after Kobe earthquake and explained the damage and failure mechanism in the subway tunnel. It was observed that shear cracks occurred on the walls of station during the earthquake. The authors pointed out that the relative movement between station and overburden soil could be the main reason of the collapse.

1
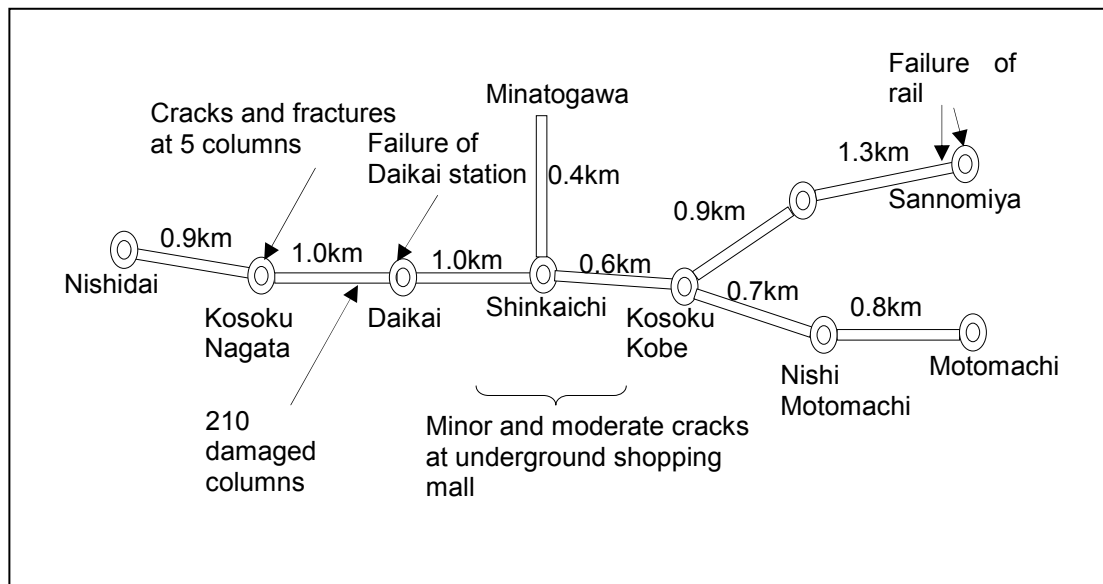
Figure 1.1. Earthquake damage map of Kobe rapid transit railway
(Sitar et al., 1995)

Parra-Montesinos et al. (2006) evaluated the collapse of Daikai Subway Station and focused on the soil structure interaction. Simplified procedures and nonlinear finite element analyses were performed to understand the dynamic behavior of the subway station during Kobe earthquake. It was emphasized that the friction between the structure and soil, soil degradation and relative movement between the soil and the structure should be taken into account in the design of underground structures against earthquakes. Besides, in order to resist the larger earthquake-induced displacements in soft ground, the authors proposed structural elements with higher ductility.

Wang et al. (2001) assessed the damage mechanism of mountain tunnels exposed to Taiwan Chi-Chi Earthquake. It was observed that 49 of 57 tunnels suffered serious cracks in Taiwan. Tunnels buried at shallow depths or near the surface experienced significant damage as compared to deeply embedded tunnels. Furthermore, It was concluded that the tunnels should be constructed far away from the surface slopes and active faults.

2

Hashash et al. (2001) reviewed the several reported case histories of underground structures prepared by Duke and Leeds (1959), Stevens (1977), Dowding and Rozen (1978), Owen and Scholl (1981), Sharma and Judd (1991), Power et al. (1998) and Kaneshiro et al. (2000). Among the case histories, San Francisco Bay area rapid transit system, Alameda tubes in California, Los Angeles metro, underground structures in Kobe / Japan, underground structures in Taiwan and Bolu tunnel were investigated. Following remarks were suggested by Hashash et al. (2001) for evaluating the performance of buried structures subjected to earthquake loading:

1) Buried structures experience less damage as compared to surface structures.

2) Case histories indicate that shallow underground structures are more prone to earthquakes than are deep underground structures. Less damage was observed as the tunnel embedment depth increases.

3) Tunnels in soils suffer more damage than tunnels in rock

4) Unlined tunnels are more vulnerable to earthquakes than are lined and reinforced tunnels. The lining and surrounding ground of a tunnel can be stabilized by grouting to reduce the earthquake induced damage.

5) Underground structures subjected to symmetrical loading are safer due to the improvement in soil-structure interaction. If the lining of structure is made stiffer without improving the surrounding soft soil, the tunnel lining may experience greater earthquake forces. Stability of shallow underground structures may be increased by reinforcing and strengthening the surrounding soil.

6) Maximum ground acceleration and velocity may affect the damage levels at the tunnels which mainly depend on location and magnitude of the earthquake.

7) Earthquake duration has a significant role on the seismic performance of underground structures. Structures may fail due to the fracture and excessive deformations.

8) Amplitude of seismic wave may increase when the wave passes through the tunnel provided that the wavelength ranges from 1 to 4 times of tunnel diameter.

9) Slope failures may cause extensive damage at and around the portal sections.

Earthquake damage on underground structures can be produced by ground failure and ground shaking. Seismically induced ground failure hazards may refer to landslides, liquefaction and fault rupture. These hazards occur in a small area and can cause significant damage on the underground structures due to large permanent ground deformations On the other hand, damage due to ground shaking affects a wide region of the buried facility. Ground shaking is produced by seismic waves including body waves and surface waves. Body waves are categorized as compressional and shear waves. Shear waves are the most destructive form of body waves that cause ovaling or racking deformation of underground structures (Wang, 1993; Hashash et al. 2001). Within the scope of this study, dynamic response of underground structures was examined by producing vertically propagating shear waves.

There are several methods for evaluating the seismic design of rectangular underground structures. Free-field deformation method is the simplest approach. This approach is based on the assumption that the structure moves in accordance with the soil during shaking. In other words, strains of the surrounding ground under seismic waves are directly applied to the rectangular underground structure. The main deficiency of this approach is the ignorance of soil-structure interaction effect. Therefore, seismic deformations may be underestimated or overestimated depending on the relative stiffness between the buried structure and surrounding ground (Wang 1993). In order to take into account soil structure interaction effect simplified frame analysis (SFA) methods are proposed by Wang (1993), Penzien (2000) and Huo et al. (2006). In SFA approach, racking deformations of the structure are estimated by considering the relative stiffness and those deformations applied as a static load to compute sectional forces. Both free field and SFA methods are displacement based approaches and are commonly preferred by engineers.

Another approach for evaluating the seismic design of underground structures is the force-based method. In this method, equivalent seismic forces caused by the inertial force of soil under earthquake loading are estimated. There is not generally accepted approach to predict the dynamic soil pressures exerted on a culvert. One widely preferred approach for predicting the dynamic earth pressures acting on the

embedded structures is the Mononobe-Okabe method. It is based on Coulomb's active pressure theory and is proposed for earth retaining structures. The dynamic force is calculated by multiplying the weight of the active wedge with the estimated seismic coefficient. It is not reasonable to use the Mononobe-Okabe method for rectangular buried structures since a yielding active wedge usually does not occur in the surrounding soil during the earthquake. Wang (1993) stated that Mononobe Okabe approach can be applied to structures having U-section or buried near the soil surface. He emphasized that as the structure embedment depth increases, the theory tends to overestimate the racking deformations. Recently, finite element and finite difference methods have been used for modeling the dynamic response of underground structures. Numerical analyses can model the complex dynamic soil structure interaction relationship between the underground structure and the surrounding soil. However, in numerical modeling, it is very difficult to simulate the non-linear behavior of soil under earthquake loading. Besides, excessive computational effort and time is required for convergence, especially for dynamic soil-structure interaction problems.

There is a lack of experimental data for evaluating the dynamic response of rectangular underground structures. Thus, more research is required in order to clarify the seismic effects on buried structure. In this study, 1-g shaking table tests and centrifuge tests were performed to investigate the dynamic earth pressures acting on the box-type underground culvert. The effect of relative stiffness between the buried culvert and surrounding ground was evaluated under harmonic motions. Moreover, the influence of acceleration on dynamic behavior of underground box-type culvert was examined. The tests provided a better understanding of the qualitative behavior of box-type embedded structures subjected to earthquake loading. As a consequence, the main objective of this study is to make a reasonable contribution to the preliminary assessment of box-type underground culverts subjected to dynamic loading.

1.2 Objective of the study

This study focuses on the dynamic response of box shaped underground structures buried in dry sand. The main objectives of the research can be summarized as follows:

1) To evaluate and to understand the dynamic pressures acting on the box-type underground culverts.

2) To study the effects of flexibility ratio and shear strain on dynamic response of box-type culverts

3) To examine the deformation of the box-type underground culvert by considering the nonlinear behavior of soil and dynamic soil-structure interaction.

4) To develop a simplified procedure for the preliminary assessment of box-type underground culverts under seismic action.

In order to achieve the goals listed above, 1-g shaking table tests were performed by applying harmonic motions. A laminar box was designed and manufactured for eliminating the boundary effects in shaking table tests. The experiments were conducted on four box-type culvert models having different rigidities. The cross section of the culvert and ground model is given in Figure 1.2. Dynamic motion was applied only in horizontal direction and accordingly the culvert model was subjected to vertically propagating shear waves as shown in Figure 1.2.
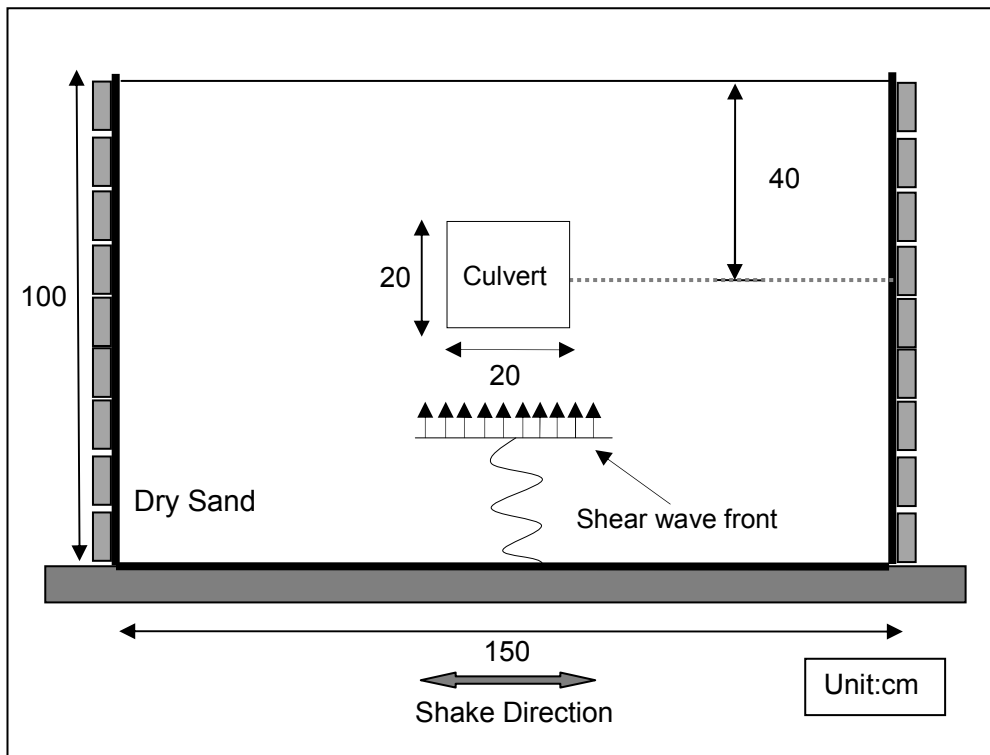
Figure 1.2. Shaking table test model

Figure 1.3 shows the shear stresses (τ) and normal stresses (σ_T, σ_N) acting on the culvert model. The total lateral pressure (σ_T) acting on the sidewalls can be defined as the superposition of static pressure (σ_s) and dynamic pressure (σ_D). Within the scope of this study, static pressures and dynamic pressures acting on sidewalls were measured separately. Based on the measurements, a dynamic pressure distribution was approximated. Furthermore, a simplified approach was developed for the preliminary assessment of the underground box-type culverts subjected to dynamic loading. For verification, centrifuge tests were conducted on a flexible box-type underground culvert and results were compared with the preliminary estimates of the proposed simplified approach.
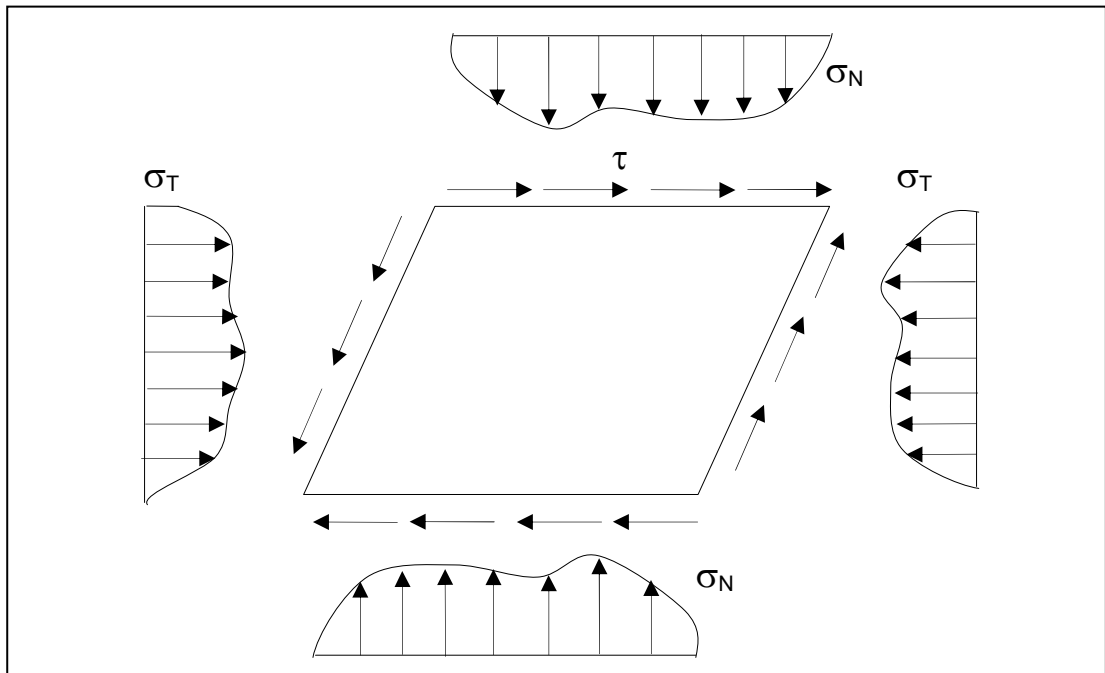
Figure 1.3. Shear and lateral normal stresses acting on the culvert model

1.3 Thesis organization

The dissertation is organized into five Chapters. A brief summary of the thesis organization is given as follows:

Chapter 1 gives a brief introduction about the significance of design of underground structures subjected to earthquake loading. The existing gaps and research needs are identified by considering the limitations and shortcomings of the current seismic design methods. The main points and objectives of the proposed research are presented.

Chapter 2 includes an overview of previous researches and presents the theoretical background for evaluating the dynamic response of underground structures. Besides, the chapter provides a summary of available analyses methods and

highlights the main factors to be considered in the design of rectangular underground structures.

Chapter 3 reports the procedure and the results of 1-g shaking table tests conducted in Middle East Technical University (METU) geotechnical dynamics laboratory. In this chapter, first, a detailed description of apparatus, data acquisition system and test instrumentation is provided. Later, the plan and the methodology of the shaking table tests are summarized. At the end of the chapter, the results obtained from the shaking table experiments are presented and discussed with the simplified approach proposed for the preliminary seismic assessment of box-type culverts.

Chapter 4 describes the centrifuge testing facility at IFSTTAR (Institut Français des Sciences et Technologies des Transports, de l'aménagement et des Réseaux) and discusses the findings of centrifuge tests conducted on a flexible box-shaped culvert model in dry sand. Furthermore, results are compared with the preliminary estimates of proposed simplified approach for validation.

Chapter 5 presents summary of the dissertation and findings obtained from the 1g shaking table and centrifuge tests. Major conclusions and limitations of the present study and recommendations for further research are discussed.

CHAPTER 2

LITERATURE REVIEW

2.1 Seismic behavior of underground structures

Seismic behavior of underground structures is significantly different from that of above ground (surface) structures which are mainly governed by inertia forces. On the other hand, underground structures are supported by the surrounding ground and compelled to move with the surrounding medium during a seismic event. This movement due to ground deformations causes a stress-strain field on the structure. Dynamic response of tunnels is categorized by three types of deformations (Owen and Scholl, 1981):

1) Axial deformation (Figure 2.1(a) and (b))

2) Curvature deformation (Figure 2.1(c) and (d))

3) Ovaling and racking deformation (Figure 2.1(e) and (f)).

Axial deformations are produced by the P-waves propagating parallel to the tunnel axis. The tunnel is under tension and compression during the passage of P-waves If the wave propagates normal to the tunnel axis there will be a hoop deformation in the tunnel cross section provided that the tunnel diameter is larger than the wavelength. In most cases, tunnel diameter is relatively short and therefore the tunnel is not exposed to high seismic stresses (St. John and Zahrah, 1987). Axial and curvature deformations are generally considered in the longitudinal direction along the tunnel axis during the design process (Wang, 1993). Ovaling and racking deformations occur when the tunnel is subjected to vertically propagating seismic waves. Wang (1993) mentioned that the tunnels are analyzed in transverse direction for determining ovaling and curvature deformations.

2.2 Seismic design approaches for underground structures

The standard method for evaluating the seismic stability of underground structures had been the pseudo-static method of analyses. Then, with the advent of dynamic analysis procedures, the seismic safety under earthquake loading have been successfully evaluated by using the numerical methods. In numerical methods, dynamic non-linear soil structure interaction is taken into account, but it is more complex and requires significant computational effort. In addition to these design methods, in order to understand the dynamic behavior of buried structures, model tests are performed. There are basically two types of model tests namely; 1-g shaking table tests and centrifuge tests.

2.2.1 Free-field ground deformation approach

Free-field ground deformation method is a practical and effective technique used in the preliminary seismic design of underground structures. In this approach, it is assumed that the underground structure moves in accordance with the surrounding ground during a seismic event. In other words, there is no interaction and relative movement between soil and the underground structure.

In the analyses, ground strains are calculated when there is no structure in the site. Those strains are then directly applied to the underground structure and accordingly deformations are computed for that structure. True values may be obtained when the rigidity of the structure is same with the soil. Otherwise, deformations may be underestimated or overestimated when the structure is more flexible or rigid relative to the surrounding ground (Hashash et al., 2001).
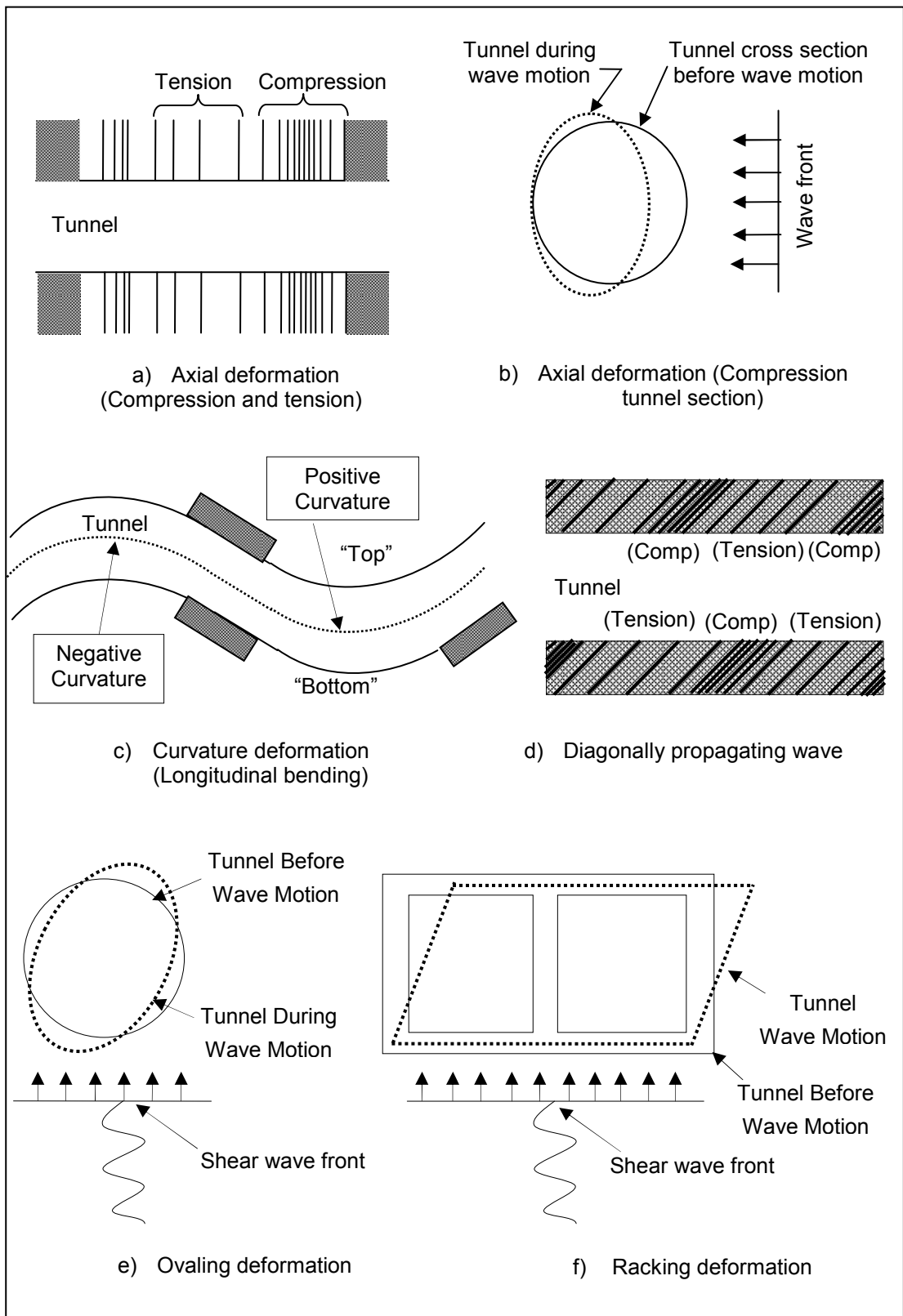
Figure 2.1. Deformation types caused by seismic waves (After Owen and Scholl, 1982, After Hashash et al., 2001)

12

2.2.1.1 Free-field axial and curvature deformations

Newmark (1968) proposed analytical procedures to estimate the free-field strains by using the theory of wave propagation in elastic, homogeneous and isotropic media. Based on the Newmark approach, St. John and Zahrah (1987) developed formulations to describe axial and curvature strains caused by seismic waves. These formulas are shown in Table 2.1. Explanations of the parameters in Table 2.1 are as follows:

V_p: Peak particle velocity due to P-wave (Compression wave)

c_p: P-wave velocity

V_s: Peak particle velocity due to S-wave (Shear wave)

c_s: S-wave velocity

V_{rp}: Peak particle velocity due to Rayleigh wave

c_R: Rayleigh wave velocity

ϕ : angle of incidence with respect to the tunnel axis

a_p: peak particle acceleration due to Pwave

a_s: peak particle acceleration due to Swave

a_{pr}: peak particle acceleration due to Rayleigh wave

St. John and Zahrah (1987) and Power et al. (1996) simplified the tunnel structure as an elastic beam for obtaining the strains in Table 2.1. Total axial strains were obtained by superposing the longitudinal strains caused by the axial and curvature deformations as given in the following equations:

$$\varepsilon_{ap} = \frac{V_s}{c_s}\cos^2\phi + \frac{Ra_p}{c_p^2}\sin\phi\cos^2\phi \quad \text{for P waves} \qquad (2.1)$$

$$\varepsilon_{as} = \frac{V_s}{c_s}\sin\phi\cos\phi + \frac{Ra_s}{c_s^2}\cos^3\phi \quad \text{for S waves} \qquad (2.2)$$

$$\varepsilon_{apr} = \frac{V_R}{c_R}\cos^2\phi + \frac{Ra_R}{c_R^2}\sin\phi\cos^2\phi \qquad \text{for Rayleigh waves} \tag{2.3}$$

where R represents the radius of the tunnel section. Free-field deformations caused by harmonic waves propagating obliquely to the tunnel axis are illustrated in Figure 2.2. In this figure, L represents the shear wave length, ϕ is the angle of incidence and D is the displacement amplitude of harmonic wave. In the design process, it is very difficult to determine the angle of incidence. Hence, to be on the safe side, the most critical angle is usually used to obtain the maximum strains (Wang, 1993).

Figure 2.2. Displacements due to harmonic shear wave propagating obliquely to the tunnel axis (After Wang,1993)

14

Table 2.1. Free-field strains and curvatures caused by seismic waves (After John St. And Zahrah, 1987)

Wave Type		Longitudinal Strain	Normal Strain	Shear Strain	Curvature
P-wave		$\varepsilon_l = \dfrac{V_p}{c_p}\cos^2\phi$ $\varepsilon_{lm} = \dfrac{V_p}{c_p}$ for φ=0°	$\varepsilon_n = \dfrac{V_p}{c_p}\sin^2\phi$ $\varepsilon_{nm} = \dfrac{V_p}{c_p}$ for φ=90°	$\gamma = \dfrac{V_p}{c_p}\sin\phi\cos\phi$ $\gamma_m = \dfrac{V_p}{2c_p}$ for φ=45°	$\dfrac{1}{\rho} = \dfrac{a_p}{c_p^{\,2}}\sin\phi\cos^2\phi$ $\dfrac{1}{\rho_m} = 0.385\dfrac{a_p}{c_p^{\,2}}$ for φ=35°16′
S-wave		$\varepsilon_l = \dfrac{V_s}{c_s}\sin\phi\cos\phi$ $\varepsilon_{lm} = \dfrac{V_s}{2c_s}$ for φ=45°	$\varepsilon_n = \dfrac{V_s}{c_s}\sin\phi\cos\phi$ $\varepsilon_{nm} = \dfrac{V_s}{2c_s}$ for φ=45°	$\gamma = \dfrac{V_s}{c_s}\cos^2\phi$ $\gamma_m = \dfrac{V_s}{c_s}$ for φ=0°	$K = \dfrac{a_s}{c_s^{\,2}}\cos^3\phi$ $K_m = \dfrac{a_s}{c_s^{\,2}}$ for φ=0°
Rayleigh wave	**Compressional Component**	$\varepsilon_l = \dfrac{V_{RP}}{c_R}\cos^2\phi$ $\varepsilon_{lm} = \dfrac{V_{RP}}{c_R}$ for φ=0°	$\varepsilon_n = \dfrac{V_{RP}}{c_R}\sin^2\phi$ $\varepsilon_{nm} = \dfrac{V_{RP}}{c_R}$ for φ=90°	$\gamma = \dfrac{V_{RP}}{c_R}\sin\phi\cos\phi$ $\gamma_m = \dfrac{V_{RP}}{2c_{RP}}$ for φ=45°	$K = \dfrac{a_{RP}}{c_R^{\,2}}\sin\phi\cos^2\phi$ $K_m = 0.385\dfrac{a_{RP}}{c_R^{\,2}}$ for φ=35°16′
	Shear Component		$\varepsilon_n = \dfrac{V_{RS}}{c_R}\sin\phi$ $\varepsilon_{nm} = \dfrac{V_{RS}}{c_R}$ for φ=90°	$\gamma = \dfrac{V_{RS}}{c_R}\cos\phi$ $\gamma_m = \dfrac{V_{RS}}{c_R}$ for φ=90°	$K = \dfrac{a_{RS}}{c_R^{\,2}}\cos^2\phi$ $K_m = \dfrac{a_{RS}}{c_R^{\,2}}$ for φ=0°

2.2.1.2 Free-field shear deformations for circular underground structures (Ovaling effect)

In circular underground structures, ovaling deformations occur due to seismic waves propagating normal to the structure axis. These deformations may be caused by different types of waves propagating horizontally, vertically or obliquely. In general, underground structure design against ovaling effect is led by the vertically propagating shear waves which produce the most critical deformation mode of the structure lining (Wang, 1993).

Wang (1993) investigated the shear distortion of the surrounding soil for perforated and non-perforated ground (Figure 2.3, Figure 2.4). Maximum diameter strains for these two cases are derived as:

$$\frac{\Delta D}{D} = \pm \frac{\gamma_{max}}{2} \qquad \text{(non-perforated ground)} \qquad (2.4)$$

$$\frac{\Delta D}{D} = \pm 2\gamma_{max}(1-\nu_m) \quad \text{(perforated ground)} \qquad (2.5)$$

where D is diameter of the tunnel, γ_{max} is maximum diameter strain, $\Delta D/D$ is diametric strain and ν_m is Poisson's ratio of soil.

Equation 2.4 and 2.5 indicate that the non-perforated shear deformations are approximately two or three times more than the perforated grounds. Maximum shear strains calculated by these equations are valid for the surrounding ground when there is no structure in the field. Perforated ground calculations are reasonable when the rigidity of the underground structure is less than the surrounding ground. If the ground stiffness is same with the stiffness of underground structure, shear distortion will be well represented by non-perforated ground deformation approach.
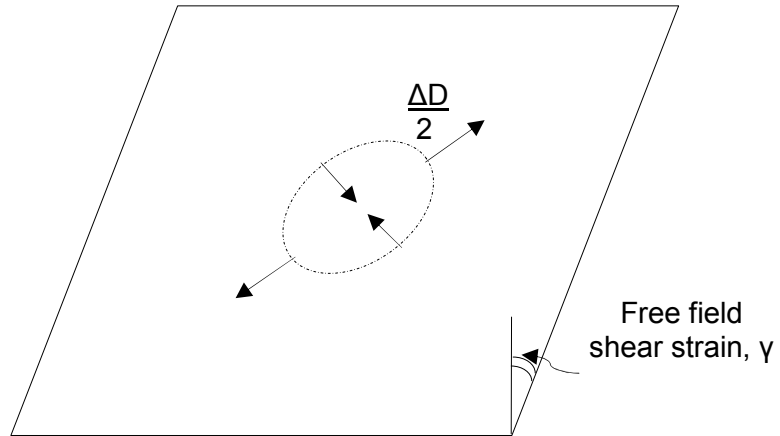
Figure 2.3. Shear distortion for non-perforated ground (After Wang,1993)
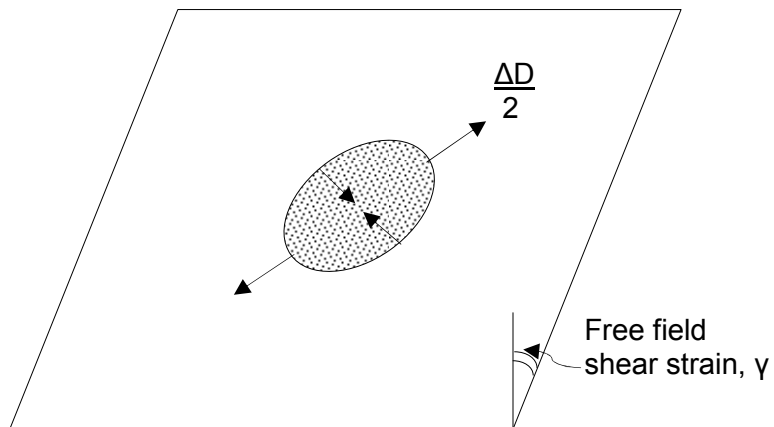
Figure 2.4. Shear distortion for perforated ground (After Wang,1993)

2.2.1.3 Free-field shear deformations for rectangular underground structures(Racking effect)

Racking type of deformation has the most significant effect on the response of underground structures subjected to seismic waves. Free-field deformation analysis is the simplest way for the evaluation of racking deflections. In this approach it is assumed that deformation of the structure is equal to the free-field racking deflection as illustrated in Figure 2.5. Analytical solutions given in Table 2.1 or one dimensional ground response analysis program such as SHAKE can be used for estimating free-field deformations.
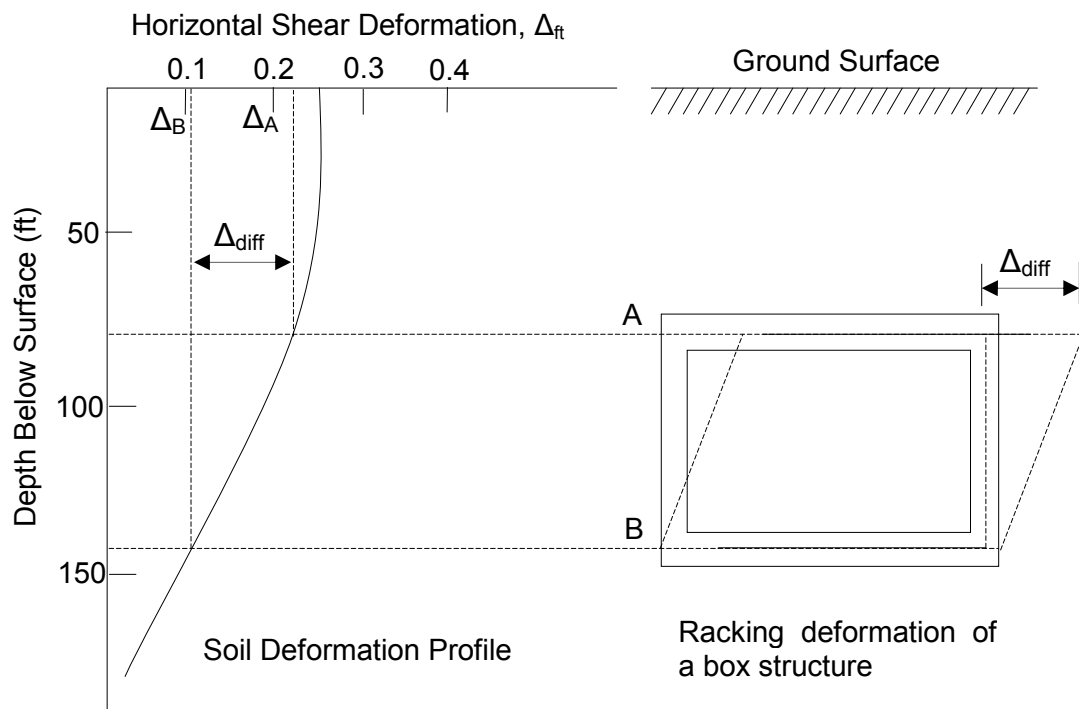
Figure 2.5. Free-field racking deformation applied on a rectangular underground structure (After Wang, 1993)

2.2.2 Soil-Structure Interaction Method

Dynamic response of the underground structures is strongly dependent on the soil-structure interaction effect. Dynamic soil-structure interaction effect is governed by the relative stiffness between underground structure and surrounding soil. Free-field deformation approach ignores this effect and cannot represent the actual behavior when the structure is too rigid or flexible with respect to the ground. Closed form solutions and design procedures of underground structures are described in the following sections.

2.2.2.1 Closed form elastic solutions for axial and curvature deformations

These solutions are specifically developed for the circular underground structures. St. John and Zahrah (1987) proposed elastic solutions for predicting the forces acting on tunnels during a ground motion. Free-field axial and curvature deformations were derived by using wave propagation theory. Elastic beam theory was applied by considering the soil-structure interaction effects. However, dynamic soil-structure interaction effect was not included in these elastic solutions due to quasi-static approximation. Forces and moments exerted on structure were calculated based on the assumption that the beam behaves as an elastic beam on elastic foundation. Figure 2.6 indicates the induced forces and moments in tunnel lining due to seismic waves.

Maximum shear forces, axial force and bending moments were derived as follows (St. John and Zahrah, 1987):

i) Maximum shear force:

$$V_{max} = \frac{(\frac{2\pi}{L})^3 E_l I_c A}{1 + \frac{E_l I_c}{K_h}(\frac{2\pi}{L})^4} \tag{2.6}$$

ii) Maximum axial force:

$$Q_{max} = \frac{(\frac{2\pi}{L}) E_l I_c A}{2 + \frac{E_l I_c}{K_a}(\frac{2\pi}{L})^2} \tag{2.7}$$

iii) Maximum bending moment:

$$M_{max} = \frac{(\frac{2\pi}{L})^2 E_l I_c A}{1 + \frac{E_l I_c}{K_h}(\frac{2\pi}{L})^4} \tag{2.8}$$

where,

K_h = Horizontal foundation modulus of the soil

K_a = Axial foundation modulus of the soil

I_c = Moment of inertia of the tunnel.

A = Free-field displacement response amplitude of a harmonic shear wave

K_a and K_h is defined by:

$$K_a = K_h = \frac{16\pi G(1-\upsilon)d}{(3-4\upsilon)L} \tag{2.9}$$

where, G is the shear modulus, d is the diameter of the tunnel, L is the wavelength and ν is the Poisson's ratio of the soil.
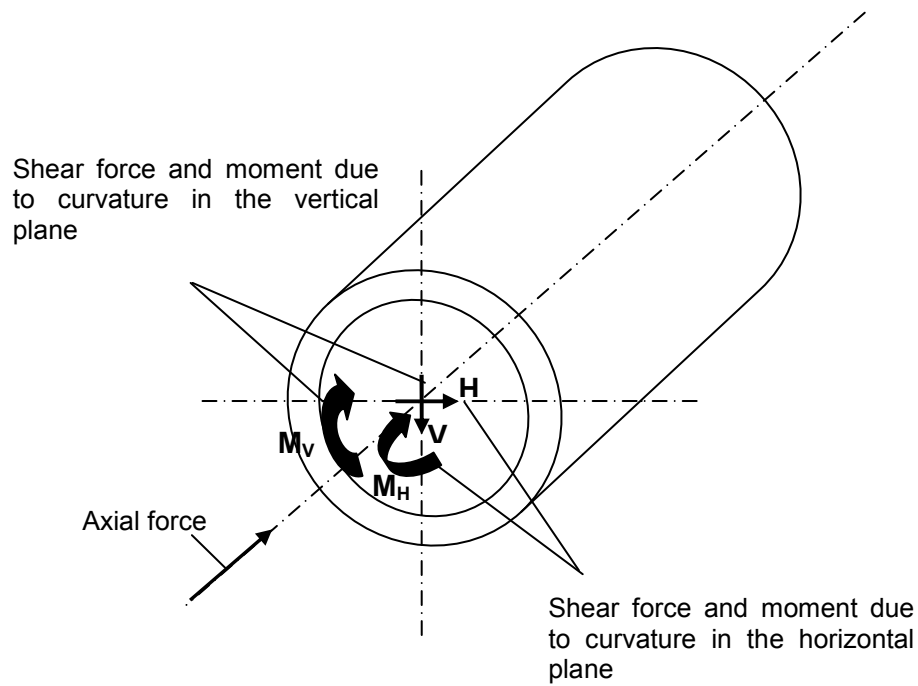
Figure 2.6. Induced forces and moments caused by waves propagation along tunnel axis (After Power et al., 1996)

2.2.2.2 Closed form elastic solutions for ovaling effect

Many researchers studied the ovaling effect of seismic waves on the underground structures during an earthquake. Schwarz and Einstein (1979), Wang (1993), Penzien (2000) and Bobet (2003) proposed to estimate the thrust, moments and displacements in tunnel lining due to ovaling deformations. Relative stiffness is represented by defining compressibility and flexibility ratio (Hoeg 1968, Peck et al. 1972). Equations for the compressibility, C, and flexibility ratio, F, are given as follows:

$$C = \frac{E_s(1-v_1^2)R}{E_l t(1+v_s)(1-2v_s)}$$

(2.10)

$$F = \frac{E_s(1 - \nu_1^2)R^3}{6E_l I(1 + \nu_s)} \tag{2.11}$$

where,

E_s=Elasticity modulus of the soil

E_l=Elasticity modulus of the tunnel lining

ν_s=Poisson's ratio of the soil

ν_l = Poisson's ratio of the tunnel lining

R= Radius of the tunnel lining

t= Thickness of the tunnel lining

I=Moment of inertia

Friction between the ground and structure was modeled for two conditions; full slip and no slip condition. Both cases are usually taken into consideration and the most critical one is used for assessing the deflections, moments and maximum thrusts. Forces and moments caused by seismic waves propagating perpendicular to tunnel axis is shown in Figure 2.7.

For full slip condition, diameter strain, maximum thrust T_{max}, maximum bending moment M_{max} were expressed as follows (Wang, 1993):

$$\frac{\Delta D}{D} = \pm\frac{1}{3}K_1 F \gamma_{max} \tag{2.12}$$

$$T_{max} = \pm\frac{1}{6}K_1 \frac{E_s}{(1 + \nu_s)} R \gamma_{max} \tag{2.13}$$

$$M_{max} = \pm\frac{1}{6}K_1 \frac{E_s}{(1 + \nu_s)} R^2 \gamma_{max} \tag{2.14}$$

$$K_1 = \frac{12(1 - \nu_s)}{2F + 5 - 6\nu_s} \tag{2.15}$$

where, K_1 is lining response coefficient.
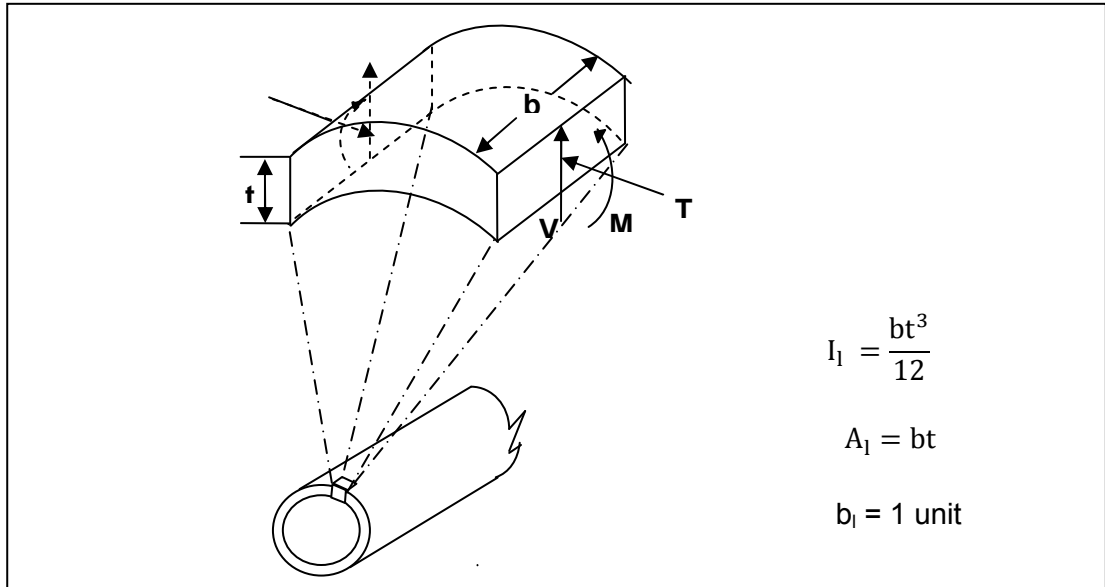
Figure 2.7. Induced circumferential forces and moments caused by waves propagating perpendicular to tunnel axis (Power et al., 1996)

For no-slip condition, maximum thrust was given by (Hoeg, 1968; Schwartz and Einstein, 1980; Wang, 1993):

$$T_{max} = \pm K_2 \tau_{max} R = \pm K_2 \frac{E_s}{2(1+v_s)} R \gamma_{max} \tag{2.16}$$

$$K_2 = 1 + \frac{[F(1-2v_s)-(1-2v_s)C]-\frac{1}{2}(1-2v_s)^2+2}{F[(3-2v_s)+(1-2v_s)C]+C\left[\frac{5}{2}-8v_s+6v_s^2\right]+6-8v_s} \tag{2.17}$$

where, K_2 is lining thrust response coefficient. Solutions of maximum moment and displacement were not given for no-slip condition. Deflections and maximum

23

moments calculated in no-slip solution are more conservative according to full-slip model results. Thus, to be on the safe side, it was suggested to use no-slip assumption for estimating the maximum moment and deflection of a circular tunnel lining. Full slip solution of a circular tunnel under simple shear condition leads to an underestimate of maximum thrust. Therefore, no-slip approach should be applied in order to evaluate the maximum lining thrust (Wang, 1993).

Penzien and Wu (1998) and Penzien (2000) proposed similar elastic solutions to assess the response of circular tunnel lining. Assuming full slip conditions, solutions for thrust, T_θ, moment, M_θ and shear V_θ are presented below:

$$T(\theta) = -\frac{12 E_l I \Delta_l^{\ n}}{D^3 (1-\nu_l)^2} \cos 2(\theta + \frac{\pi}{4})$$

(2.18)

$$M(\theta) = -\frac{6 E_l I \Delta_l^{\ n}}{D^2 (1-\nu_l)^2} \cos 2(\theta + \frac{\pi}{4})$$

(2.19)

$$V(\theta) = -\frac{24 E_l I \Delta_l^{\ n}}{D^3 (1-\nu_l)^2} \sin 2(\theta + \frac{\pi}{4})$$

(2.20)

where, D is outside diameter of the circular lining, Δ_l^n is the lining diametric deflection and θ is the angular position. Figure 2.8 shows the forces and moments acting on circular lining. Diameter change of the lining due to soil-structure interaction is expressed as:

$$\pm \Delta_l^{\ n} = \pm R^n \Delta_{ff}$$

(2.21)

where, Δ_{ff} is free-field deformation, R is lining soil racking ratio and α_s is the stiffness ratio which can be given as:

$$R = \pm \frac{4(1-\nu_s)}{(\alpha_s + 1)}$$

(2.22)

$$\alpha_s^{''n} = \frac{12E_lI(5-6v_s)}{D^3G_s(1-v_l^2)} \tag{2.23}$$
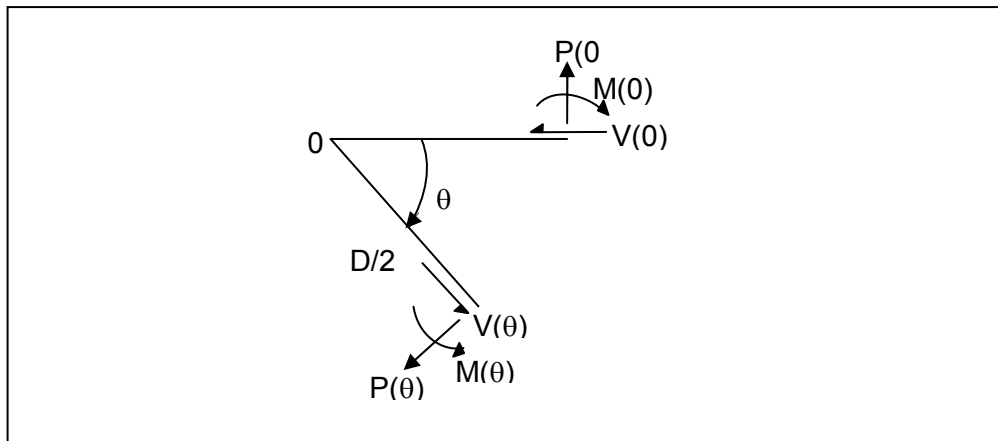
Figure 2.8. Sign convention for axial,shear forces and moments (After Penzien, 2000)

Recommended analytical solutions by Penzien (2000) for no-slip condition are as follows:

$$P(\theta) = -\frac{24E_lI\Delta_l}{D^3(1-v_l)^2}\cos2(\theta+\frac{\pi}{4}) \tag{2.24}$$

$$M(\theta) = -\frac{6E_lI\Delta_l}{D^2(1-v_l)^2}\cos2(\theta+\frac{\pi}{4}) \tag{2.25}$$

$$V(\theta) = -\frac{24E_lI\Delta_l}{D^3(1-v_l)^2}\sin2(\theta+\frac{\pi}{4}) \tag{2.26}$$

25

For no slip condition, Bobet (2003) proposed the following equations:

$$T = (1 - C_3) R \tau \cos 2(\theta + \frac{\pi}{4}) \tag{2.27}$$

$$M = \frac{1}{2}(1 + C_2 + C_3) R^2 \tau \cos 2(\theta + \frac{\pi}{4}) \tag{2.28}$$

where,

$$C_2 = (-2) \frac{(1 - v_s)^2 C^* + (1 - v_s) - \dfrac{3[(1 - v_s)C^* + 4]}{F^*}}{(1 - v_s)^2 C^* + (1 - v_s)(3 - 2v_s) + \dfrac{3[(1 - v_s)(5 - 6v_s)C^* + 4(3 - 4v_s)]}{F^*}} \tag{2.29}$$

$$C_3 = \frac{1}{3} \frac{(1 - v_s)C^* - 2 - C_2[(1 - v_s)C^* + 4v_s]}{(1 - v_s)C^* + 2} \tag{2.30}$$

2.2.2.3 Racking effect on rectangular underground structures

Racking is the main effect governing the design of rectangular underground structures. This action is caused by the seismic waves propagating perpendicular to the tunnel axis. Racking deformations of the underground structures are strongly dependent on the soil-structure interaction. This interaction is mainly affected by the relative stiffness between the underground structure and the soil. Other factors affecting the seismic performance of rectangular underground structures can be given as follows (Wang, 1993):

-Structure type and dimensions

-Ground shaking

-Depth of the underground structure

Simplified procedures were proposed by Wang (1993), Penzien (2000) and Huo et al. (2006) so as to design rectangular underground structures exposed to seismic ground motions. These procedures are given in the following sections.

i) Simplified procedure of Wang (1993)

Wang (1993) defined the shear strain and flexural stiffness of a soil element (Figure 2.9) under simple shear condition as follows:

$$\gamma_s = \frac{\Delta}{H} = \frac{\tau}{G_s} \tag{2.31}$$

$$\frac{\tau}{\gamma_s} = \frac{\tau}{\Delta/H} = G_s \tag{2.32}$$

Where, Δ is the racking deformation, H is the height of the structure and τ is the simple shear stress and G_s is the shear modulus of the soil. Considering that the rectangular underground structure is distorted under same shear stress, Wang (1993) obtained a concentrated force P and proposed following equations for estimating shear strain of the underground structure:

$$\gamma_s = \frac{\Delta}{H} = \frac{P}{HS_1} = \frac{\tau L}{HS_1} \tag{2.33}$$

$$\frac{\tau}{\gamma_s} = \frac{\tau}{\Delta/H} = \frac{S_1 H}{L} \tag{2.34}$$

where L is the width of the structure and S_1 is the force required for unit racking deformation of rectangular underground structure. If Equation 2.33 is divided by Equation 2.35, the flexibility ratio, F, representing the relative stiffness between the rectangular underground structure and the soil is calculated as:

$$F = \frac{G_s L}{S_1 H} \tag{2.35}$$
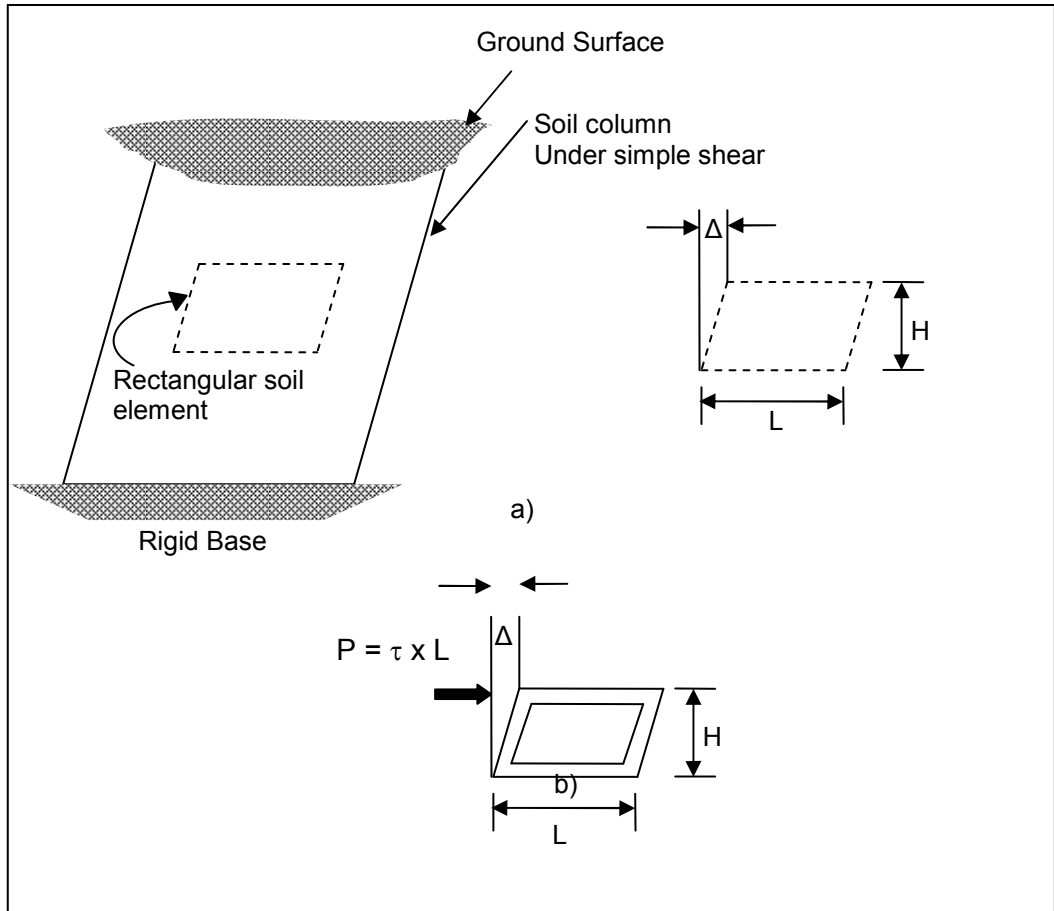
Figure 2.9. Racking deformation of soil and structure under s'mple shear (After Wang, 1993)
a) Free-field deformation of soil
b) Racking deformation of rectangular underground structure

The flexibility ratio can be found by conducting simple frame analysis for any type of rectangular underground structure. In order to calculate the flexibility ratio of a single frame, following equation is proposed by (Wang, 1993):

$$F = \frac{G_s}{24}\left(\frac{H^2 W}{EI_W} + \frac{HW^2}{EI_R}\right) \tag{2.36}$$

where, E is the elastic modulus of the structure, H is the height and W is the width of structure, I_W is the moment of inertia for side walls and I_R is the moment of inertia

for upper and lower slabs. Physical meaning of the flexibility ratio can be described as follows (Wang,1993;Hashash et al. 2001):

- For F=0 condition: Since the structure is infinitely rigid, it will not be deformed under seismic waves.

- For F<1 condition: The underground structure is more rigid as compared to surrounding soil. It will deflect less than the surrounding soil during a seismic event.

- For F=1 condition: Stiffness of the structure and the ground is equal to each other. This means that the underground structure conforms to free-field ground deformations.

- For F>1 condition: Structure is more flexible as compared to surrounding ground. Hence, It will deflect more than the surrounding ground.

- For F=∞ condition: Since the structure is infinitely flexible, it acts like a perforated ground under dynamic excitations.

Wang (1993) performed finite element analyses in order to investigate the soil-structure interaction effect on dynamic response of underground structures. In the analyses, a detailed numerical modeling study was performed by considering the factors such as flexibility ratio, structure geometry, input motion characteristics and tunnel embedment depth. Results showed that flexibility ratio is the main factor to be considered in the design of underground structures.

Variation of racking ratio, R, was plotted with respect to flexibility ratio in Figure 2.10 (Wang 1993). This figure shows that racking ratio increases at a decreasing rate with flexibility ratio. In the design process, if free-field deformations are estimated, structural racking deformations can be easily determined by using the Figure 2.10. Wang (1993) compared the racking ratios of circular and rectangular tunnels for a given flexibility ratio (Figure 2.11). Based on this comparison the author suggested that the charts proposed for circular underground structures may be used as an upper bound for rectangular underground structures.
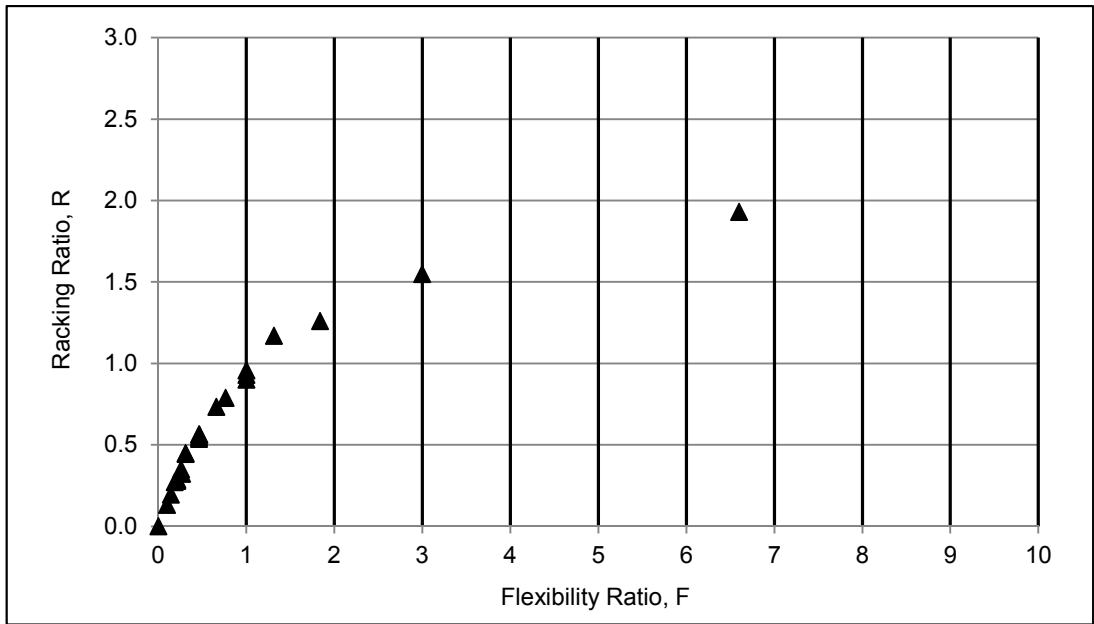
Figure 2.10. Variation of racking ratio with respect to flexibility ratio for rectangular tunnels (Wang, 1993)
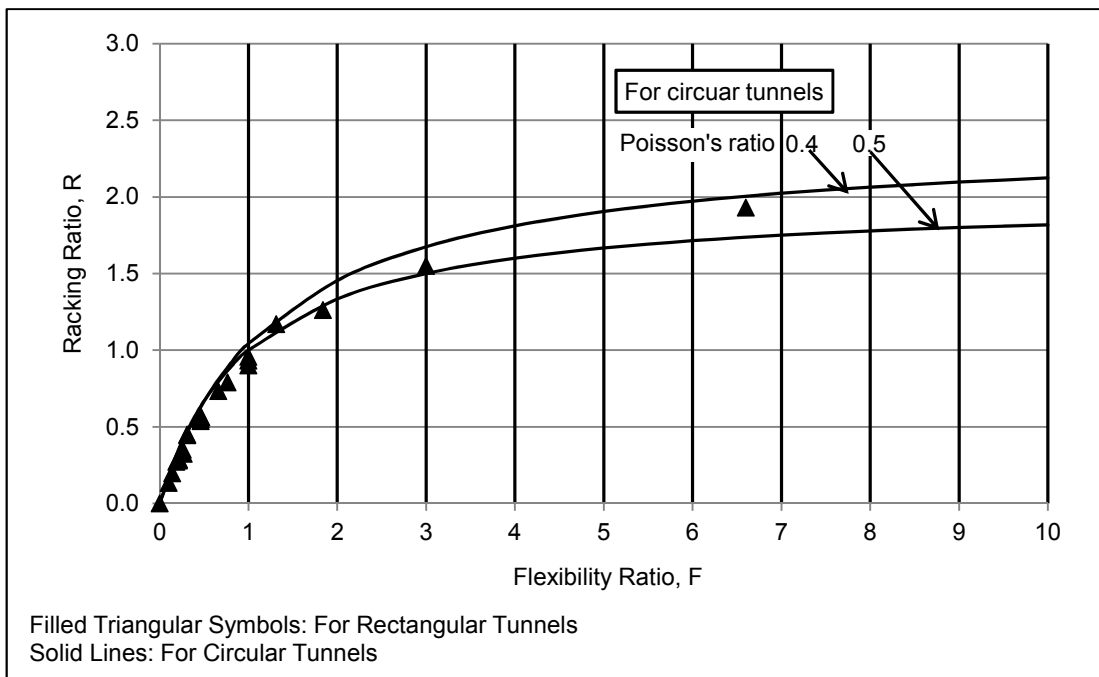
Figure 2.11. Variation of racking ratio with respect to flexibility ratio for circular and rectangular tunnels (Wang, 1993)

Wang (1993) proposed simplified frame analysis models for deep and shallow tunnels. The author mentioned that racking deformation of a deep tunnel is mainly caused due to shear force acting on the interface between upper slab and soil. Hence, a simplified frame with a pseudo-concentrated force (Figure 2.12a) was proposed for modeling the dynamic response of structure under racking deformation. For a shallow tunnel, shear force has relatively little effect on the racking deformations due to smaller overburden pressure. It was estimated that the racking deformations were caused by lateral pressures acting on the side walls. Thus, a triangular pressure distribution (Figure 2.12b) was suggested for the design of shallow rectangular underground structures against racking. Wang (1993) recommended the following design procedure for rectangular underground structures:

1) Determine the soil properties from field and laboratory tests.

2) Specify and assess the important parameters related to earthquake such as magnitude, maximum ground acceleration and site-specific design spectra

3) Perform static analysis for the preliminary assessment of underground structure.

4) Predict the free-field soil deformations (Δ_{ff}) at mid-depth of the structure by applying Newmark method or one dimensional ground response analysis. Newmark method is appropriate for the deeply tunnels embedded in homogeneous soil. For shallow tunnels buried in heterogeneous soil, one dimensional ground response analysis should be used.

5) Find the flexibility ratio using the Equation 2.35.

6) Determine the racking ratio, R from Figure 2.10 and Figure 2.11.

7) Compute the racking deformation (Δ_s) of underground structure by multiplying the free-field deformation by racking coefficient $\Delta_s = R\Delta_{ff.}$

8) Perform structural analysis by applying the racking displacement on simplified frame models shown in Figure 2.12 and obtain internal member forces.

9) Apply loading criteria given for maximum and operating design earthquake and make a design.

Main assumptions and limitations from the study of Wang (1993) can be summarized as follows:

- Equations for estimating the relative stiffness between the soil and underground structure are given for elastic structures with rigid connections.

- Thickness of the overburden soil changes between 4.5 and 7m. Finite element analyses were performed only for this range.

- Soil is homogeneous and the models have a rigid base.

- No-slip occurs on the soil-structure interface.

- Transmitting boundaries were used to reduce the boundary effects.
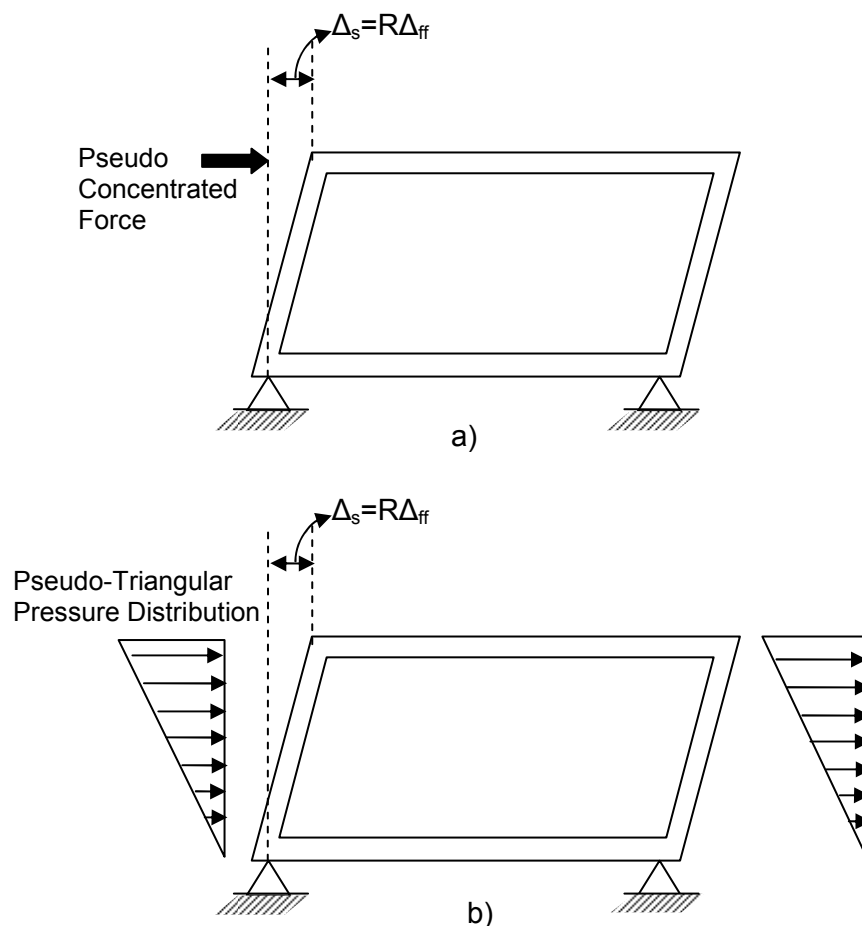
Figure 2.12. Simplified frame models for design of underground structures (After Wang, 1993) a) For deep tunnels b) For shallow tunnels

ii) Simplified procedure of Penzien (2000)

Penzien (2000) proposed a simplified approach for estimating the racking deformation of rectangular underground structures. In this methodology, it is assumed that the wavelength of the motion is larger than the height of the tunnel and inertia effects due to soil structure interaction are negligible. On this basis, racking deformation of rectangular underground structure was evaluated under constant shear stress and quasi-static conditions.

Figure 2.13 represents the deformation of a rectangular cavity under simple shear stress. In this figure, γ_{ff} is the free-field shear strain and γ_c is the cavity shear strain. When the shear stress, τ_{ff}, acting on the cavity is removed, γ_c can be found by using the Equation 2.37 and 2.38. Equation 2.38 is an approximate relation for estimating racking ratio which is originally developed for determining the racking ratio of circular cavity.

$$\gamma_c = \pm\beta\gamma_{ff} \tag{2.37}$$

where

$$\beta \doteq 4(1-\upsilon_s) \tag{2.38}$$

where υ_s is the Poisson's ratio of the soil.

Soil and lining stiffness coefficients, k_{so} and k_l, were defined to investigate the soil-structure interaction under free-field shear strain. Unit racking deflection of the soil surrounding cavity and the lining are indicated in Figure 2.14 and Figure 2.15 respectively. Lining stiffness, k_l, can be determined by performing frame analysis under simple shear loading (Penzien 2000).
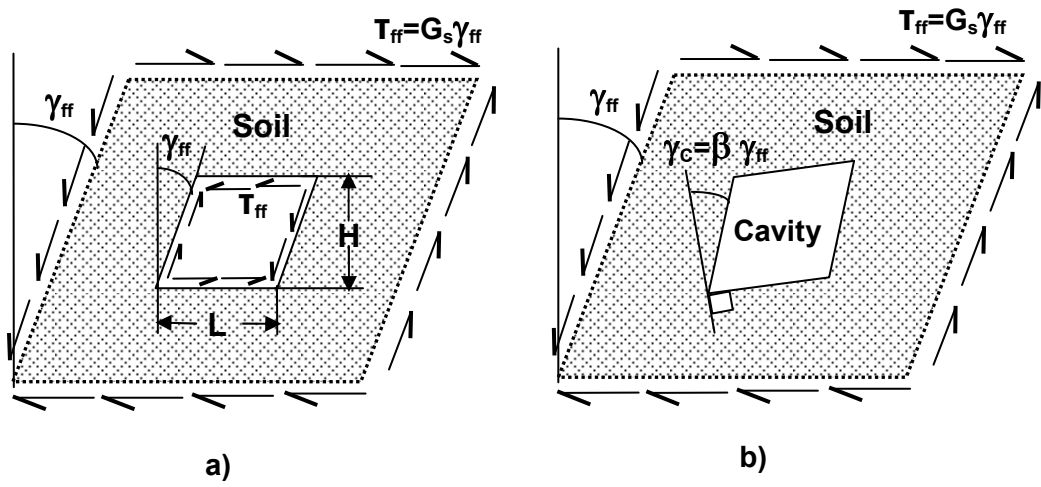
Figure 2.13. Deformation of rectangular cavity subjected to a uniform shear-strain environment (after Penzien 2000) a) with free-field shear stress distribution applied to cavity surface; b) with free-field shear stress distribution removed from cavity surface
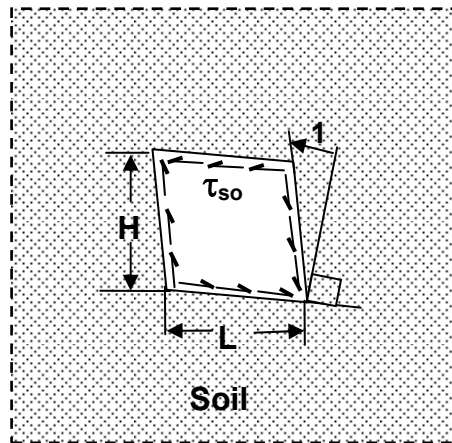
Figure 2.14. Stiffness coefficient $k_{so}=\tau_{so}$ for soil outside of cavity (After Penzien, 2000).
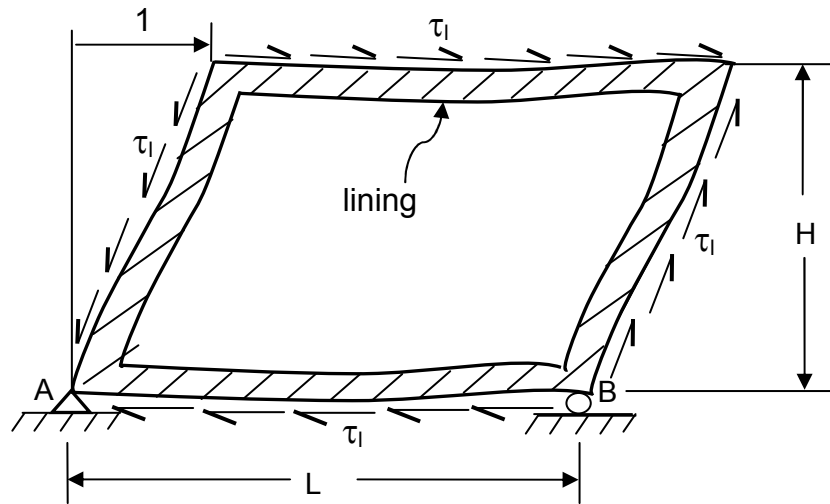
Figure 2.15. Stiffness coefficient $k_l \equiv \tau_l$ for rectangular lining (After Penzien 2000).

Soil stiffness coefficient k_{so}, can be calculated by using the following equation:

$$k_{so} = \frac{G_s}{(3 - 4\upsilon_s)H}$$

(2.39)

where, G_s is the shear modulus of the surrounding soil and the H is the height of the structure. A second soil coefficient acting on the outside of the soil is defined as:

$$k_{si} = \frac{G_s}{H}$$

(2.40)

Using the derived soil and lining coefficients, Penzien (2000) obtained the following relationship for estimating racking ratio:

$$R = \frac{4(1 - \upsilon_s)}{1 + \alpha_s}$$

(2.41)

where

$$\alpha_s = (3 - 4\upsilon_s) \frac{k_l}{k_{si}} \tag{2.42}$$

Penzien (2000) presented the variation of racking ratio with respect to stiffness ratio for different values of Poisson' ratio υ_s, 0.4 and 0.5 (Figure 2.16). It was observed that Penzien's (2000) approach give closer results to the dynamic finite element solutions (filled triangular symbols in Figure 2.16) of Wang (1993). Based on the comparison given in Figure 2.16, Penzien (2000) mentioned that inertia of the structure may be negligible when assessing the racking deformation of rectangular underground structures. Besides, the author pointed out that "the normal stresses produced on lining surface during its interaction with the soil have a secondary effect on racking of the lining".
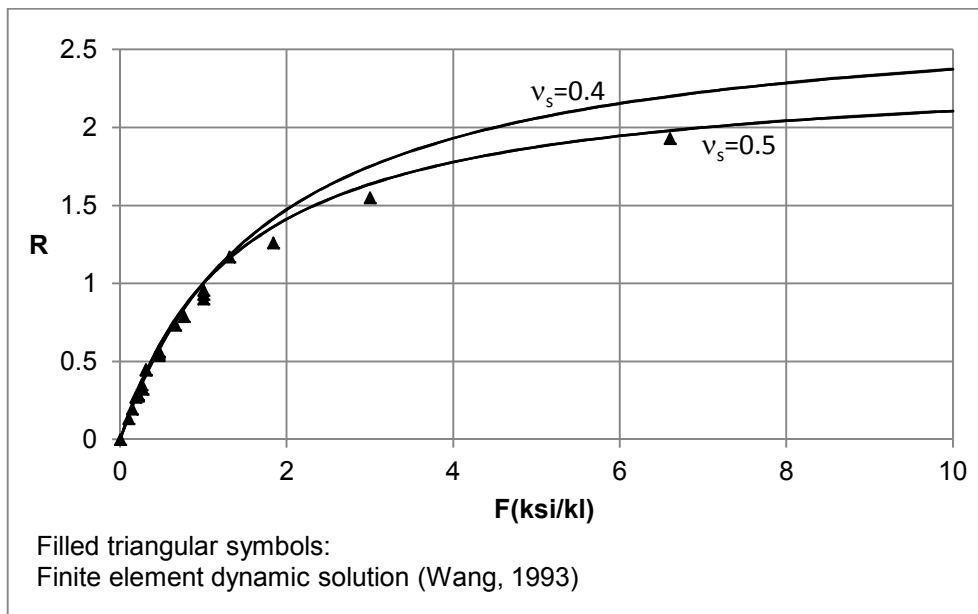
Figure 2.16. Racking ratio R versus stifness ratio k_{si}/k_l for discrete values of Poisson's ratio υ_s (After Penzien, 2000)

iii) Simplified procedure of Huo et al. (2006)

Huo et al. (2006) proposed a closed-form solution depending on the relative stiffness and on geometry of underground structure. Differently from the studies of Wang (1993) and Penzien (2000), Huo et al. (2006) considered the lateral stresses acting on the sidewalls. A uniform shear stress distribution and a linear normal stress distribution were estimated for the simplified solution. Shear and normal stress distributions and the structure deformations are illustrated in Figure 2.17. Assumptions and limitations of the solution are given as follows:

1) Deeply buried rectangular underground structure in homogeneous and isotropic soil
2) Plain strain conditions are valid.
3) Soil and the structure remain in elastic range under seismic loading.
4) Only bending deformations in structural frame members are taken into account.

Huo et al. 2006 provided the following methodology for design of underground structures:

1) Internal dimensions of the opening, a and b, are specified for the condition a>b.
2) Shape ratio, λ (λ=a/b), is determined with the mathematical parameter k. For a square underground structure λ=a/b=1, k is 0.25.
3) Stiffness ratio, Ω, is computed by using the following equation

$$\Omega = \frac{E_{str}I_{str}}{G_s b^3} \tag{2.43}$$

where,

E_{str} = Elastic modulus of the underground structure
I_{str} = Moment of inertia of the underground structure
G_s = Shear modulus of the soil

(a) Loading   (b) Deformations
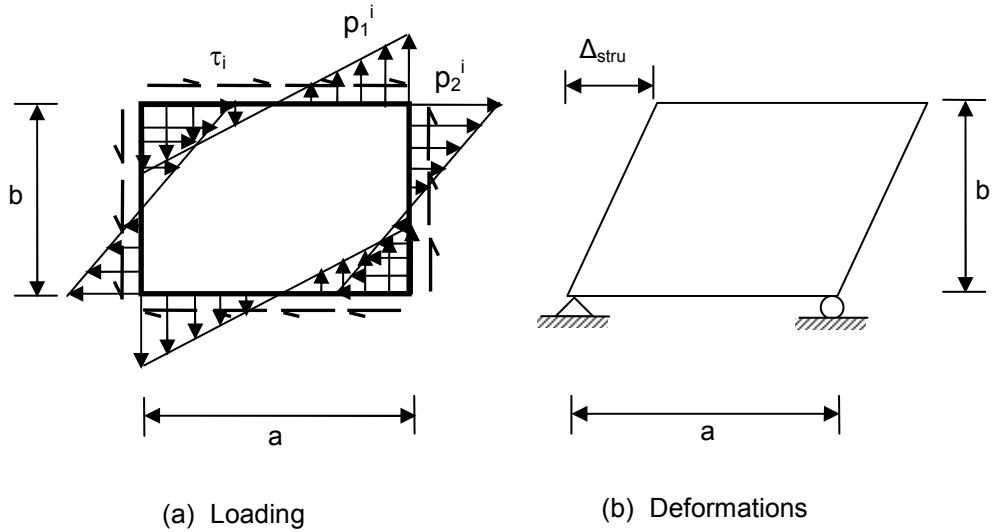
Figure 2.17. Structure loading and deformations (After, Huo et al., 2006)

4) For a simple structure, deformation of the structure due to shear stress (Δ_{τ^i}) and deformation of the structure due to a linear normal stress distribution ($\Delta_{p_2^{\,i}}$) can be obtained by Equation 2.44 and Equation 2.45. Otherwise, structure analysis is used.

$$\Delta_{\tau^i} = \frac{1}{24}\lambda b^4 \frac{\dfrac{2}{(EI)_c}\left[\dfrac{\lambda}{(EI)_s} + \dfrac{1}{(EI)_W}\right] + \dfrac{\lambda}{2(EI)_s}\left[\dfrac{3\lambda}{2(EI)_s} + \dfrac{2}{(EI)_W}\right]}{\dfrac{2}{(EI)_c} + \dfrac{1}{(EI)_W} + \dfrac{3\lambda}{(EI)_s}} \qquad (2.44)$$

$$\Delta_{p_2^{\,i}} = \frac{1}{4} b^4 \frac{\dfrac{2}{45(EI)_c}\left[\dfrac{\lambda}{(EI)_s} + \dfrac{1}{(EI)_W}\right] + \dfrac{\lambda}{480(EI)_s}\left[\dfrac{7\lambda}{2(EI)_s} + \dfrac{5}{(EI)_W}\right]}{\dfrac{1}{3(EI)_c} + \dfrac{1}{6(EI)_W} + \dfrac{\lambda}{2(EI)_s}} \qquad (2.45)$$

38

For a rectangular underground structure having slabs and walls with equal stiffness, and no central column,

$$\Delta_{\tau^i} = \frac{(1+\lambda)}{24 E_s I_s} \lambda b^4 \tag{2.46}$$

$$\Delta_{p_2^i} = \frac{(1+\lambda)}{60 E_s I_s} b^4 \tag{2.47}$$

where,

$(EI)_c$=Bending rigidity of central columns.

$(EI)_s$=Bending rigidity of the upper and lower slabs.

$(EI)_W$=Bending rigidity of the side walls.

5) Parameters M,N and L are determined from the charts given in Figure 2.18 & Figure 2.19.

6) Racking deformation of the rectangular underground structure is found by using Equation 2.48.

$$\frac{\Delta_{str}}{\Delta_{ff}} = \frac{G\Delta_{str}}{\tau_{ff} b} = (1 - \upsilon_s^2) \left[N \Delta_{p_2^i} + (M \Delta_{p_2^i} + \Delta_{\tau^i}) L \right] \frac{G}{b} \tag{2.48}$$

Analytical solution was verified with the numerical analyses and compared with the studies of Wang (1993) and Penzien (2000). For flexibility ratios larger than 2, the analytical solution gives larger deformations with respect to Wang (1993) and Penzien (2000) approaches. The difference may be due to following reasons (Huo et al., 2006):

-Wang (1993) used beam elements in finite element models. These elements with rigid connections which can limit the deformations of the ground. Solutions of Wang (1993) did not taken into consideration the inertia effects. These effects are not considered in a pseudo-static approach.

- A rectangular opening is assumed as a circular opening in Penzien's (2000) solution.
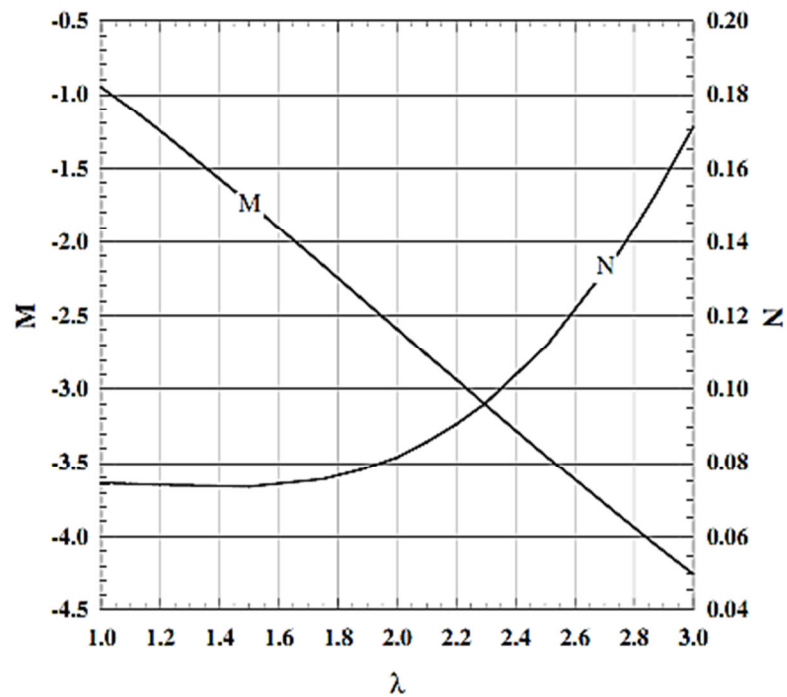
Figure 2.18. Parameter M and N values (After, Huo et al., 2006)
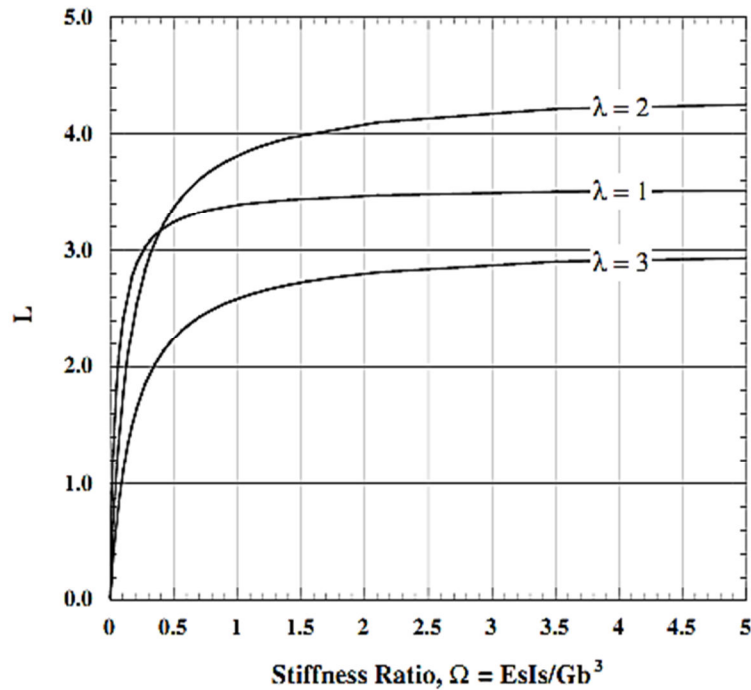
Figure 2.19. Parameter L values (After, Huo et al., 2006)

2.2.2.4 Dynamic pressures acting on underground structures

There is not generally accepted procedure for estimating the dynamic earth pressures acting on underground structures subjected to ground motions. Mononobe-Okabe (1929) approach is widely preferred by engineers to determine the dynamic soil pressures. This approach was specifically given for the seismic analysis of retaining walls. It assumes that there is a definite active wedge failure surface behind the wall. However, an underground structure moves with the surrounding ground, accordingly no wedge occurs during seismic motion. Thus, assumptions and simplifications of Mononobe-Okabe method results in illogical findings for design of underground structures (Hashash et al., 2001).

2.2.2.5 Numerical analyses for design of underground structures

Numerical analyses methods have some advantages compared to other approaches for evaluating the dynamic response of underground structures. Complicated geometries and ground conditions can be modeled during the analyses. Soil-structure interaction effect is well represented and the nonlinear behavior of the soil can be taken into consideration in this approach. The main disadvantage of this method is the complex and time consuming analyses. Several studies have investigated the dynamic stability of underground structures by using numerical methods. Mostly, finite element and finite difference methods have been applied in these studies by using computer software programs, such as FLUSH, ABAQUS and FLAC.

Matsuda and Tanaka (1996) investigated the damage of Kamisawa station collapsed during the 1995 Hyogoken-Nambu earthquake. The authors applied two-dimensional finite element analyses in order to evaluate the seismic stability of the underground structure. Analyses results showed that the wall deformation of the underground structure coincided with the deformation of surrounding soil (Figure 2.20). Besides, it was concluded that the main cause of the damage is the larger shear stress at intermediate columns. The authors suggested conducting three-dimensional seismic response analysis to obtain more representative results.

Gomez Masso and Attala (1984) conducted numerical analyses for several simplified tunnel models. It was pointed out that the simplified methods lead to conservative results. Sweet (1997) performed linear and non-linear analyses in order to evaluate the dynamic response of Los-Angeles Metro System. Results showed that racking displacements obtained from non-linear analyses are larger than that of linear analyses (Hashash et al., 2001). Navarro (1992) conducted numerical analyses by using the finite element program FLUSH. The pressure distributions obtained in the study did not represent the thrust predictions of Mononobe-Okabe. Furthermore, it was mentioned that the dhear stresses obtained from vertically propagating shear wave were much higher than those due to Rayleigh and P-waves.
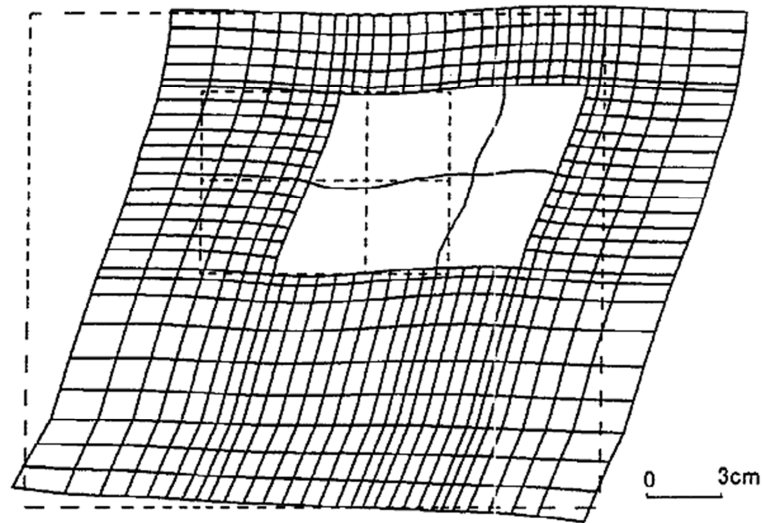
Figure 2.20. Deformation scheme of obtained from the numerical analyses (Matsuda and Tanaka, 1996)

Park et al. (2006) evaluated the dynamic response of a tunnel in Bangkok MRT subway. FLAC^{2D} finite difference software package program was used to perfrom numeric analyses. Moments and thrusts calculated from the Wang (1993) and Bobet (2003) were slightly higher than the numerical findings. Results obtained from Penzien's (2000) solution were underestimated. Bagherzadeh and Ferdowsi (2009) modeled the Esfahan metro tunnels subjected to earthquake loading by using finite difference numerical approach. Findings of dynamic analyses were compared with the findings of analytical solutions proposed by Wang (1993) and Penzien (2000). Calculated moments by numerical analyses were in close agreement with the moments obtained from Wang (1993) and Penzien (2000) analytical approaches. It was emphasized that Penzien's (2000) solution underestimates the axial forces.

Huo et al. (2005) carried out finite element analyses to evaluate the dynamic behavior of underground structures by considering the soil-structure interaction. For this purpose, the authors investigated dynamic response of Daikai subway station failed due to Hyogoken-Nambu earthquake. Numerical model was prepared and

analyzed by the finite element tool ABAQUS. The results from the dynamic analyses were quite interesting. Following conclusions were derived based on these results:

1) Transferring a free-field deformation to the structure depends on the relative stiffness and the interface friction between structure and ground.

2) Freestanding columns of buried structures are very vulnerable to small deformations like aboveground structures.

3) If the structure is more rigid than the ground, it prevents the movement of the surrounding soil during the dynamic excitation. Thus, surrounding soil deform less than free field and accordingly shear modulus exhibits little degredation.

4) If the friction between the underground structure and surrounding soil is large, shear stress will increase and shear modulus degradation will reduce. If there is no friction shear stress, shear stress will be zero, thus, high normal stresses will occur at the interface.

2.3 Physical modeling of underground structures

2.3.1 Shaking table tests (1-g physical modeling)

Shaking table test modeling (1-g Physical modeling) systems has been used by many researches to evaluate the dynamic responses of geotechnical structures. The system has three main parts, namely the shaker (generates dynamic motion), shaking table and container. Harmonic or real earthquake motions can be applied by different type of shakers such as electrical or hydraulic actuators. Shaking table is the platform that transmits the dynamic motion to the container. Laminar box is an ideal flexible container to be used in shaking table and centrifuge tests. It consists of several horizontal layers that can move easily with the movement of soil inside. Shapes of the most common used laminar boxes are either circular or rectangular. Choice of shape of the laminar box is mostly related with the geotechnical structure

to be analyzed. For pile foundation analyses a circular box may be better, but for underground structure analyses, a rectangular one is more suitable to represent the plain strain conditions.

Large shaking table test is more appropriate for the analyses of the geotechnical structures subjected to seismic waves. However, design and fabrication of a large shake table is difficult due to economic reasons. 1-g shaking table tests on reduced scale models cannot model the stress-strain behavior due to the low stress field in soil container. Thus, these tests are mostly used for clarifying the complex behavior of geotechnical structures subjected to seismic motions. Few researchers performed 1-g shaking table tests for evaluating the load transfer mechanisms, failure types and effect of different parameters.

There are several factors affecting the performance of the laminar box. Prasad et al. (2004) investigated the efficiency of the laminar box used in 1-g shaking table tests. Authors explained the design and calibration of a rectangular shaped laminar box. Calibration of the laminar box was made by considering the following factors:

-Influence of inertia of the laminar box
-Influence of bearing friction
-Influence of stiffness of the membrane
-Influence of boundaries or sidewalls of the laminar box

Che and Iwatate (2002) studied the seismic response and damage characteristics of Daikai Station which collapsed in the 1995 Hyokogen-Nanbu earthquake. Shaking table tests and numerical analyses were performed to evaluate the dynamic lateral earth pressures and bending strains exerted on the underground structure. A laminar box with a height of 100cm and a width of 120cm was developed for the 1-g shaking table tests. The model ground was formed of two sand layers as indicated in Figure 2.21. A 1/30 scaled box type structure made of polyvinyl chloride resin was used to model the Daikai Station. Results and conclusions obtained from the study can be summarized as follows:

-Lateral earth pressures due to vertical motions can be ignored.

-Rocking motions were observed during horizontal motion.

-Bending strain in the center columns was almost five times larger than the strains in the sidewalls.

-Connection type had a significant effect on bending strains. Flexible joint reduced the strains about 1/5 of that for fixed type joint.

Nishiyama et al. (2000) conducted 1-g shaking table tests using two and three span rectangular models to evaluate the dynamic behavior of cut and cover tunnels. To satisfy the similitude requirements a silicon ground model was used in the tests. Model ground and the layout of the transducers are indicated in Figure 2.22.

Nishiyama et al. (2000) mainly focused on the friction between underground structure and the ground. No-slip condition was met by the adhesive strength of silicon ground. For full-slip condition, teflon sheets were installed on the exterior surface of rectangular box model. Findings of the study can be given as follows:
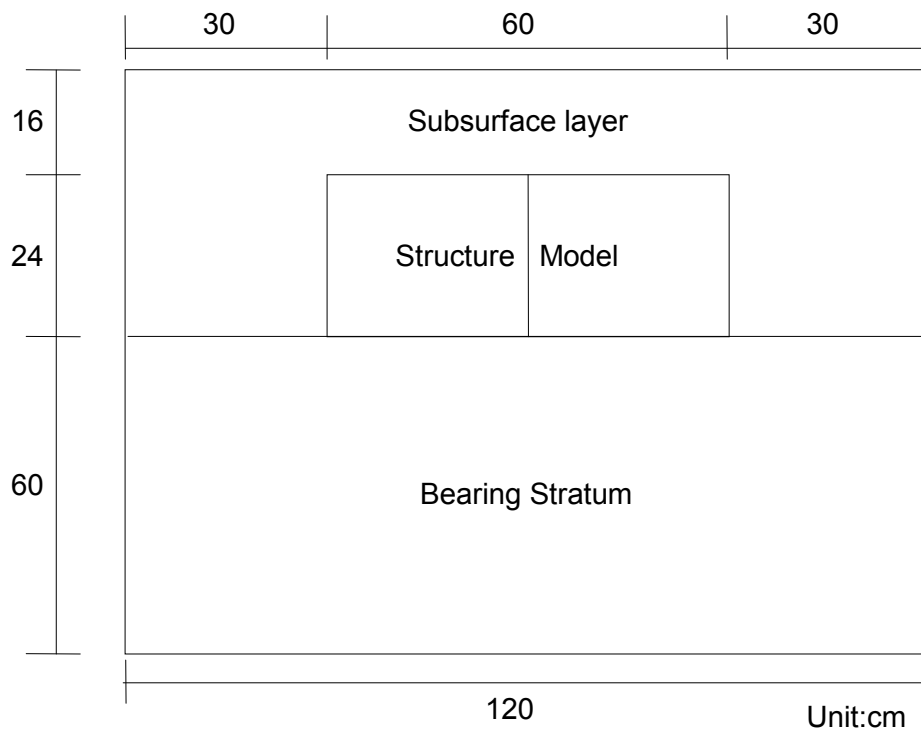
Figure 2.21. General view of model ground and subway model (Che and Iwatate, 2002)
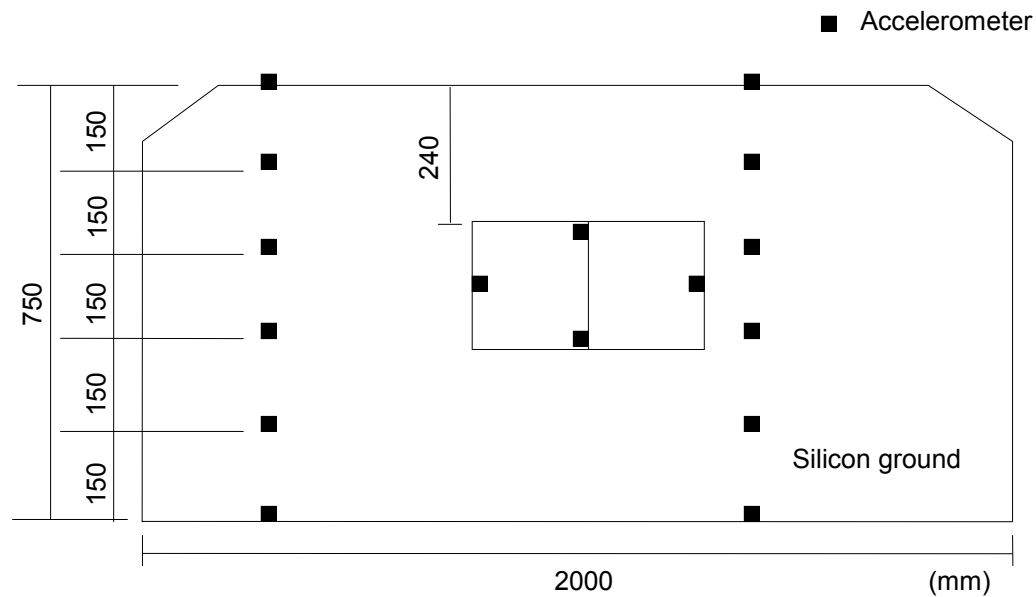
Figure 2.22. Layout of the instrumentation (Nishiyama et al., 2000)

-Shear stresses at the ceiling and normal pressures acting on the sidewalls decrease with decreasing friction between the underground structure and the ground.

- Separation and slipping effect is small when the tunnel is more flexible with respect to the ground. Similarly, separation and slipping effect is not so big for stiffer tunnels.

In a later research, Che et al. (2006) performed 1-g shaking table tests and numerical analyses for evaluating the dynamic response of buried long span corrugated steel culverts. Two elliptical shaped models in 1/16 scale were used in the shaking table tests,. The models had dimensions of 457mm (short radius) x 650mm (long radius) x 800mm (width) and 2mm thickness. Ground was constructed from dry fine sand and models were made of vinyl chloride resin. 1-g shaking table tests were conducted under random vibrations recorded during the Hyogoken-nanbu earthquake and harmonic motions. Several transducers were used to measure accelerations, strains and dynamic soil pressures. Instrumentation details are given in Figure 2.23. At the end of the study, following results were presented by Che et al. (2006):

47

-Large bending strains occurred at the corrugated culvert due to dynamic soil pressures. However, maximum bending strain did not reach the allowable strain of the corrugated culvert. Since the normal strain of the culvert was too small, it could be ignored.

-Absolute maximum dynamic soil pressure values measured under Hyokogen-nanbu earthquake motion were nearly identical to the values obtained from static analyses of soil.

-Bending strains and dynamic pressures did not cause structural failure under Hyogoken-nanbu earthquake motion.
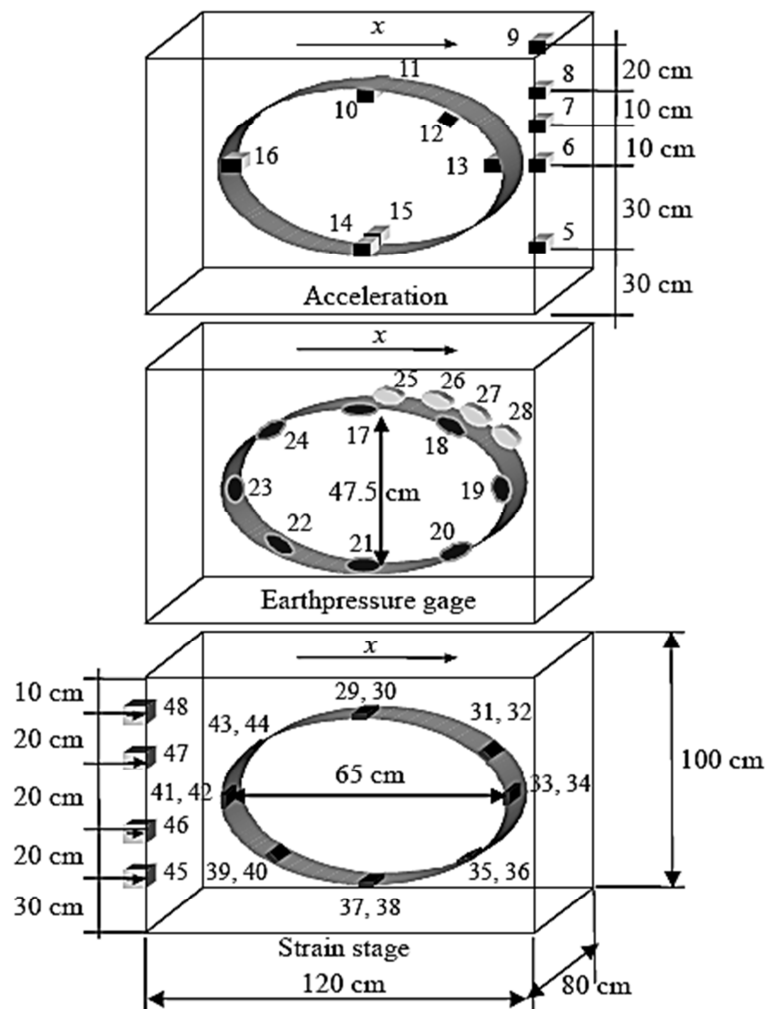
Figure 2.23. Layout of the transducers (Che et al., 2006)

Matsui et al. (2004) investigated the seismic performance of two-span rectangular underground reinforced concrete (RC) structures. For this purpose, the authors conducted large shaking table test and verified the results with numerical analysis. Aim of the study was to develop a nonlinear finite element model for assessing the dynamic response of underground RC structures. The FEM model considered the effects of nonlinear behavior of RC model and dynamic soil structure interaction.

Two-span underground RC structure model was built and fixed to the bottom of shake table (Figure 2.24). The ground was constructed by dry sand with a relative density of approximately 87%. Pressures, displacements and accelerations were measured during the shaking table tests. Figure 2.25 indicates the lateral dynamic soil pressures and sidewall curvature measurements at a certain time of the shaking. Dynamic soil pressures caused compressive forces along the sidewall and accordingly center of the wall tended to deform inward. Due to this deformation, bending cracks occurred at the top and bottom of outer surface and uniform horizontal cracks were observed on the inner surface of the sidewall as indicated in Figure 2.26. Besides, measurements showed that the underground structure conformed to ground deformations.
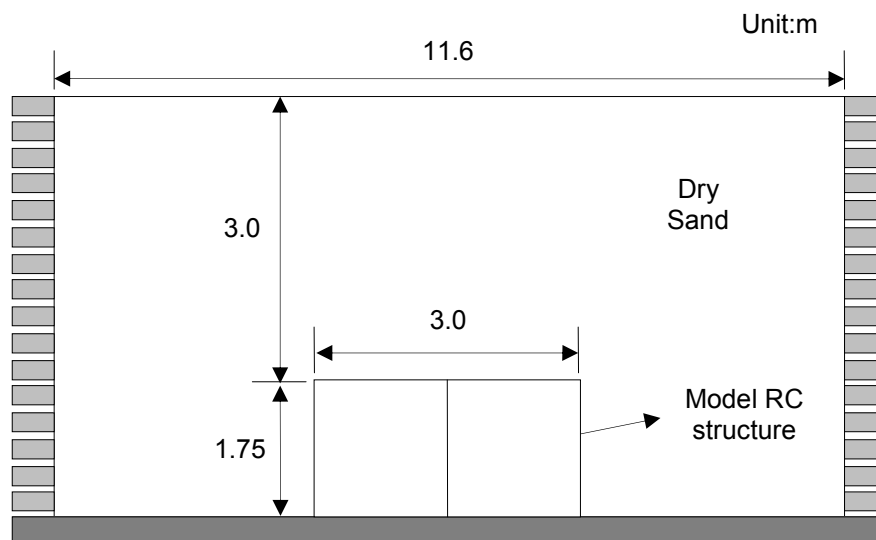
Figure 2.24. Shaking table test model (Matsui et al., 2004)
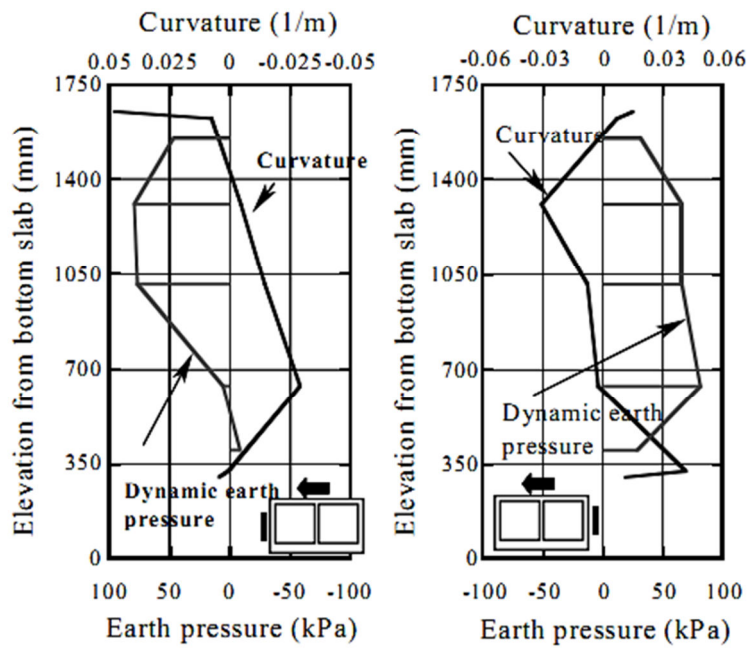
Figure 2.25. Lateral dynamic pressures along the sidewall and curvature of sidewalls (Matsui et al., 2004)
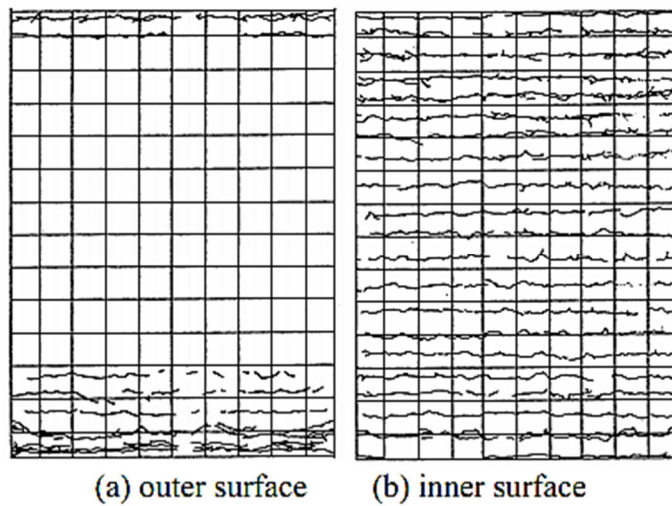
Figure 2.26. Cracks observed at sidewalls of the two-span RC culvert (Matsui et al., 2004)

Crosariol (2010) studied the dynamic response of rigid underground structures buried in soft clay. For this purpose the author performed shaking table tests and explored the effects of dynamic soil-structure interaction. A 1/10-scale model was developed to represent San Francisco Bay Area Rapid Transit subway located in United States. Crosariol (2010) derived scaling relationships for satisfying the similitude rule. Based on the geometric similarity, the author defined a scale factor, N, and provided the scaling relations as given in Table 2.2.

Table 2.2. Scale factors used for the shaking table test model
(After Crosariol, 2010)

Variable	Scale factor	For N=10
Soil density	1	1
Force	N^3	1000
Stiffness	N^2	100
Modulus	N	10
Acceleration	1	1
Shear wave velocity	$N^{1/2}$	3.16
Soil damping	1	1
Poisson's ratio	1	1
Time	$N^{1/2}$	3.16
Frequency	$N^{-1/2}$	0.316
Length	N	10
Stress	N	10
Strain	1	1
Flexural rigidity	N^5	100000
Dimensionless Quantities	1	1

In order to obtain a representative clay model of San Francisco Young Bay Mud, a mixture of soil was prepared by using kaolinite, bentonite. Prepared mix was filled into a ring type box conforming to ground deformations under simple shear. Shaking table tests were performed by using 1979 Imperial Valley, 1992 Landers and 1999 Chi-Chi input motions. Remarks of the study can be summarized as follows:

i) The author pointed out that further study was required to understand the effect of deformation mode on the dynamic response of underground structures.

ii) Structure deformations are small compared to corresponding free-field deformations due to dynamic soil-structure interaction.

iii) Racking deformations are highly dependent on the input accelerations and racking deformation increases linearly with increase of accelerations.

2.3.2 Centrifuge Tests

Full-scale tests may be the best type of physical modeling technique to investigate the dynamic response of geotechnical structures. Actual field conditions can be well represented. However, those tests are costly and require a great deal of effort and time to prepare the prototype model. Besides, it is not possible to carry out an extensive research by employing full-scale tests in order to observe the effects of different parameters. Hence, the centrifuge test has become an alternative technique for the study of dynamic behavior of geotechnical structures. The primary principle of the centrifuge test is to simulate the in-situ stresses by generating a high acceleration field. The model is mounted at the end of a rigid arm and rotated with a centrifugal acceleration of Ng. Thus, in-situ stresses are obtained and prototype dimensions are scaled down by a factor of N.

Buckingham (1914) pi theorem stated that if a problem contains n variables involving m fundamental dimensions, then a set of n-m dimensionless groups can be developed by the original variables. The physical problem can be expressed as by the following equation:

$$f(X_1, X_2, \ldots, X_n) = 0 \qquad (2.49)$$

where $X_1, X_2, \ldots, X_n$ are the physical variables. There are a total of n-m dimensionless products:

$$g(\pi_1, \pi_2, \ldots, \pi_n) = 0 \qquad\qquad (2.50)$$

Based on this theorem, a dynamic problem in geotechnical engineering can be defined by:

$$f(\sigma, L, \rho, g, t, u) = 0 \qquad\qquad (2.51)$$

where,

σ = stress

L=length

ρ=density

g=gravitational acceleration

t=time

u=displacement

Dimensionless pi (π) groups for this physical problem are given as follows:

$$\pi_1 = \frac{\sigma^*}{\rho^* g^* L^*} = 1 \qquad\qquad (2.52)$$

$$\pi_2 = \frac{u^*}{g^* t^*} = 1 \qquad\qquad (2.53)$$

$$\pi_3 = \frac{u^*}{L^*} = 1 \qquad\qquad (2.54)$$

where, the asterisk (*) sign on a physical variable shows the ratio of the quantity in the model to the quantity in the prototype. (e.g. $L^*=L_{model}/L_{prototype}$). Kutter (1995) stated that the main objective of the centrifuge test is to obtain the same stiffness and strain in reduced scale model and in full-scale prototype. Furthermore, the author emphasized that the density of material should not be scaled in order to obtain identical soil mechanical properties. In other words, the density of soil in the model should be same as the density in the prototype. Based on these identifications, scale factors derived from the following assumptions:

$$\sigma^* = 1 \qquad\qquad\qquad (2.55)$$

$$\rho^* = 1 \qquad\qquad\qquad (2.56)$$

$$L^* = \frac{1}{N} \qquad\qquad\qquad (2.57)$$

Common scaling factors for centrifuge modeling are presented in Table 2.3.

Table 2.3. Scaling Factors for Centrifuge Modeling

Parameters		Model	Prototype	Scaling Factor
Length	L^*	1	N	1/N
Area	A^*	1	N^2	$1/N^2$
Volume	V^*	1	N^3	$1/N^3$
Mass	M^*	1	N^3	$1/N^3$
Force	F^*	1	N^2	$1/N^2$
Energy	E^*	1	N^3	$1/N^3$
Stress	σ^*	1	1	1
Strain	ε^*	1	1	1
Soil density	ρ^*	1	1	1
Acceleration	a^*	N	1	N
Time (dynamic)	t_{dyn}^*	1	N	1/N
Time (diffusion)	t_{dif}^*	1	N^2	$1/N^2$
Velocity	v^*	1	1	1
Frequency	f^*	N	1	N

There are several effects that must be taken into account in the centrifuge modeling (Taylor, 1995). The effects can be summarized as follows:

1) Scaling rules derived for centrifuge modeling are based on the equality of the stresses between model and prototype. Vertical stresses in the model (σ_{vm}) and prototype (σ_{vp}) are given by:

$$\sigma_{vm} = \rho N g h_m \qquad (2.58)$$

$$\sigma_{vp} = \rho g h_p \qquad (2.59)$$

where, ρ is the mass density, h_m and h_p are the heights of model and prototype, respectively. If $\sigma_{vm} = \sigma_{vp}$, then $h_p = N h_m$. Linear dimension factor between prototype and model is N. When a centrifuge rotates with an acceleration of Ng, acceleration varies through the model due to radius change. Nonlinear variation of stress in the model can be depicted as in Figure 2.27.
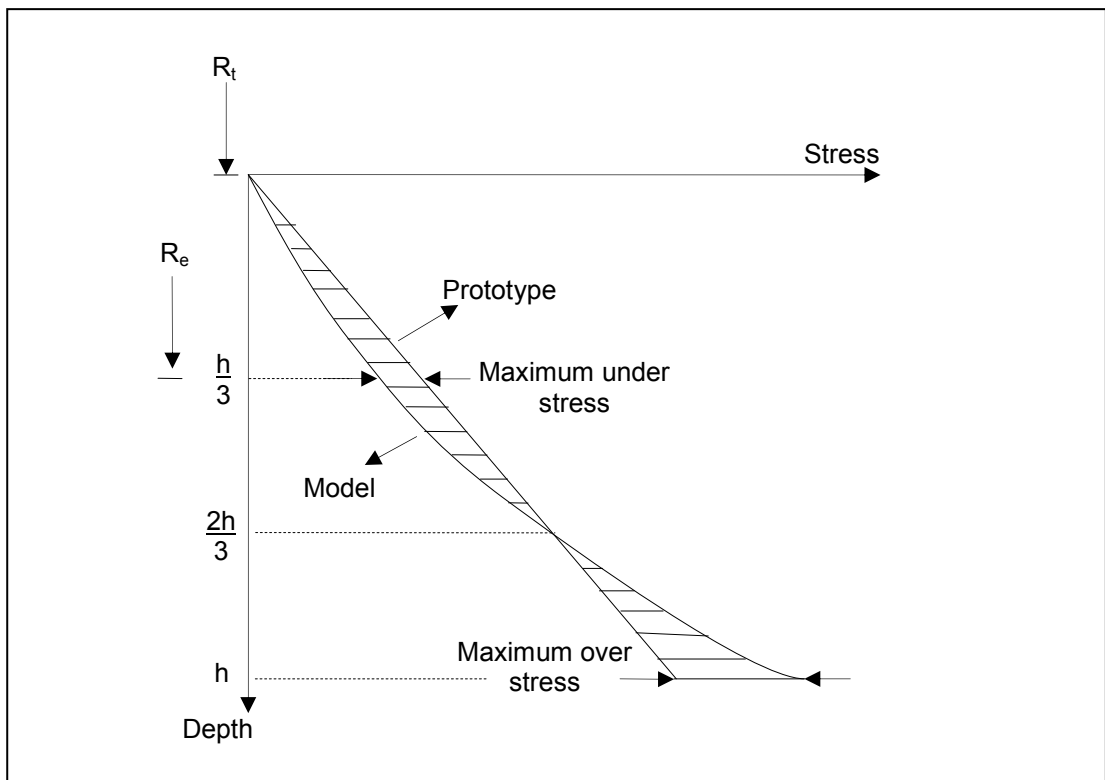
Figure 2.27. Vertical stress distribution in a centrifuge model and its corresponding prototype (Taylor, 1995)

Centrifugal acceleration Ng can be expressed as follows:

$$Ng = \omega^2 R_e \tag{2.60}$$

where, R_e is the effective centrifuge radius and ω is the natural circular frequency. If R_t is the centrifuge radius measured from rotation axis to the top of the model, vertical stress at depth z can be calculated by:

$$\sigma_{vm} = \int_0^z \rho\omega^2 (R_t + z)\, dz = \rho\omega^2 z(R_t + \frac{z}{2}) \tag{2.61}$$

Substituting Equation 2.60 into Equation 2.58 gives:

$$\sigma_{vm} = \rho Ngh_m = \rho\omega^2 R_e h_m \tag{2.62}$$

Considering that the vertical stress in centrifuge model and prototype is equal to each other at a depth of $z=h_i$, using Equation 2.60, 2.61 and 2.62 following relationship between R_e and R_t can be obtained as:

$$R_e = R_t + 0.5h_i \tag{2.63}$$

In order to minimize the overall error in vertical stress distribution, ratio of maximum under stress to prototype stress (r_u) at a depth of $0.5h_i$ is equalized with the ratio of maximum over stress to prototype stress (r_o) at the base of the model (h_m). Following equations are obtained from equalization of the ratios r_o and r_u :

$$h_i = \frac{2}{3} h_m \tag{2.64}$$

Maximum error is given by;

$$r_u = r_o = \frac{h_m}{6R_e} \tag{2.65}$$

Centrifuge effective radius becomes:

$$R_e = R_t + \frac{h_m}{3} \qquad\qquad (2.66)$$

Taylor (1995) mentioned that the maximum error in the vertical stress remains below 3% when R_e is at least five times larger than h_m

2) Dimensions of the prototype are reduced by a scale factor of N when preparing the model for centrifuge test. Applying this rule for soil particle size is not logical for some conditions. For example, if fine sand in prototype is scaled by a factor of 100, a clay material must be used to satisfy the scaling rules. This is not reasonable since the stress-strain characteristics of clay and sand are quite different from each other. In most cases, particle size effect is neglected and same soil in prototype is used in the centrifuge model to capture the soil composition and stress-strain behavior. This assumption may be valid when the soil is homogeneous, continuum and fine grained. For coarse-grained soils scaling depends on the relative size between the particles and the model. Fugslang and Ovesen (1988) observed that there is no scale effect when the model dimensions are at least 30 times the average grain size. Iglesia et al. (2011) stated that logical results can be obtained without scaling the particle size provided that the ratio of model size to average grain size is larger than 20.

3) In the centrifuge model, time scale factor for the consolidation and seepage is $1:N^2$. In the dynamic problems time scale factor for the duration of the earthquake motion is 1:N. As understood, there is a conflict in time factors for the dynamic problems including seepage. Dynamic test on saturated cohesionless soils is a good example for that conflict. In these tests, excess pore pressure dissipation occurs during the seismic motion. To overcome the time scale problem, the modelers usually use a fluid N times more viscous than water while having same density. Taylor (1995) emphasized that modelers should avoid affecting the mechanical properties of soil by changing the fluid. Wilson (1988) investigated the damping effect of a more viscous fluid on the results. The author found that damping of the soil increases with the increasing viscosity of fluid.

4) Model containers used in centrifuge tests should satisfy the following design criteria:

-The sidewalls of the container should be flexible and conform to soil deflection modes during shaking so that the reflection of P-waves from the end walls is minimized. For this purpose, a laminar box or an equivalent shear box can be used as a model container in the centrifuge tests.

-Friction between the soil and wall should be high enough to resist the complementary shear stresses occurred due to dynamic motion. Rough sheets or friction rods are usually used to sustain the complementary shear stresses.

-Side walls of the container should be frictionless to prevent the development of shear stress at the contact surface. Thus, soil can move easily during the seismic motion.

-The vertical settlement of the soil at the boundaries should be the same to avoid initial stresses at the end walls.

5) Selection of appropriate scale factor for centrifuge model tests depends on several factors such as the model size, container size, stress levels and centrifuge capacity. Considering that the instrumentation is quite difficult in small models, model size should be maximized by choosing the scale factor as small as possible.

6) In centrifuge test, the direction of the inertial acceleration change along the width of the model container. The maximum error occurs at the boundaries of the container. Thus, it is better to study and focus in the central region of the centrifuge model box.

Since 1980s, centrifuge modeling has been widely used in geotechnical earthquake researches. However, there were only limited geotechnical centrifuge studies regarding the dynamic behavior of underground structures. Ha et al. (2010) investigated the earthquake faulting effects on buried pipelines by performing centrifuge tests. Results were compared with a case history of pipe failure during Izmit (1999) earthquake in Turkey. The authors proposed that it was better to design pipe route almost perpendicular to the fault trace to be on the safe side.

Furthermore, ASCE (1984) methodology for estimating the maximum lateral force at the soil-pipe interface was validated by centrifuge test results.

Ling et al. (2003) studied the seismic response of large diameter pipe in liquefiable ground. Centrifuge model tests were conducted under 30g gravitational field. Nevada sand was prepared as model ground with a relative density of 38%. Pipe model and the instrumentation are presented in Figure 2.28.
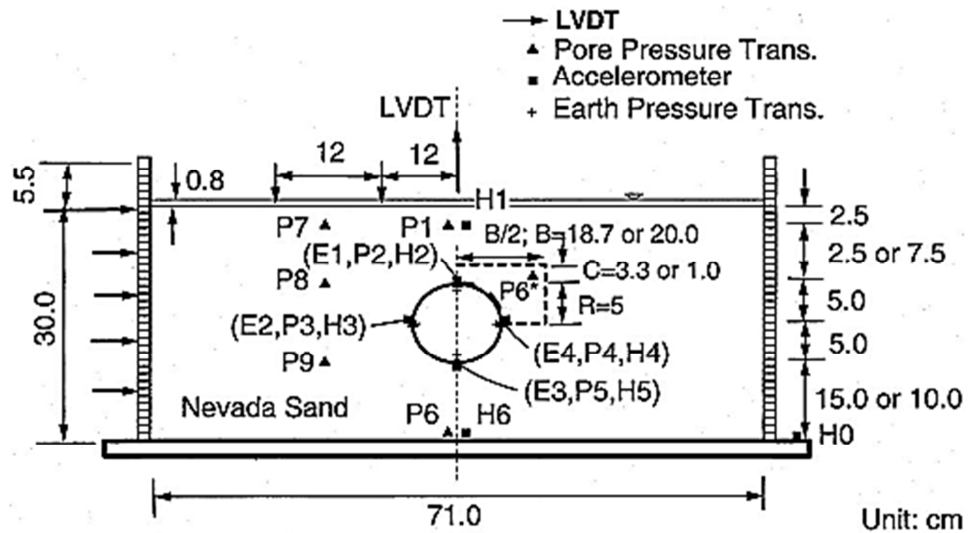
Figure 2.28. Pipe model and layout of the transducers in centrifuge model test
(Ling et al., 2003)

Ling et al. (2003) proposed a simplified procedure to evaluate the seismic performance of a large-diameter pipe against liquefaction and developed a mitigation method for flotation. The design is based on the limit equilibrium approach. Burial depth of the pipe was determined by assuming that soil has no shear strength during liquefaction. A soil prism including overburden soil and pipe weight was considered (Figure 2.29). This prism was reinforced by adding gravels with geogrid. Thus, added forces improve stability of pipe by increasing the resisting forces against buoyancy force. Besides, it was observed that the lateral earth

59

pressure reached maximum value during liquefaction and then reduced with dissipation of excess pore pressure.

O'Rourke et al. (2003) focused on the response of buried pipelines subjected to permanent ground deformation. For this purpose, centrifuges tests were performed on a model pipeline and confirmed with finite element analyses. A split box consisting of two halves was used to simulate the peak ground deformation. Model pipeline and surrounding ground are obliged to shear along the horizontal plane in the split box. Results showed that for a fault displacement of 2m, pipe strains were remained in the elastic range. Strains obtained from the finite element analyses are in close agreement with the recorded strains in centrifuge tests. Finally, the authors pointed out that the bending strains govern the seismic response of pipeline when the pipe axis is perpendicular to fault trace.

Figure 2.29. Soil prism considered in the limit equilibrium stability analysis of the pipe (Ling et al., 2003)

CHAPTER 3

SHAKING TABLE MODEL TESTS ON BOX CULVERTS UNDER DYNAMIC LOADING

3.1 Shaking table test system

Shaking table tests were carried out in the dynamic laboratory of Civil Engineering department of Middle East Technical University. The shaking table system was mounted on main steel frame having plan dimensions of 3.5m x 1m. The main frame was connected to reinforced concrete foundation by welding the anchor plates. The whole system was designed and constructed by Calisan (1997). There were three main parts of the shaking table system, namely, motion generating system (actuators), model container and data acquisition system.

In this study, the system was modified by using a motor driver and laminar box. A motor driver was added to the motion generating system to control the frequencies and to obtain a soft start during the shaking. A laminar box was designed and fabricated in the Ostim Organized Industry. The rigid box (Figure 3.1) was removed from shaking table system and replaced with the laminar box. General view of the shaking table system with laminar container is given in Figure 3.2.

Figure 3.1. Previous shaking table system with rigid box (Cilingir, 2005)
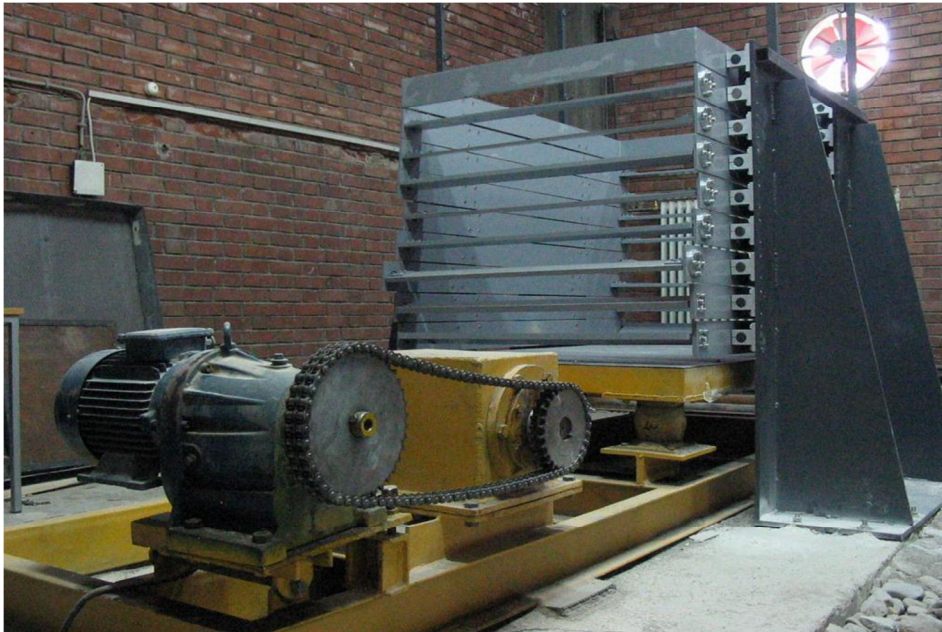
Figure 3.2. General view of the modified shaking table system with laminar box

3.1.1 Motion generating system

In the shaking table system, uni-axial horizontal motion was generated by an AC (Alternating Current) electrical motor as shown in Figure 3.4. In the previous motion generating system, when the motor starts to operate, an impact force was generated instantaneously. In order to prevent this undesirable situation, a motor driver (Figure 3.3) was added to the shaking mechanism. The motor driver enabled the operator to apply smoother operation and to adjust frequencies of the motion.

Gears and chain were used for transmitting rotary motion from electric motor to a rigid shaft. The rotary motion is converted to horizontal harmonic motion by means of the rigid shaft connected to the shaking table platform. Displacement of the rigid shaft or amplitude of motion is adjusted by two attached discs as shown in Figure 3.5. The eccentricity between the discs is provided by using one fixed and five removable screws.

Figure 3.3. The motor driver
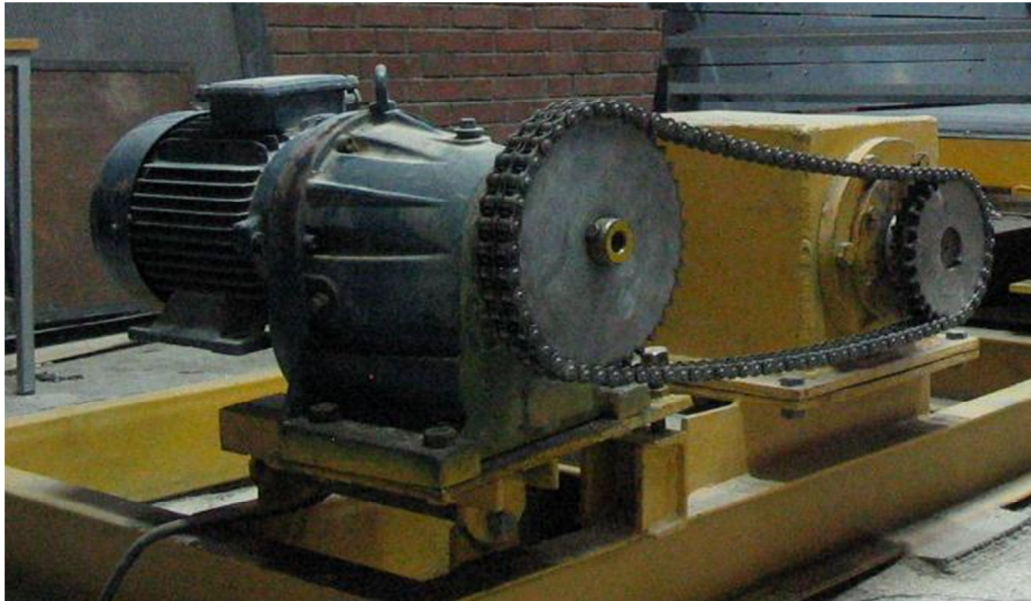
Figure 3.4. AC Electrical motor, chain and gear system

Figure 3.5. Rigid shaft and two attached discs

The maximum displacement limit of the motion generating system is 6mm and frequency range is between 0.5Hz–10Hz. Considering the simple harmonic motion equation (Equation 3.1) given below, acceleration (Equation 3.2) can be calculated by taking second derivative of displacement with respect to time. Peak accelerations used in the tests vary from 0-0.5g.

$$X = A\sin\omega t \tag{3.1}$$

$$\ddot{X} = -A\omega^2 \sin \omega t \tag{3.2}$$

where,

$\ddot{X}$=Acceleration
X=Displacement
A=Displacement amplitude
ω=Angular frequency
t=Time

3.1.2 Soil container

In the previous shaking table system the soil container was a rigid box. Rigid containers usually are not preferred for the dynamic tests due to following reasons:

- Rigid container does not conform to soil deformation pattern during shaking.
- Rigid box generate P-waves during shaking

In this study, available system was renovated by using a laminar box instead of rigid box so as to eliminate the boundary effects. A rectangular laminar container was preferred rather than a ring type container considering the plain strain conditions for a box-type underground structure. Typical laminar box is constructed of several horizontal rectangular or circular metal frames stacked together. The frames are free to move on linear roller bearings in the direction of motion. Thus, the box is able to

conform to the soil deformation pattern during shaking. The stiffness resisting to the movement of soil is the friction between the layers and linear roller bearings. For this reason, the main purpose in the design of laminar box is to minimize the friction as much as possible. Within the scope of this study, a laminar box (Figure 3.6) was designed and manufactured in Ostim Organized Industry. It is rectangular in cross section with dimensions of 1m (width) x 1.5m (length) x 1m (height). The box is composed of nine rectangular steel frames. Each frame is 10cm deep and the spacing between the frames is 1cm. There are linear bearings connected to the outside rigid supporting frame on the long side (Figure 3.7). Linear bearings are fixed in transverse direction while they are free to move in longitudinal direction. The short sides of laminar frames (Figure 3.8) are connected to long sides by means of hinge joints allowing rotation in transverse direction. Hence, the sidewalls of the box conform to soil deformation and boundary effects are minimized.
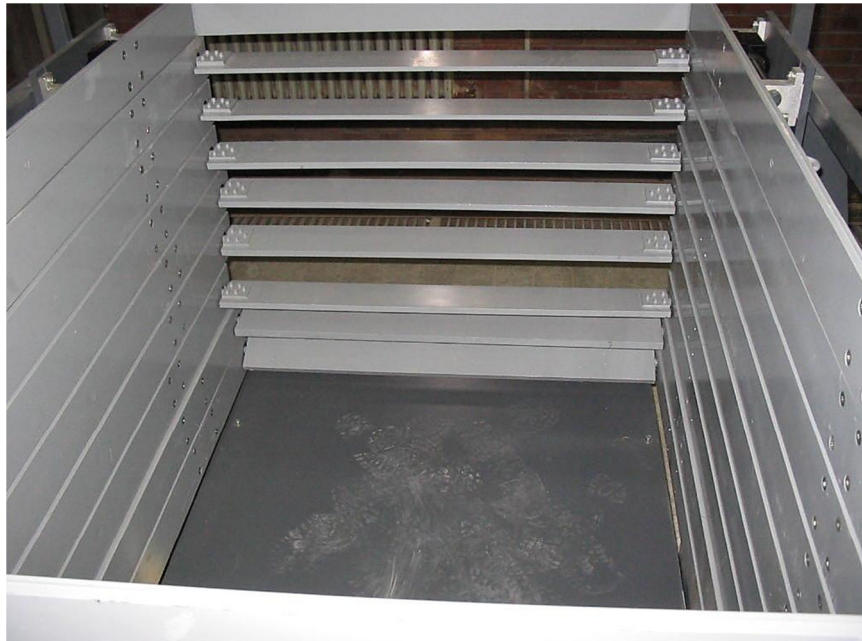
Figure 3.6. General view of laminar box
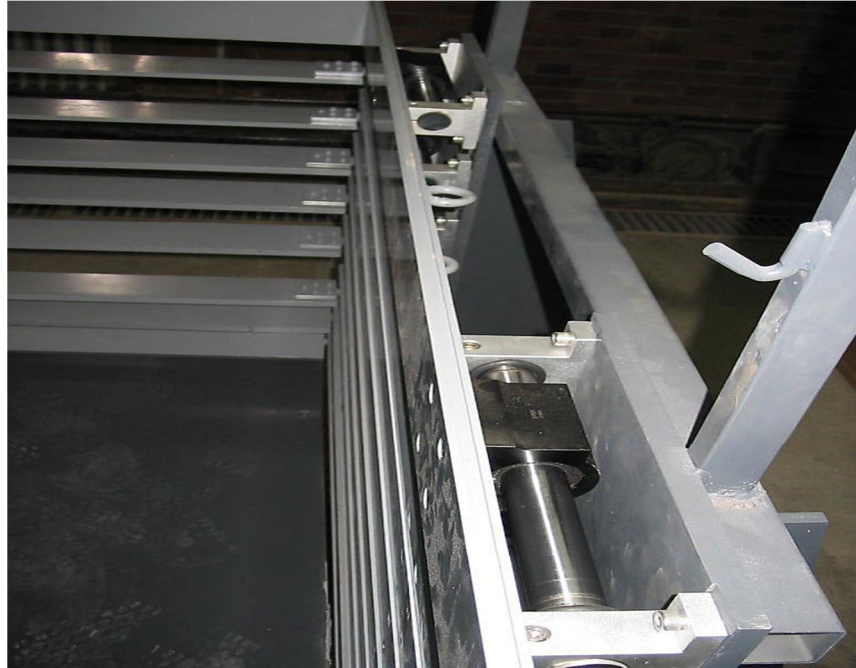
Figure 3.7. Linear bearings connected to outside rigid supporting frame

Figure 3.8. Short side of the laminar box

3.1.3 Friction and boundary effect

i) Friction effect

Long side of the laminar layer slides on the linear bearings connected to the outside frame. During the sliding, friction between the laminar layer and linear bearings resists to the motion. In order to determine this effect, maximum friction forces were measured on each layer. Results are given in Table 3.1.

Table 3.1. Friction forces of laminar layers

Layers of Laminar Box	Maximum Measured Friction Force (N)
Layer 1	25
Layer 2	30
Layer 3	28
Layer 4	30
Layer 5	26
Layer 6	25
Layer 7	27
Layer 8	28
Layer 9	25

If the ground was considered to be made of several layers having thicknesses of 10cm, shear force at the base of top layer can be given as:

T=m.a (3.3)

where m is the soil mass and a is the acceleration of the soil layer. Considering a low acceleration of 0.05g, the shear force at the base of top layer will be around 1160N. Hence, the friction effect of the layer is approximately 2.6%. For higher accelerations it would be rather small, thus it could be ignored.

ii) Laminar box boundary effect

Two acceleration sensors were placed into the soil to analyze the boundary effect of the laminar box during the shaking table tests. Both sensors were at the same depth. One was in the center and the other was 3 cm away from the laminar box wall. Comparison of the acceleration records of those sensors indicates that boundaries have very small effect ground motion. Results are shown in Section 3.5.1.

3.1.4 Data acquisition system

Data acquisition (DAQ) system mainly consists of four major parts: transducers, signal conditioning, DAQ hardware (A/D converter) and personal computer. The flow diagram of overall process for DAQ system is given in Figure 3.9. In the first stage, the physical properties such as acceleration, pressure or displacement were measured with the transducers. Transducers converted the physical properties into corresponding voltage signals. In dynamic tests, transducers usually produce outputs in milivolt (mV) range. Then, signal conditioning modules were used to amplify the mV outputs of transducers for meeting the requirements of DAQ card. Later, DAQ card converted the conditioned transducer signals to digital values. In the final stage, a software program was used to make connection with the DAQ card

for controlling and processing the digitized data. General view of the DAQ system used in shaking table test is illustrated in Figure 3.10.
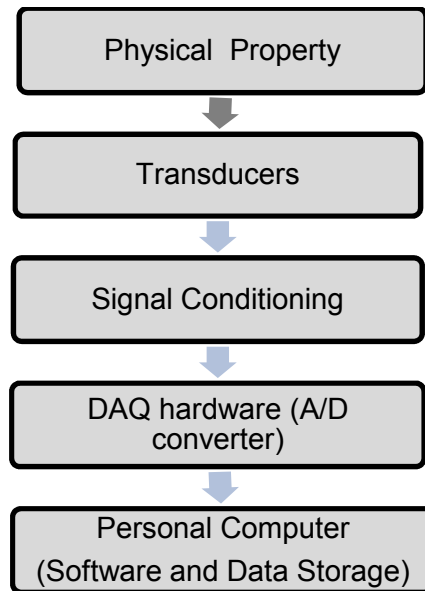
Figure 3.9. Flow diagram for the DAQ system

Figure 3.10. General view of the data acquisition system

3.1.4.1 Transducers

Several transducers were used in the shaking table experiments, namely, acceleration, pressure and displacement transducers. All of the transducers were strain gage-type sensors. Strain gages are used to measure the strains of an object subjected to forces. Resistance of the strain gage increase or decrease depending on the subjected forces. Acceleration, force, stress or displacement can be determined and calibrated by measuring this change in resistance.

i) Acceleration transducers

TML ARF-A (Figure 3.11) type acceleration transducers were used in the tests. There were nine accelerometers, seven of them had a capacity of $10m/s^2$ and two of them had a capacity of $50m/s^2$. They are sufficiently small and lightweight to be used in shaking table model tests. They can only detect acceleration in one axis and be easily placed on the models using adhesives. Mechanical and electrical properties of acceleration transducers are summarized in Table 3.2.

Table 3.2. Mechanical and electrical properties of acceleration transducers

Type	ARF-10A	ARF-50A
Capacity	$10m/s^2$	$50m/s^2$
Rated Output	0.5mv/v	0.5mv/v
Nonlinearity	1%	1%
Frequency Response	50Hz	130Hz
Operating Temperature	-10 to 50 Celcius	-10 to 50 Celcius
Over Load	300%	300%
Input/Output Resistance	120 Ohm	120 Ohm
Recommended Excitation Voltage	Less than 2V	Less than 2V
Allowable Excitation voltage	5V	5V
Weight	13g	13g

Figure 3.11. Acceleration transducer used in shaking table tests

There are two main points to be taken into consideration when placing the acceleration transducers inside the soil. First, the transducers must be stable and remained in a straight position during excitation. To accomplish this, acceleration transducers should be mounted on a rigid plate. Second, the accelerometers and soil should move together during shaking table tests. There should be no relative movement between transducer and soil. For the present study, rigid thin wood plates having light weight were used as an acceleration transducer assembly. Thus, accelerometers could move in accordance with the soil.

Acceleration transducers can make measurements in one axis. As illustrated in Figure 3.12, in the first position it provides constant 1g acceleration. A simple rotation of 90 degree produces 1g change in acceleration level and acceleration becomes 0g in the second position. In the third position, 180 degree rotation from its first position produces 2g change in acceleration value and acceleration becomes 1g. For all these conditions, corresponding output voltages were measured and calibration coefficient was calculated by drawing a linear calibration curve.
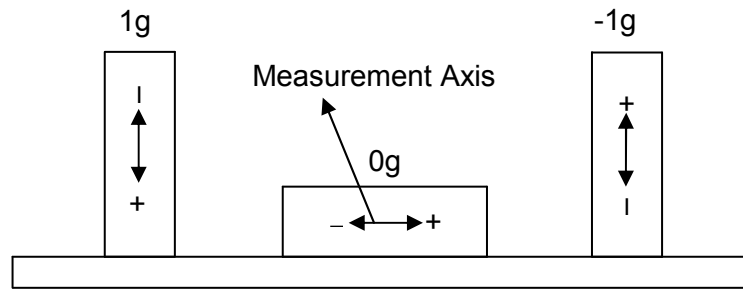
Figure 3.12. Posititons of acceleration transducer during calibration

ii) Pressure transducers

Four Honeywell ABH006PGC1B type pressure sensors and one TML type KDF-200kPa soil pressure gauge were used in the shaking table experiments. TML type KDF-200kPa pressure transducers have an outer diameter of 50mm and sensing area diameter of 34mm. For the Honeywell ABH006PGC1B (Figure 3.13) pressure transducers, outside diameter is 23.8mm and pressure sensitive surface diameter is 19mm. Specifications of the pressure transducers are given in Table 3.3 and Table 3.4, respectively.

Table 3.3. Specifications of TML KDF-200KPA transducer

Type	KDF-200KPA
Capacity	200kPa
Rated Output	0.3mv/v
Non-linearity	2%RO
Temperature Range	-20 to 60 Celcius
Input/Output Resistance	350 Ohm
Recommended Excitation Voltage	Less than 3V
Allowable Excitation voltage	10V
Weight	160g

Table 3.4. Specifications of Honeywell AB/HP pressure transducer

Measurement Type	Gage
Signal Conditioning	Unamplified
Pressure Range	0 to 42kPa
Supply Voltage	5.0 Vdc, 6.0 Vdc max.
Maximum Overpressure	15 kPa
Burst Pressure	50kPa
Port Style	Flush Diaphragm
Temperature Compensation	Yes
Output Type	0 mV to 100 mV
Accuracy	0.5% full scale BFSL
Response Time	less than 0.5 ms
Input Impedance	150 ohms
Output Impedance	115 ohms
Insulation Resistance	1000 Mohms @ 50 Vdc max.
Output Calibration	Yes
Termination Type	0,91 m [3 ft] 4-Conductor Shielded
Weight	57 grams [2.0 ounces]
Full Scale Span	100 mV ± 1 mV
Operating Temperature Range	-54 ºC to 93 ºC
Compensated Temperature Range	-1 ºC to 71 ºC

a)   b)

Figure 3.13 Pressure transducers used in shaking table tests, a) Honeywell pressure transducers b)TML type soil pressure gages

As stated above, there were two types of pressure transducer used in shaking table tests; TML Type soil pressure gauge and Honeywell AB/HP stainless steel flush mounted pressure sensor. There is a rigid diaphragm in TML type pressure sensor. This diaphragm moves rigidly under forces, hence the transducer can be calibrated using deadweights utilized for testing. The pressure sensor was placed on a smooth surface and after applying deadweights, changes in voltage were recorded by means of data acquisition system.

Honeywell AB/HP pressure transducer has a different working principle. In order to obtain accurate readings, the forces acting on sensitive area of this pressure sensor, should be uniformly distributed. Calibration of this sensor was done with water by using a pipe. The pressure sensor was mounted properly under the pipe and leakage of water was prevented. During calibration process, voltage outputs were obtained for different levels of water in the pipe.

iii) Displacement transducers (LVDT)

Two TML SDP-100C type displacement transducers (Figure 3.14) were used in the tests. Displacement transducers have 100mm capacity; their specifications are summarized in Table 3.5. Displacement transducers were calibrated in a simple way. First, the transducer was fixed in a horizontal position and sensing rod was pressed to certain amount of displacements. Corresponding voltage values were measured and calibration coefficient was calculated.

Figure 3.14. Displacement transducers used in shaking table tests.

Table 3.5. Specifications of displacement transducer

Type	SDP-100C
Capacity	100mm
Rated Output	2.5mV/V
Sensitivity	50×10^{-6} strain/mm
Non-linearity	0.2%RO
Spring force	5.9N
Temperature Range	0 to 60 Celcius
Input/Output Resistance	350 Ohm
Recommended Excitation Voltage	Less than 2V
Allowable Excitation voltage	5V
Weight	350g

3.1.4.2 Signal conditioning

In the experiments, eight ADVANTECH ADAM 3016 strain gage input modules (Figure 3.15a) and eight PCLD-7702 signal amplifiers (Figure 3.15b) were used for conditioning the output signals generated by the transducers. Output voltages of

transducers were measured and amplified by changing the gain settings of signal conditioners. Thus, signals were adjusted for the data acquisition card.
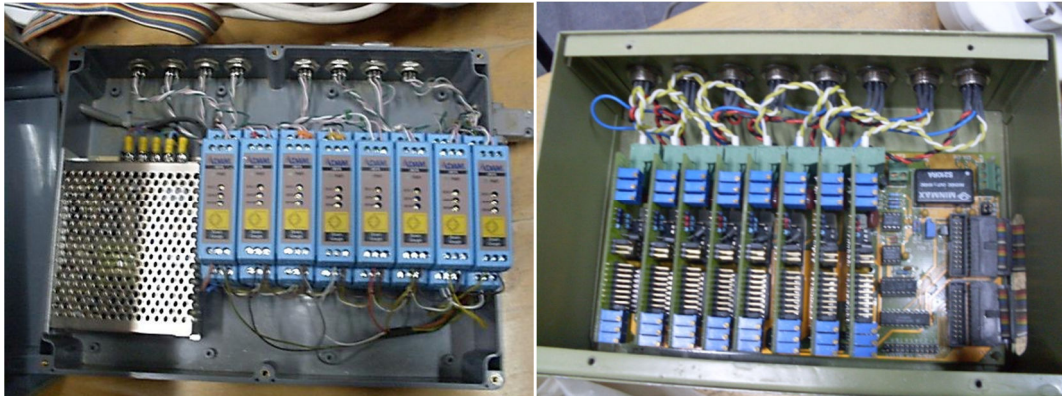
a)   b)

Figure 3.15. Signal conditioning modules and amplifiers a) ADAM strain gage input modules b) PLCD 772 signal amplifiers

3.1.4.3 Data acquisition card

ADVANTECH PCL 818 HD data acquisition card (DAQ) was used for converting analog data to digital data. It is a PCI bus 12 bit DAQ card providing 16 single-ended and 8 differential inputs up to 100 kHz sampling rate. In the shaking table tests, sampling rate adjusted for each channel was 500hz. This sampling rate is adequately enough to capture the input motion frequencies. The PCL 818 card has 12-bit resolution. The resolution indicates the number of smallest input voltage that can be distinguished by the data acquisition card. Resolution (R) can be calculated using the following formula:

$R=2^n$ (3.4)

where, n is the bit number. The PCL card resolution is:

R=2^{12}=4096

When measuring the 0-10V input voltage, the smallest voltage signal change captured by the card is:

10/4096=2.44 mV

Specifications of data acquisition card are given in the following table:

Table 3.6. Specifications of data acquisition card

Channels	16 single ended or 8 differentials
Resolution	12 bits
Max. Sampling Rate	100kS/s for all input ranges
Overvoltage Protection	±30 V_{DC} max.
Input Impedance	10MΩ
Sampling Modes	Software, Pacer or External
Input Range	V, software programmable ±10V,±5V,±2.5V,±1.25V,±0.625V

3.1.4.4 Data storage and processing

MATLAB software program was used to store the data in personal computer's memory. Digital voltage values converted by the card were acquired by using the data acquisition toolbox of MATLAB. MATLAB includes special functions to design a bandpass filter. The frequency range of the filter is between 0.5 Hz to 25 Hz. For the evaluation of measurements, all processed data in MATLAB were exported into EXCEL spreadsheets.

3.1.4.5 Membrane

In shaking table tests, an elastic rubber membrane was used to prevent sand leaking out of the laminar box. Thickness of the membrane is 1mm. Its thickness was kept as thin as possible to allow horizontal shear during shaking. In other words, a membrane with small stiffness as compared to soil was selected for the tests. In order to obtain a membrane having same dimensions with the inside dimensions of laminar container, a mould was constructed using plywood. The mould was covered with the membrane end the corners of the membrane were stuck with adhesives. After drying up, it was taken out and placed into the laminar box.

3.2 Soil properties

3.2.1 Physical properties

Air dried Çine sand was used to construct the model ground in the shaking table tests. Based on the Unified Soil Classification System (USCS), the soil can be identified as SP: poorly graded slightly silty medium sand. The grain size distribution curve of the sand (Figure 3.16) was determined through dry sieve analysis. Parameters derived from distribution curve can be given as follows:

D_{10} = 0.15mm
D_{30} = 0.27mm
D_{50} = 0.45mm
D_{60} = 0.53mm

D_{10}, D_{30}, D_{50} and D_{60} are the particle size diameters corresponding to 10%, 30%, 50% and 60% passing in the grain size distribution curve.

Coefficient of uniformity,

$$C_u = D_{60} / D_{10} = 3.53 \qquad (3.5)$$

Coefficient of curvature,

$$C_c = D^2_{30} / (D_{60} \times D_{10}) = 0.92 \qquad (3.6)$$
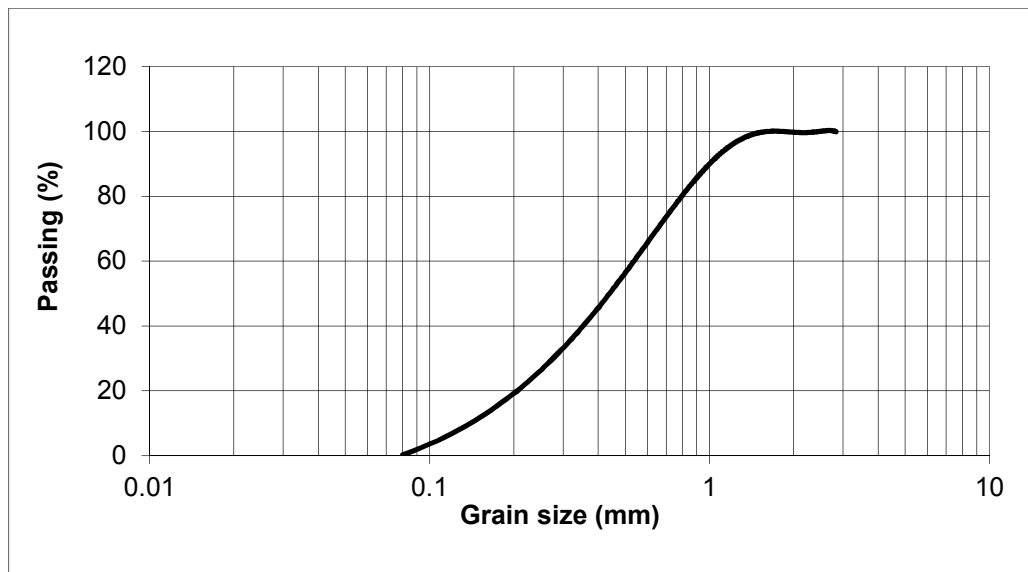
Figure 3.16. Grain size distribution curve of Çine Sand

The minimum density of dry sand was determined by using two methods. In the first method a cylinder tube was filled with sand and converted upside down by covering the top of the tube. Then, the tube was brought back to its original position and volume of sand was measured. In the second method sand was poured into a jar by using a funnel. The fall height was kept as minimum as possible to obtain the loosest state. Minimum dry density and corresponding maximum void ratio were found as 14.50kN/m³ and 0.80, respectively. Maximum dry density was determined by tamping. Sand was placed into a mould and compacted with a vibration tamper. Maximum dry density and corresponding minimum void ratio were obtained as

18.10kN/m^3 and 0.44, respectively. Table 3.7 shows the physical properties of Çine Sand.

Table 3.7. Physical properties of Çine Sand used in shaking table tests

	Çine Sand
Water content	%0.1
Specific gravity	2.66
Minimum void ratio	0.44
Maximum void ratio	0.80
Minimum unit weight (kN/m^3)	14.50
Maximum unit weight (kN/m^3)	18.10
Coefficient of uniformity (C_u)	3.53
Coefficient of curvature (C_c)	0.92
Mean diameter (D_{50}) (mm)	0.45
Fines content (%)	1.15
Poisson's Ratio	0.3

Direct shear and triaxial tests were conducted to find the shear strength parameters of the soil. Normal stress range in direct shear and triaxial tests changes between 14kPa to 50kPa. For a relative density of 60%, Çine Sand has a friction angle of 43°.

3.2.2 Dynamic soil properties

The model ground was modeled in one dimensional ground response analyses program SHAKE91 and the results were calibrated with obtained free-field shear

strains at mid-depth of culvert in shaking table tests. Figure 3.17 illustrates the comparison between SHAKE91 and experimental results.
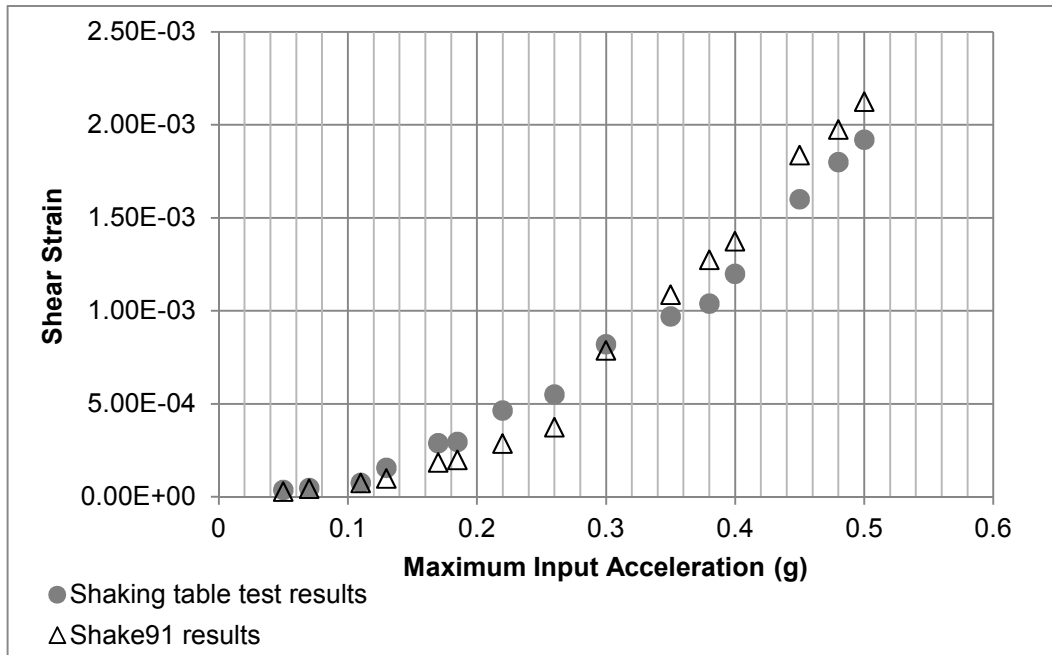
Figure 3.17. Comparison of shaking table test and SHAKE91 results

Based on the SHAKE91 result, maximum shear modulus and shear modulus reduction curves of the Çine sand were estimated. For a relative density of 60%, the maximum shear modulus of the ground surrounding culvert was predicted as 13000kPa. Figure 3.18 shows the shear modulus reduction (G/G_0) obtained from back-analyses of free-field shaking table results by using SHAKE91. Shear modulus degradation curve proposed by Darendeli (2001) is given in the same figure for reference. The curve was plotted for a mean effective stress (3.6kPa) representing the stress levels of culvert depths in shaking table tests. G_0 is the initial (low-strain) shear modulus and G is the shear modulus at any strain level. The reference strain (γ_r) is approximately 3.9×10^{-4} which corresponds to the shear strain when shear modulus falls to one half of initial shear modulus.
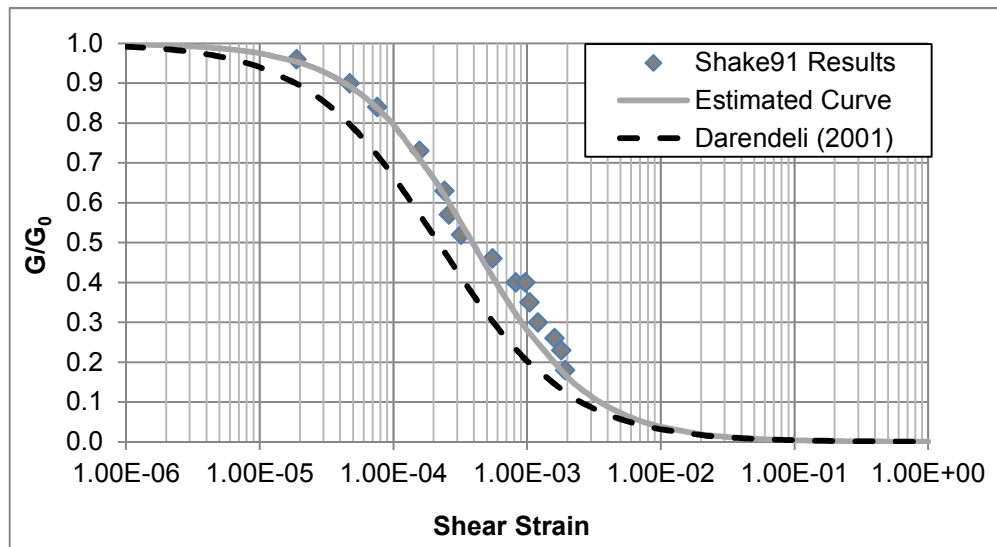
Figure 3.18 Variation of normalized shear modulus with respect to shear strain

3.3 Preparation of model ground

Raining method was conducted to prepare the model ground throughout the shaking table tests. In order to obtain a homogeneous model ground and a uniform density throughout the laminar box, sand was pluviated into the laminar box from a height of 60cm by using a sieve (Figure 3.19). The sieve is rectangular in cross section with dimensions of 0.98m (width) x 1.48m (length) and the mesh size of 2.36mm. When constructing the model ground, first, a sand bed with a thickness of 20cm was placed into the box in two layers and compacted with a vibration tamper (Figure 3.20). Later, the remaining part of the sand was placed into the laminar box in layers of 10cm thickness by pluviation. During the sand raining, five small boxes were buried into the soil at different locations to determine the relative density of the sand. Measurements with small boxes show that a uniform density and homogeneous ground model can be obtained by sand pluviation. Relative densities of the sand bed and overlying sand changed between 80 to 85% and 60 to 65%, respectively. General view of the laminar box after filling sand is shown in Figure 3.21.

Figure 3.19. Diffuser with 2.36mm sieve size located on top of the laminar box

Figure 3.20 Tamping for preparation of sand bed

Figure 3.21 Laminar box after filling sand

3.4 Box-type culvert models

Four different types of steel box culvert models were used in shaking table tests. Each model is 20cm by 20cm in cross section and 80cm in length. Side walls of the box structure model have four kinds of thickness: 2mm, 3mm, 5mm and 10mm. The culverts were labeled as C1, C2, C3, C4 respectively. Upper and lower slabs of the culvert models were relatively thick and rigid as compared to that of sidewalls. Thus, dynamic lateral earth pressures will be monitored by eliminating structural effects due to bending of the slabs. Cross sections of the box models are illustrated in Figure 3.22.

Box models were manufactured considering the flexibility ratio which represents the relative stiffness between the soil and structure. As discussed in Chapter 2, flexibility ratio of the structure can be given as (Wang, 1993):

$$F = \frac{G_s W}{S_1 H}$$

(3.7)

where, G_s is the shear modulus, W is width and H is the height of the structure, S_1 is the force required to cause a unit racking deflection of the structure. Computed S_1 values were presented in Table 3.8.

Table 3.8. Calculated S_1 values for the culvert models

Culvert Type	S_1 kN/m/m
C1 Upper and Lower Slab=10mm Side Walls=2mm	396.8
C2 Upper and Lower Slab=10mm Side Walls=3mm	1314.5
C3 Upper and Lower Slab=10mm Side Walls=5mm	5555.5
C4 Upper and Lower Slab=10mm Side Walls=10mm	25000

The flexibility ratio of a single barrel box can be directly calculated by using the equation proposed by Wang (1993). The equation is given by:

$$F = \frac{G_s}{24}\left(\frac{H^2 W}{EI_W} + \frac{HW^2}{EI_R} \right) \tag{3.8}$$

where G_s is the shear modulus of soil, H is the height and W is the width of box structure, I_w is the moment of inertia of walls, I_R moment of inertia of slabs. The physical meaning of the F (flexibility ratio) values can be described as follows:

For F<1, the structure is more flexible as compared to the soil.

For F>1, the structure is more rigid as compared to the soil.

For F=1, rigidity of structure is same with the soil.
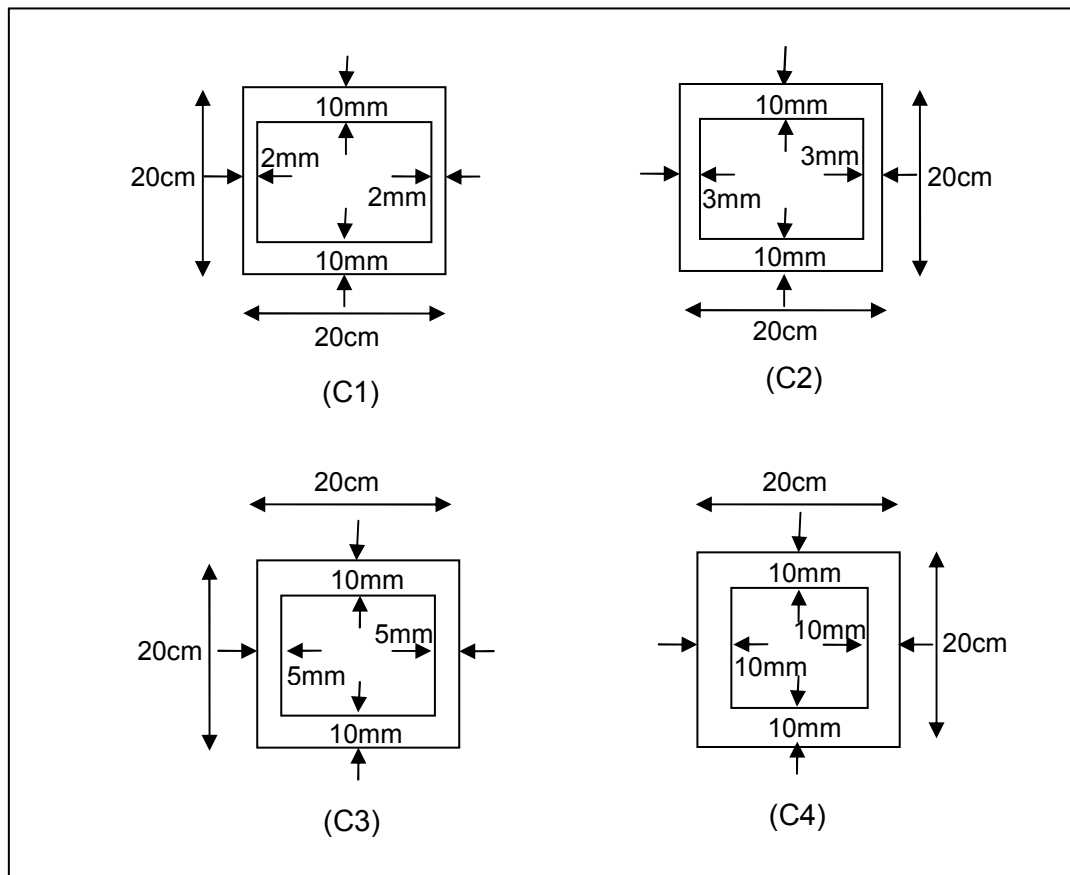
Figure 3.22. Cross sections of the steel culvert models used in shaking table tests

Configuration of the structure model and layout of the transducers are depicted in Figure 3.23 and Figure 3.24, respectively. The box culvert model (Figure 3.25) was buried in sand at a depth of 40cm. Embedment depth ratio h/H is 2 where h is mid-depth of the structure and H is structure height. In order to minimize the laminar box boundary effects, the model and transducers were placed in the middle of the container. Seven pressure transducers were mounted on the box model to measure the dynamic soil pressures. One accelerometer was placed at the bottom of culvert model for evaluating inertia of the structure. Five accelerometers were buried in the ground model to determine soil accelerations and deformations, and one accelerometer was placed on the shaking table to measure the input motion.
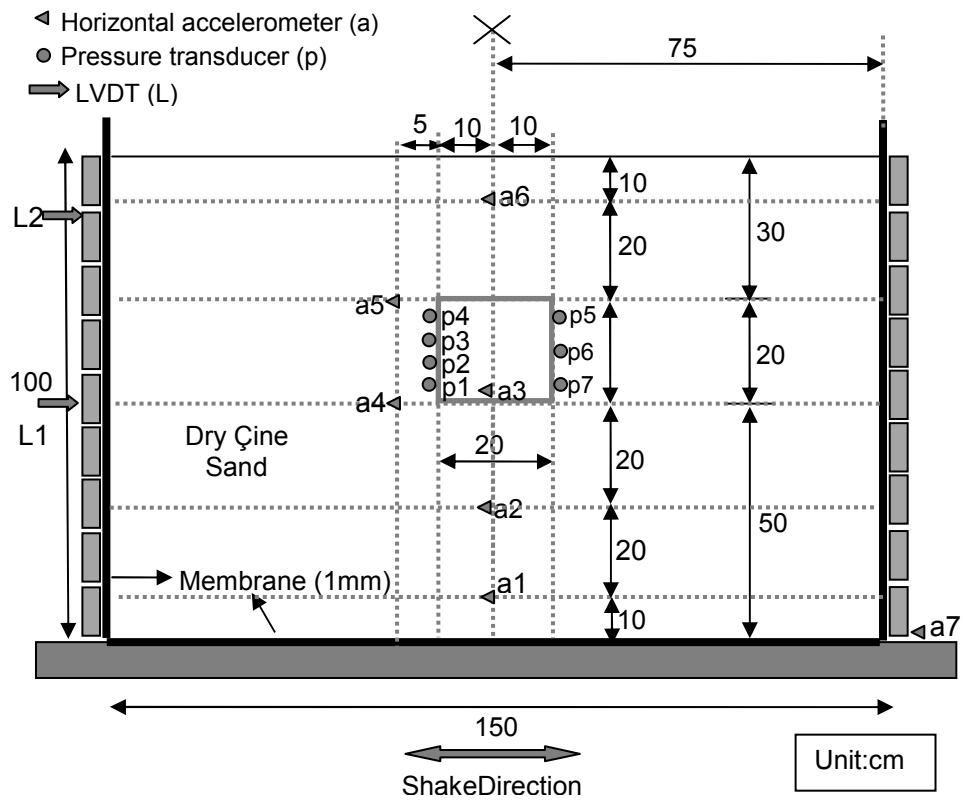
Figure 3.23. Schematic illustration of shaking table test instrumentation
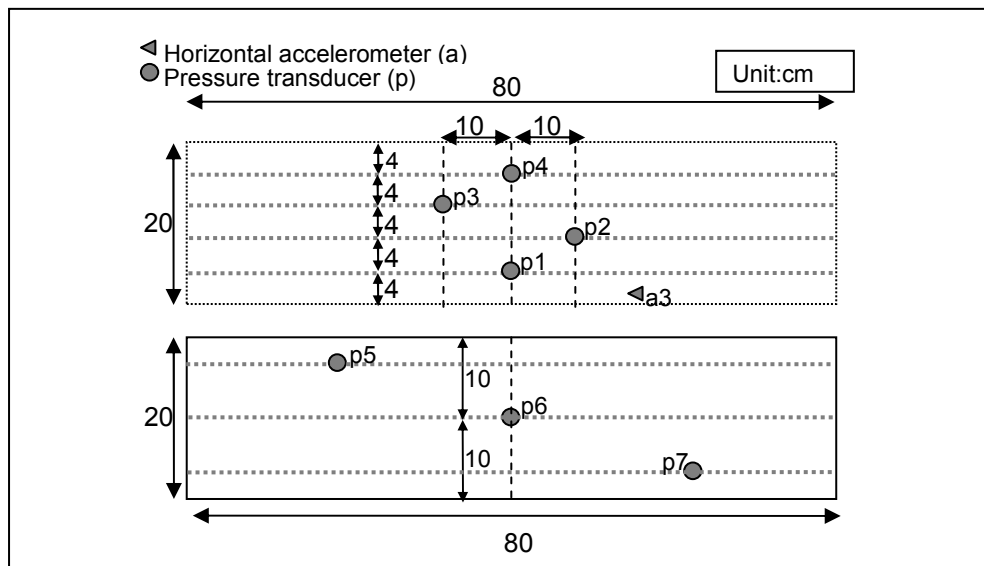
Figure 3.24. Layout of pressure and acceleration transducers on the box model
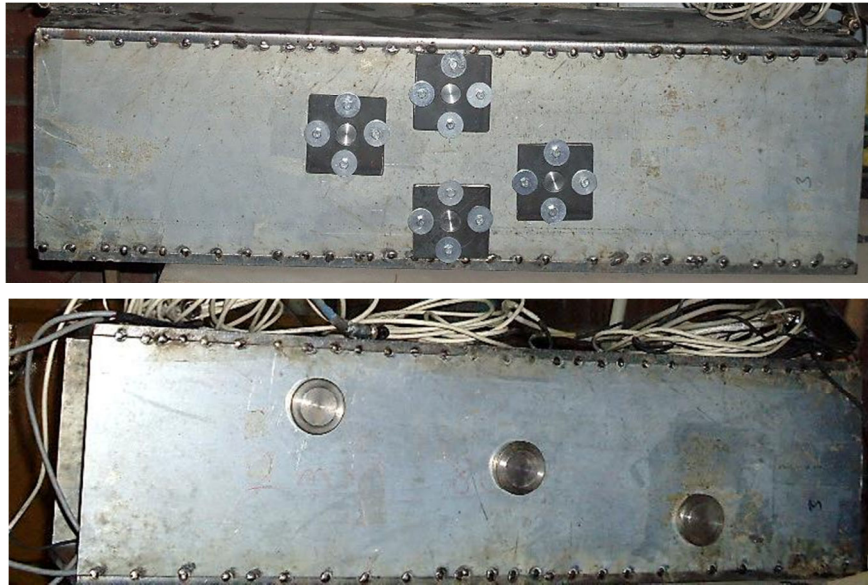
Figure 3.25. General view of a culvert model and mounted pressure transducers

3.4.1 Testing program and procedure for shaking table tests

There are totally 91 shaking table tests performed under different input motions having various acceleration amplitudes and frequencies. The testing program includes different cases given as follows:

- Free-field response tests
- Model tests for 4 different culvert models (C1, C2, C3, C4), when the model was buried at a depth of 40cm (h/H=2).
- Model tests for 2 different culvert models (C1, C4), when the model was buried at a depth of 60cm (h/H=3)

The procedure for the tests can be summarized as follows:

1) The laminar box was fixed with locking bars for holding the laminar layers together during filling process.

2) Pressure and acceleration transducers were mounted on the culvert models before tests.

3) For the preparation of sand bed, the sand was placed into the box in two layers and compacted with a vibration tamper. The height of the sand bed was 20cm.

4) The sieve was placed 60cm above the sand bed and the sand was filled in layers of 10cm thickness until 50cm height. During the pluviation process, density measurement boxes and accelerometers were buried into the soil.

5) The culvert model was put into the box and leveled in both longitudinal and transverse directions. The transducers were connected to data-acquisition system and initial voltage readings were recorded.

6) The remaining part was filled by pluviation and displacement transducers connected to a rigid stable outside frame were placed at heights of 50cm and 90cm.

7) The static data was recorded and fixing bars were taken out for the dynamic tests. Input motion frequency was tuned manually by using the motor driver control panel and the displacement was adjusted by changing the eccentricity of the discs.

8) The system was turned on and the soil container was shaken about 15 seconds with a harmonic input motion. All recorded data were saved and transferred into a Matlab file.

9) For free-field condition tests; step 5 was absent in the procedure.

The testing program applied for all culvert models can be tabulated as shown in the Table 3.9.

Table 3.9. Testing program applied in shaking table experiments

Test Number	Acceleration Amplitude of Input Motion (g)	Frequency of Input Motion (Hz)	Duration (Seconds)
1	0.05	2	10
2	0.07	2	10
3	0.11	3.1	10
4	0.17	3.1	10
5	0.19	3.1	10
6	0.22	3.1	10
7	0.26	4.2	10
8	0.30	4.2	10
9	0.35	5.3	10
10	0.4	5.3	10
11	0.45	6.4	10
12	0.48	6.4	10
13	0.50	6.4	10

3.5 Results and discussions

3.5.1 Boundary effect of laminar box

Boundary effect of laminar container on ground motion was investigated by using accelerometers. One accelerometer (a6) was placed near sidewall at a distance of 5cm from membrane and the other accelerometer (a3) was placed in middle of the laminar container (Figure 3.30). Both accelerometers were at the same level at mid-height of the laminar box. Acceleration time histories at those locations were recorded during shaking table tests. Results indicate that the acceleration record near sidewall is very similar to acceleration record in the middle of container

91

(Figure 3.26 and Figure 3.27). There was almost no phase difference between the acceleration time histories, only the amplitudes change. The ratio of the acceleration amplitude near the sidewall to the acceleration amplitude at the center was plotted against the input acceleration in Figure 3.28. As seen in Figure 3.28, there is minor variation of about 5% and 10% between the wall and center accelerations. Hence, it can be said that walls of the laminar container do not have significant boundary effect on the ground motion. In this study, the model was placed at the center of container to minimize boundary effects.
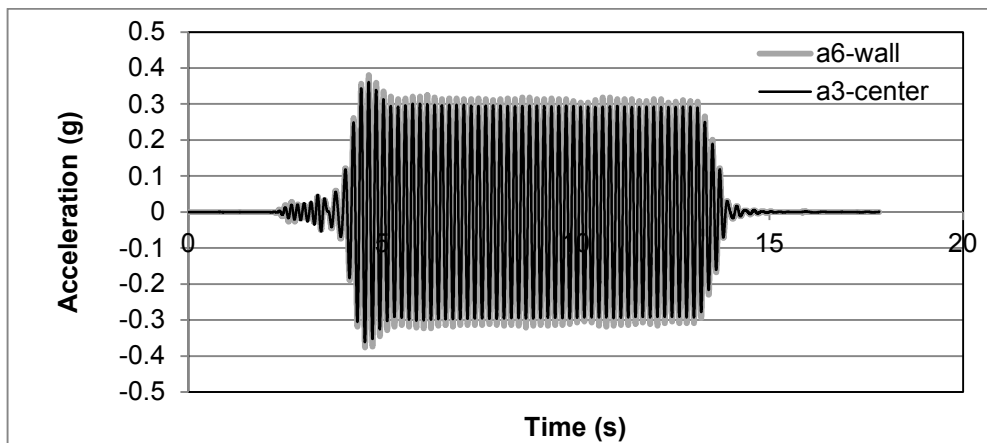
Figure 3.26. Comparison of accelerations recorded at the center and near container sidewall
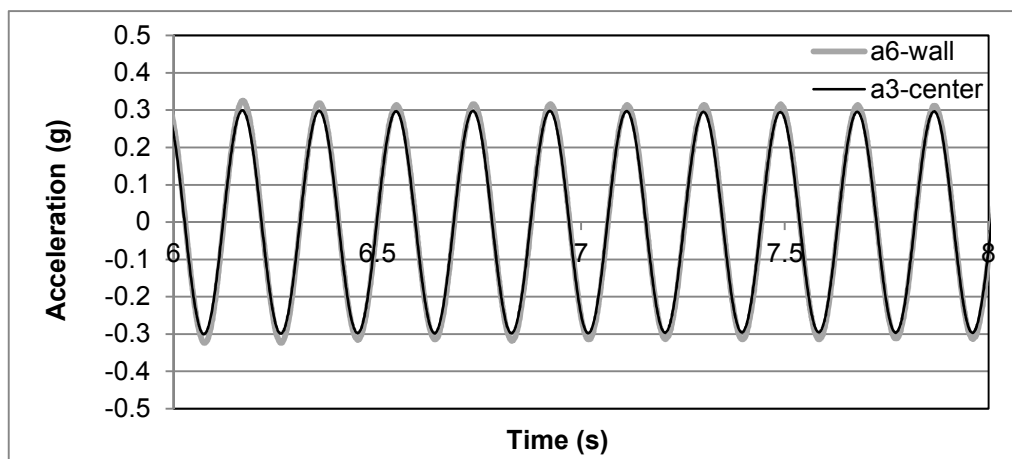
Figure 3.27. Closer view of Figure 3.26.
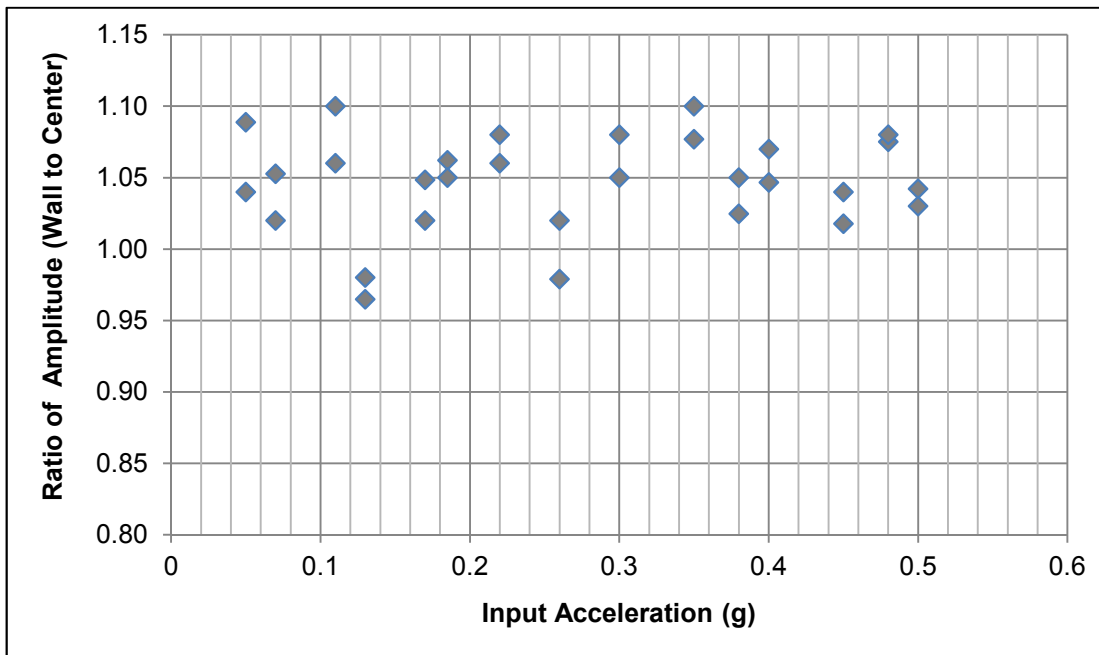
Figure 3.28. Variation of acceleration amplitude ratio (wall to center) with respect to input acceleration

3.5.2 Determination of flexibility ratio for culvert models

Flexibility ratio (relative stiffness) is defined as the ratio of soil stiffness to structural stiffness. It has significant role on the dynamic response of underground culverts; hence special attention should be given to the determination of flexibility ratio. In dynamic soil culvert interaction analyses relative stiffness is represented by the ratio of shear modulus of the surrounding ground to structural racking (flexural) stiffness. The main difficulty in determining the flexibility ratio is the assessment of shear modulus. Shear modulus is strongly dependent on the intensity of the dynamic motion. It decreases with increasing shear strain of the soil. Therefore, different flexibility ratios can be obtained under different dynamic motions for the same culvert. Based on this conclusion, the flexibility ratios of the four culvert models were determined at different strain levels. First, the shear strains of the surrounding soil

were computed from the shaking table test results for different input motions. Next, degraded shear modulus values were determined at those strains. Finally, the flexibility ratios were calculated by dividing degraded shear modulus to structural racking stiffness. Following table (Table 3.10) presents the flexibility ratio values for the culvert models at different input accelerations.

Table 3.10. Flexibility ratio values for the culvert models at different input accelerations.

Maximum Input Acceleration (g)	Flexibility Ratio for C1	Flexibility Ratio for C2	Flexibility Ratio for C3	Flexibility Ratio for C4
0 (Static Condition)	32.8	9.9	2.3	0.52
0.05	31.50	9.49	2.25	0.50
0.07	30.47	9.20	2.18	0.49
0.11	28.83	8.70	2.06	0.48
0.13	27.52	8.31	1.97	0.46
0.17	23.91	7.22	1.71	0.45
0.185	19.66	5.93	1.40	0.44
0.22	14.74	4.45	1.05	0.43
0.26	14.41	4.35	1.03	0.41
0.3	13.76	4.15	0.98	0.34
0.35	12.78	3.86	0.91	0.31
0.38	11.47	3.46	0.82	0.26
0.4	11.14	3.36	0.80	0.23
0.45	11.14	3.36	0.80	0.23
0.48	10.48	3.16	0.75	0.21
0.5	8.85	2.67	0.63	0.19

3.5.3 Comparison of measured static lateral coefficients with Jaky's formula

There were totally seven pressure transducers mounted along the sidewalls of the culvert model. Four of them were located at the left side and three of them were located at right side of the box culvert. First, initial voltage values were registered when there was no overburden soil on the culvert model. Later, the final voltage values were recorded after filling the laminar container. Table 3.11 gives the measured static pressures along the sidewalls of four culvert models with respect to depth ratio. Depth ratio is represented by d/H where d is the distance from pressure transducer to upper corner of the culvert and H is the culvert height. Besides, flexibility ratio is denoted by FR which is given for the static condition as presented in Table 3.10.

Table 3.11. Lateral static earth pressures acting on the culvert models.

		C1	C2	C3	C4
	Depth Ratio (d/H)	Lateral Soil Pressure (kPa)	Lateral Soil Pressure (kPa)	Lateral Soil Pressure (kPa)	Lateral Soil Pressure (kPa)
Left Side Wall	0.2	1.35	1.38	1.59	1.68
	0.4	1.52	1.80	1.77	2.13
	0.6	1.68	2.05	2.22	2.25
	0.8	1.98	2.30	2.47	2.58
Right Side Wall	0.25	1.57	1.52	1.63	1.68
	0.5	1.66	1.88	2.10	2.18
	0.75	1.92	2.05	2.34	2.42

Figure 3.29 shows the variation of lateral earth pressure coefficients (K) with respect to depth ratio (d/H). For comparison, two lines indicating at rest and active earth pressure coefficients, K_0 and K_A, were drawn in the same plot. K_0 was calculated from the following empirical relationship proposed by Jaky (1948):

$$K_0 = 1 - \sin\phi'$$
(3.9)

where ϕ' is the drained friction angle. K_A was determined by using the Equation 3.10 suggested by Rankine (1857). For an internal friction angle of 42°, K_0 and K_A were calculated as 0.33 and 0.2, respectively.

$$K_a = \frac{1 - \sin\phi'}{1 + \sin\phi'}$$
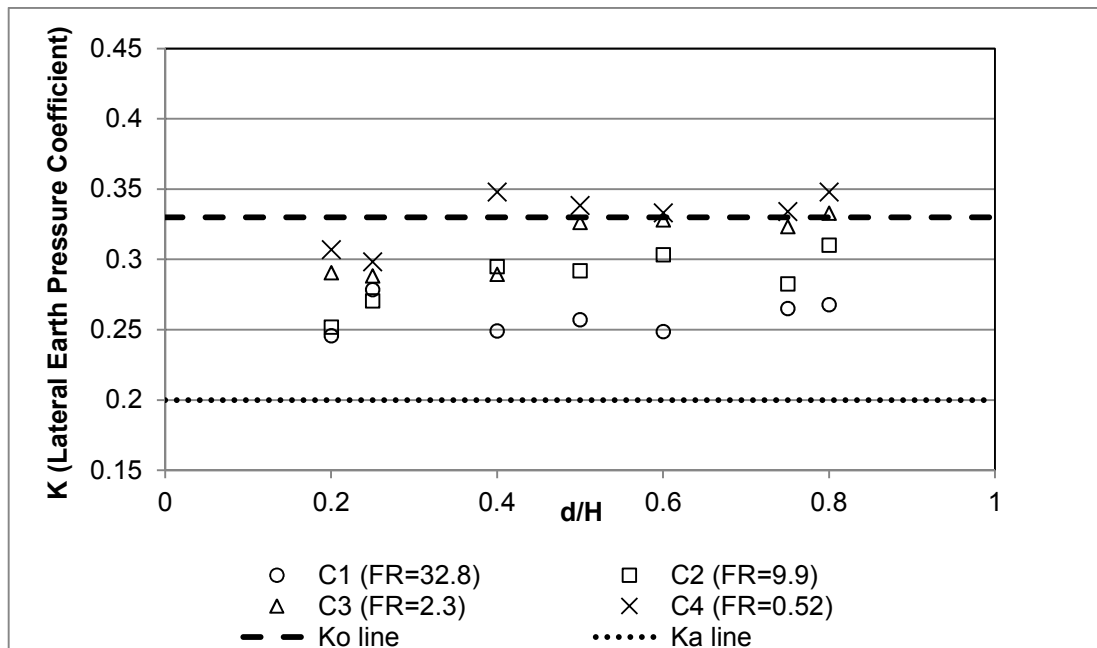(3.10)

Figure 3.29. Variation of learth pressure coefficient (K) with respect to depth ratio (d/H)

As seen from Figure 3.29, all measured earth pressure coefficient values are above the K_A line. K values obtained for the culvert models C3 and C4 are in close agreement with the K_0 line. On the other hand, for relatively flexible culverts C1 and C2, smaller K values were found as compared to C3 and C4. These values fall into the region bounded by K_0 and K_A lines. The results showed that lateral earth pressure coefficient decreases with increasing flexibility ratio as expected. The sidewall of the flexible culverts deforms more than that of rigid culverts and accordingly the walls are subjected to low soil pressure.

3.5.4 Maximum acceleration along the depth of ground model

In order to investigate the variation of maximum acceleration along the depth of soil model, the accelerometers were placed at 5 different depths in the soil as seen in Figure 3.30. Recorded maximum accelerations at those depths normalized with the maximum shaking acceleration and plotted versus soil depth as given in Figure 3.31 and Figure 3.32. As seen in Figure 3.31, the normalized acceleration (amplification ratio) is very low and changes around 1 for the maximum input accelerations 0.02g, 0.06g, 0.12g. This means that the soil behaves as a rigid mass at low strain levels. The amplification ratio starts to increase at 0.17g and at the top layer of the soil it becomes approximately 1.1. Figure 3.32 shows the variation of normalized acceleration along the depth of soil model for the maximum input accelerations of 0.22g, 0.26g, 0.30g, 0.34g, 0.4, 0.45g and 0.50g. In the figure, it is observed that the amplification ratio near the surface changes between 1.2 and 1.4. Higher accelerations at the upper region of the model ground may occur due to reflection and refraction of the seismic waves from the surface. Besides, it should be noted that the frequency of the input motion is higher at higher accelerations.
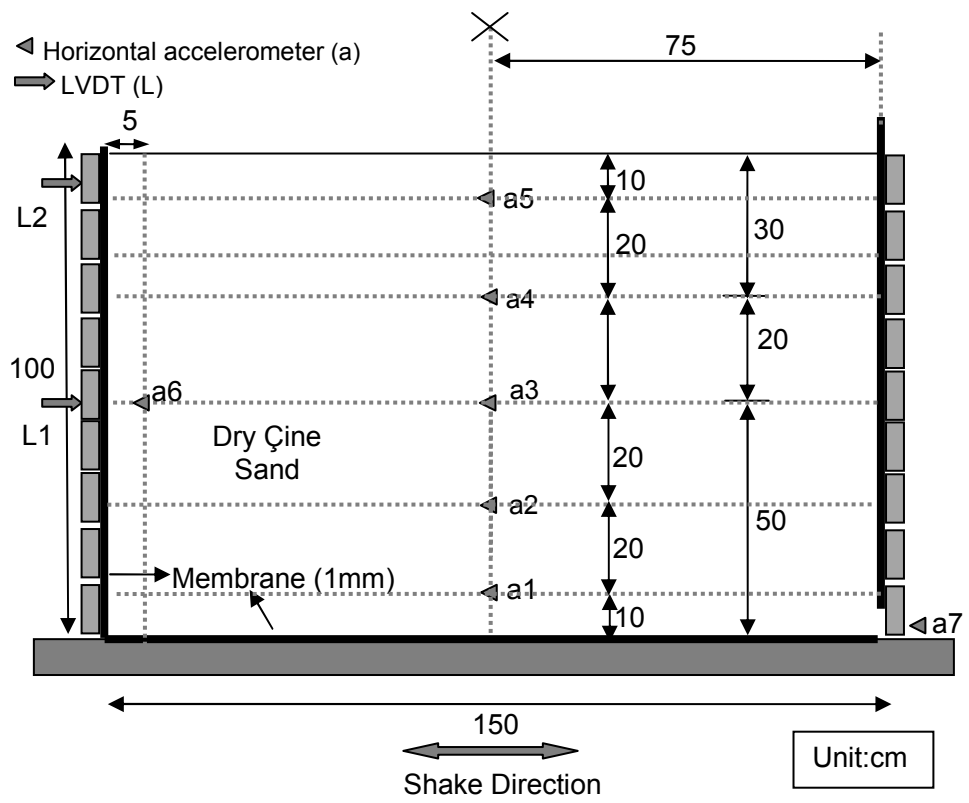
Figure 3.30. Layout of the transducers in free-field shaking table tests.
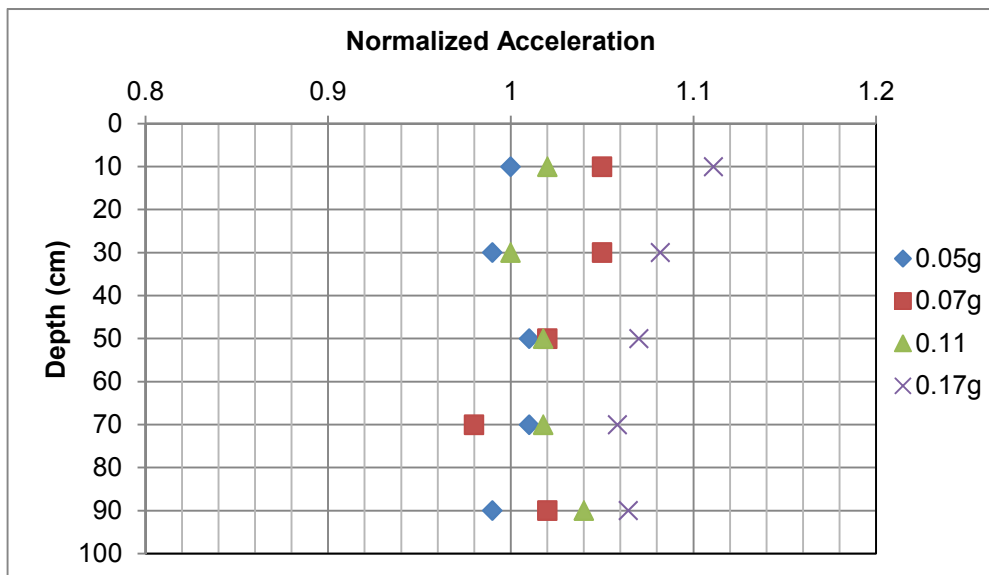
Figure 3.31. Variation of maximum acceleration along the soil profile for maximum input accelerations (0.05g, 0.07g, 0.11g, 0.17g)
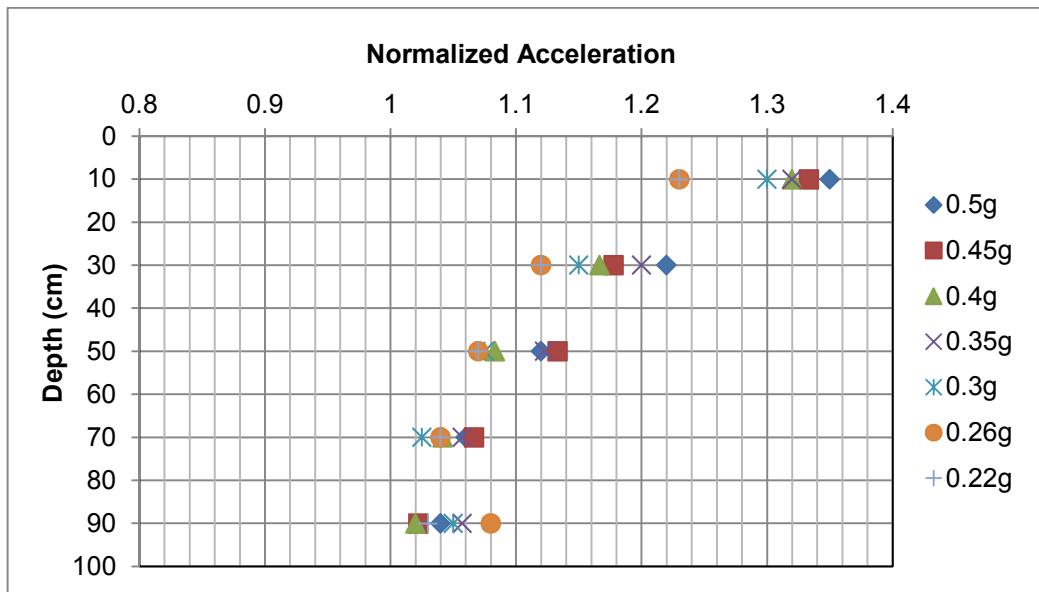
Figure 3.32. Variation of maximum acceleration along the soil profile for maximum input accelerations (0.22g, 0.26g, 0.3g, 0.35g, 0.4g, 0.45g, 0.5g)

3.5.5 Evaluation of displacements and shear strains

Displacement of laminar box and soil were measured by using linear variable transducers and accelerometers respectively. LVDT measures the displacements directly. In contrast to the LVDT, the accelerometer may provide an indirect measure of displacement by integrating the acceleration time history twice. Before the integration process the data must be filtered to prevent the unwanted errors or misleading results. For this reason, recorded acceleration time histories were filtered by a bandpass filter between 1Hz and 20Hz (high pass at 1 Hz and low pass at 20Hz). Thus, high frequency noise and drift due to spurious low frequency components were eliminated for enhancing data quality.

The accelerometers were placed at different heights in the soil model. As explained above, the displacements were computed by double integrating of acceleration

records. Assuming that the displacement is varying linearly between two accelerometers located at point 1 and 2, the shear strain can be calculated by:

$$\gamma = \frac{d_2 - d_1}{z_2 - z_1} \qquad (3\text{-}11)$$

where γ is the shear strain, d_1, d_2 are the displacements at points 1, 2 and z_1, z_2 are the heights at points 1, 2, respectively. Based on this approach, soil shear strain around the culvert model was obtained for the input motions having different acceleration amplitudes. Figure 3.33 shows the variation of free-field shear strain at culvert's mid-depth with respect to maximum input acceleration.
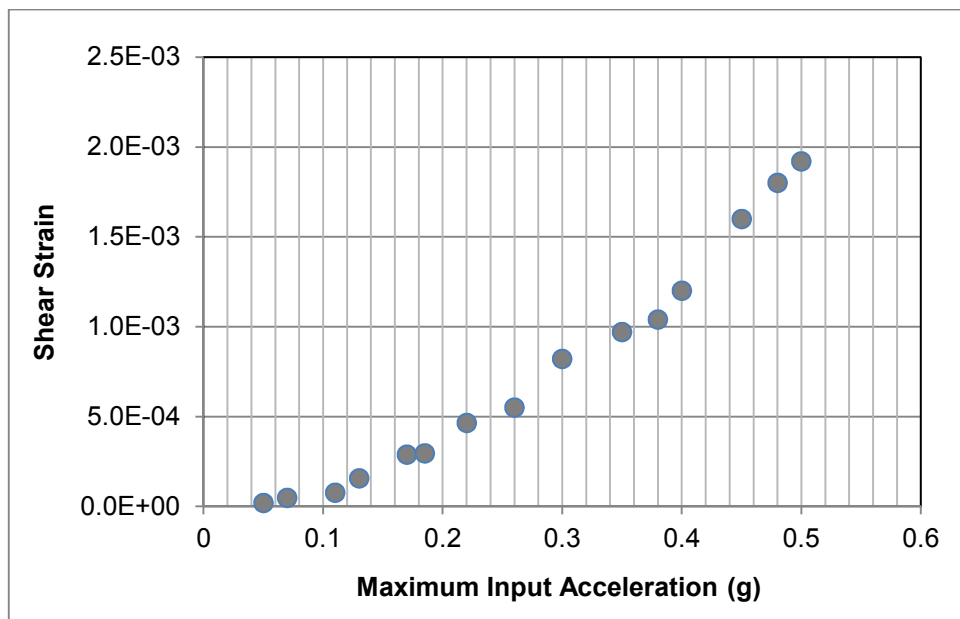
Figure 3.33. Variation of free-field shear strain at culvert depth with respect to maximum input acceleration

Two displacement transducers, L1 and L2, were placed at mid height (50cm elevation) and near the top (90cm elevation) of laminar box. Displacement time histories were analyzed at different acceleration levels 0.11g and 0.4g. It is observed that the relative displacement between L1 and L2 increases with increase in acceleration as expected. Moreover, there is small phase shift at higher accelerations. Following figures (Figure 3.34, Figure 3.35) gives the comparison between the displacement time histories recorded by L1 and L2 for different accelerations.
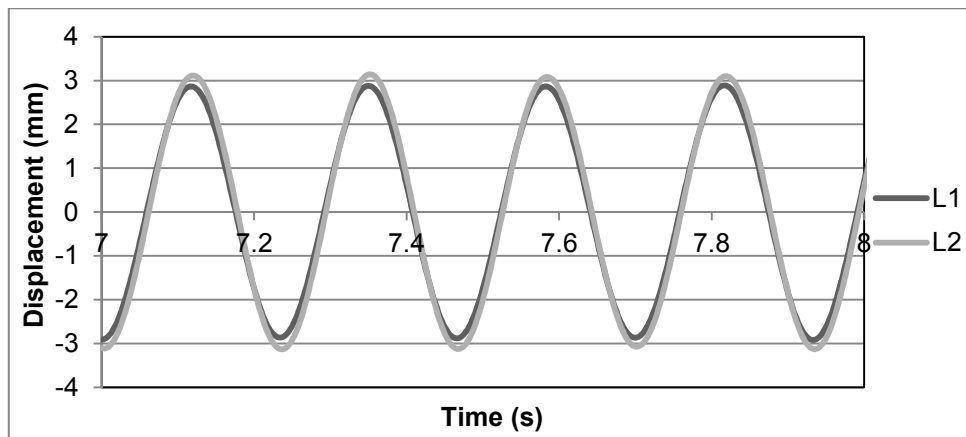
Figure 3.34. Displacement time histories recorded by L1 and L2 at 0.11g maximum input acceleration
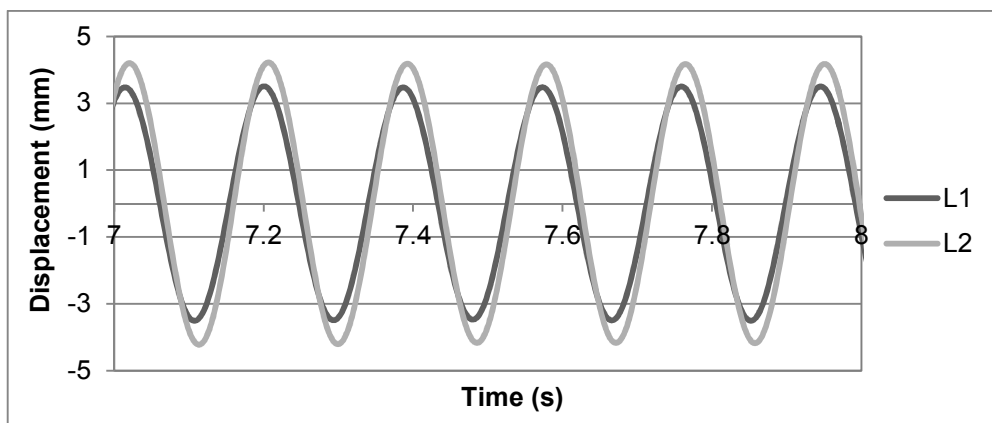
Figure 3.35. Displacement time histories recorded by L1 and L2 at 0.4g maximum input acceleration

3.5.6 Dynamic soil pressures acting on sidewalls of the culverts

In shaking table tests lateral soil pressures were measured at each sidewall of the culvert models. During the tests, static and dynamic pressures were measured separately. For this purpose, first, the static pressure was recorded then dynamic pressures were measured by taking the initial values as static pressures. Figure 3.36 is an example of the dynamic pressure record. The negative values in this figure do not represent the suction or negative forces acting on the culvert model. They indicate the reduction in the static pressure under cycling loading.

There are four pressure transducers at the left side and three pressure transducers at the right side of the culvert model. Figures from 3.37 to 3.44 shows the variation of recorded maximum dynamic pressures at those sensors with respect to free field shear strain (at mid-depth of culvert) and input acceleration for different culvert models used in the shaking table tests.

Maximum pressures at each cell were measured at different times during the excitation. In other words, they don't act on the sidewalls of the culvert, simultaneously. As seen from the figures maximum dynamic pressure increases with increase of shear strain and rigidity of the structure as expected. Moreover, it was observed that maximum dynamic pressures occur near the corners of culvert model.
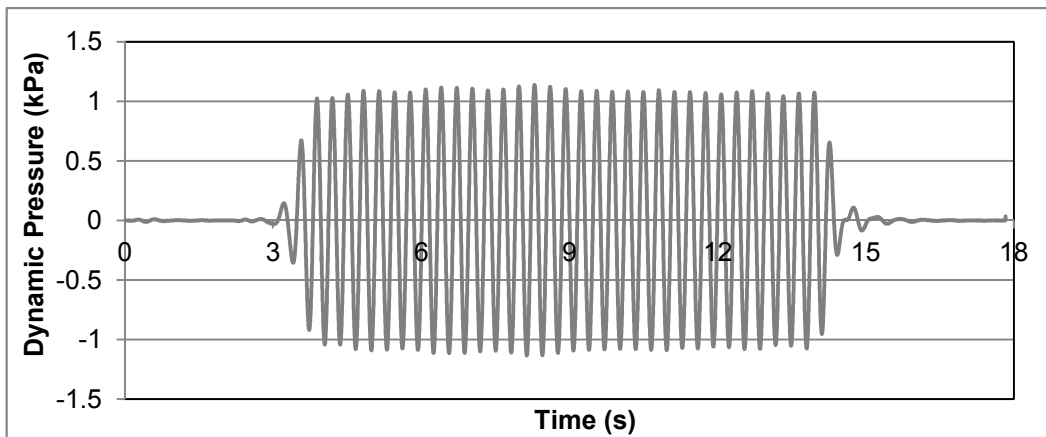
Figure 3.36. An example of dynamic pressure record
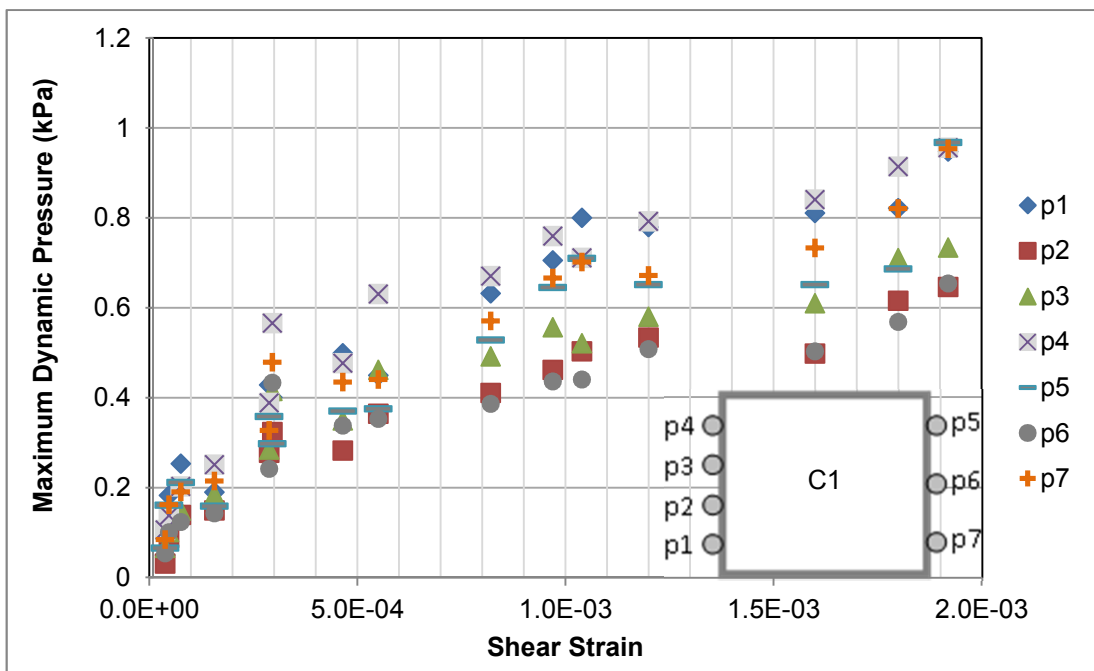
Figure 3.37. Maximum dynamic pressure variation with respect to field shear strain at culvert mid-depth for model C1.
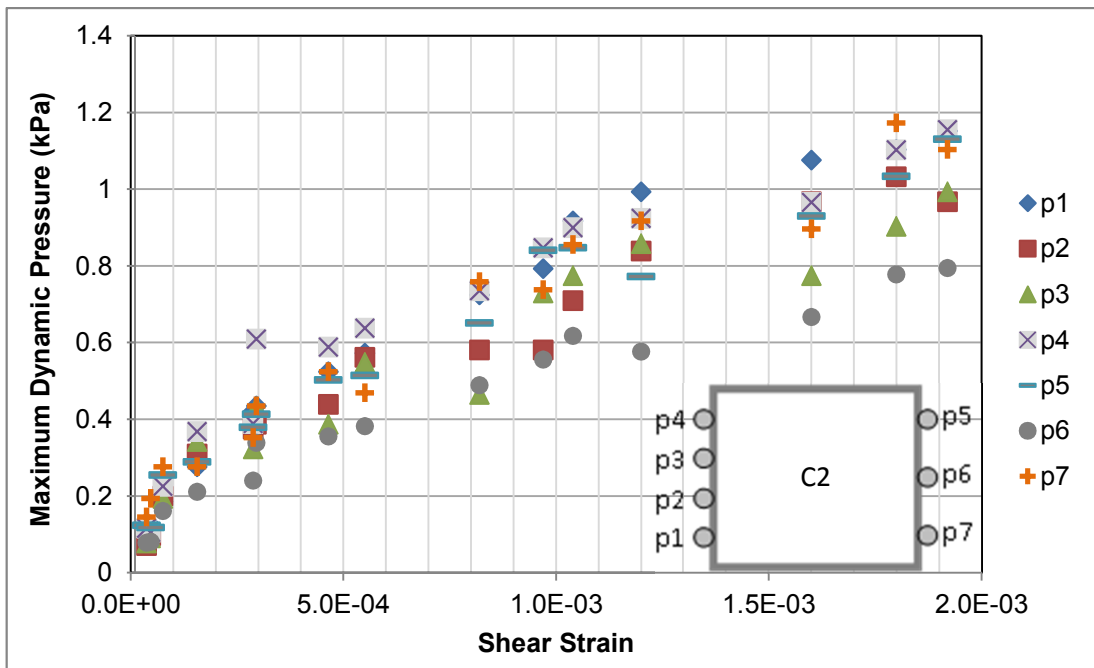
Figure 3.38. Maximum dynamic pressure variation with respect to field shear strain at culvert mid-depth for model C2.
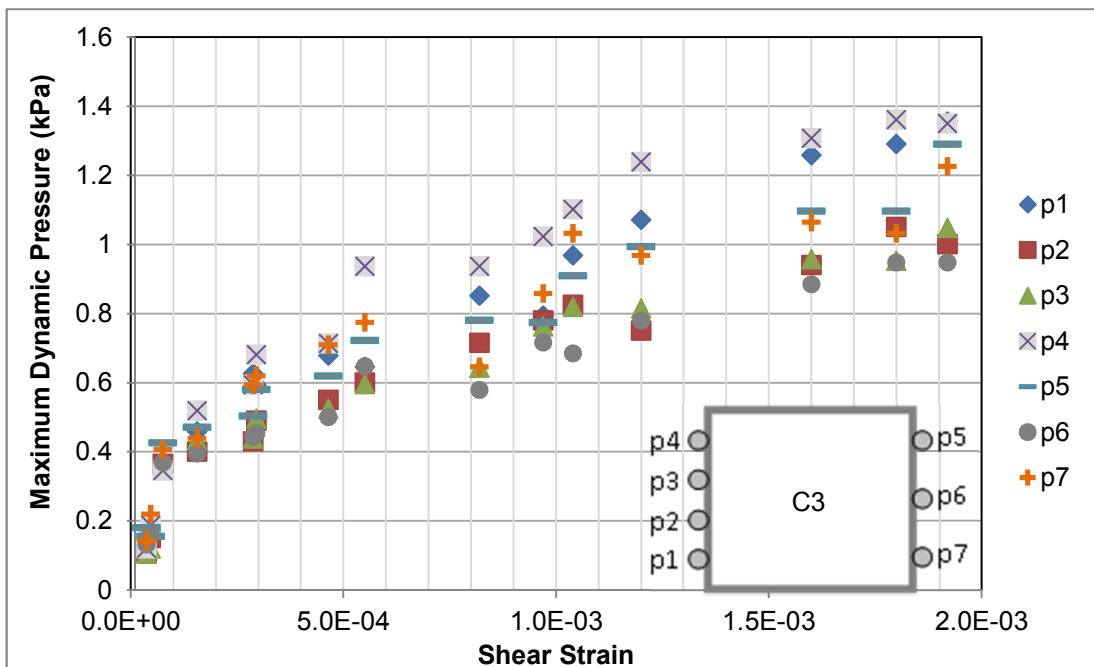
Figure 3.39. Maximum dynamic pressure variation with respect to field shear strain at culvert mid-depth for model C3.
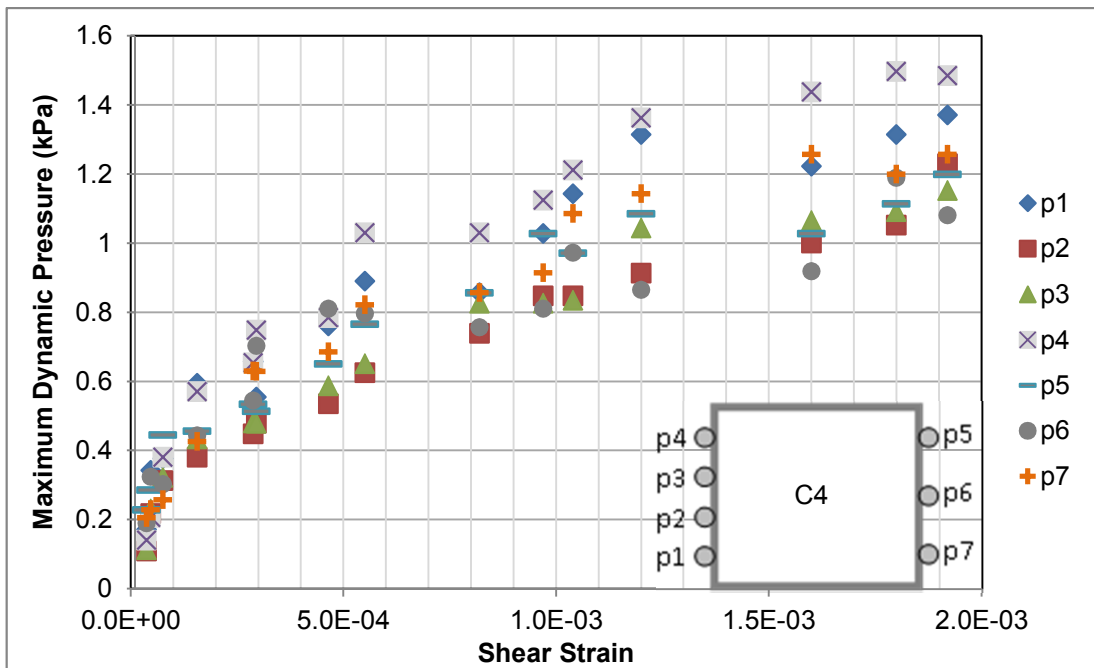
Figure 3.40. Maximum dynamic pressure variation with respect to field shear strain at culvert mid-depth for model C4.
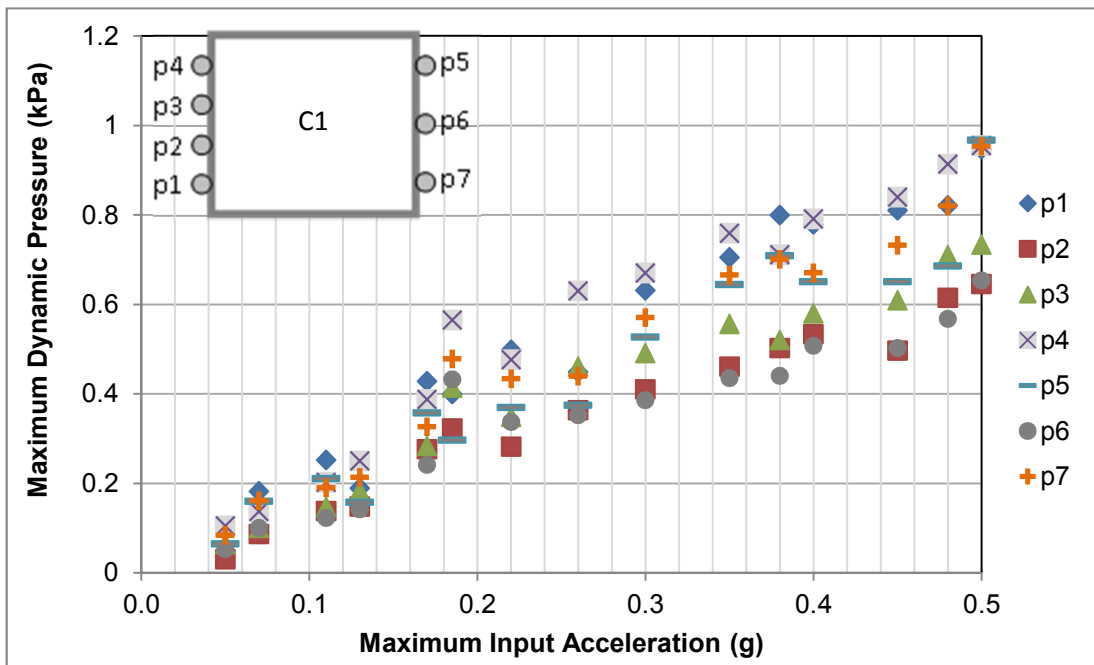
Figure 3.41. Maximum dynamic pressure variation with respect to input acceleration for culvert model C1.
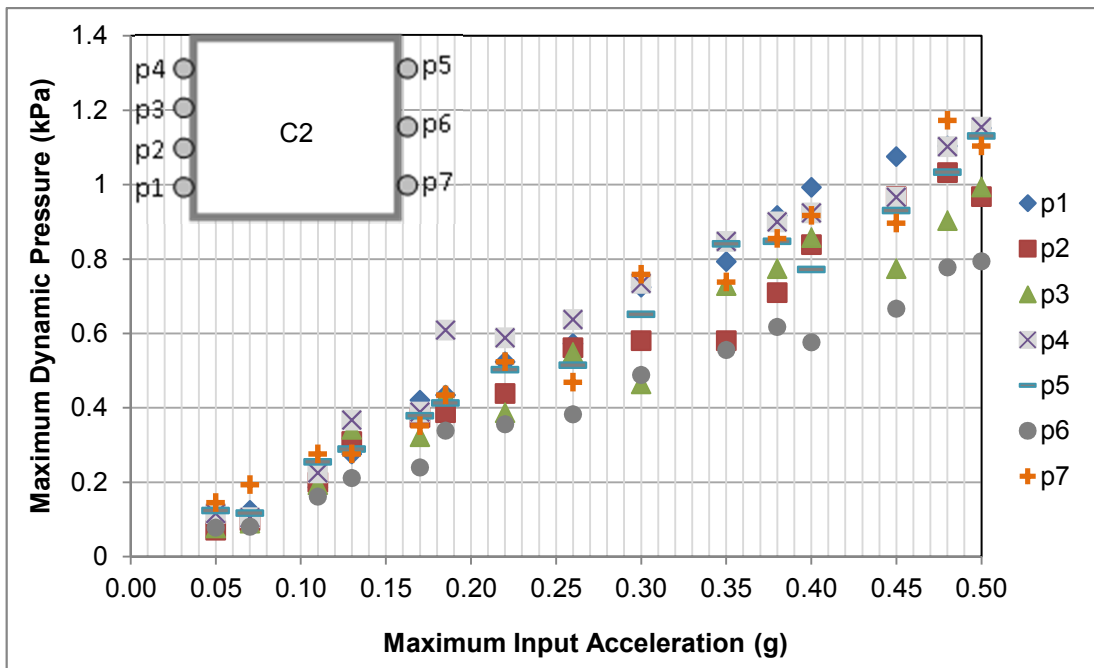
Figure 3.42. Maximum dynamic pressure variation with respect to input acceleration for culvert model C2.
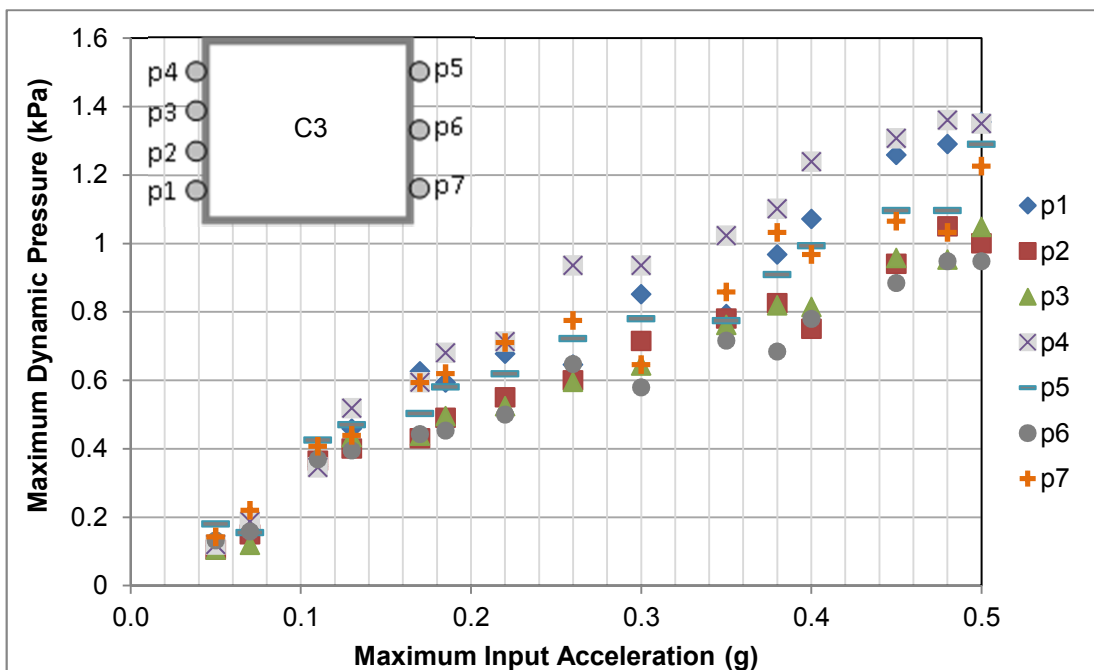
Figure 3.43. Maximum dynamic pressure variation with respect to input acceleration for culvert model C3.

106
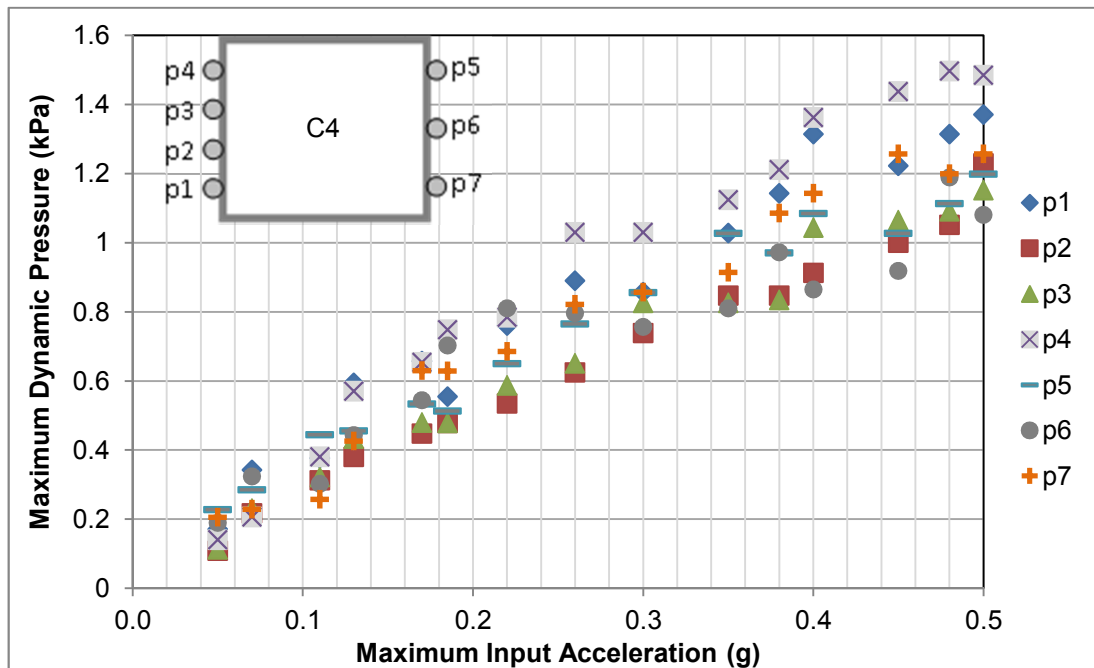
Figure 3.44. Maximum dynamic pressure variation with respect to input acceleration for culvert model C4.

3.5.7 Dynamic pressure distribution

Dynamic lateral soil pressures acting on the sidewalls of the culvert model are not constant and change during the excitation. This results in a rapidly varying pressure distribution along the sidewall of the culvert model. In order to evaluate the critical dynamic pressure distribution acting on the culvert model, the maximum bending moment at the lower slab of the culvert was calculated by considering the racking as most critical deformation mode. Based on this analysis, the pressure distributions giving the maximum bending moments were determined. In the obtained pressure distribution, there is an opposite phase angle between the recorded pressure values at same levels of left and right side of the culvert models as found in the studies of Che et al. (2006) and Nishiyama et al. (2000). When the upper left corner, UL, of the

box model is in compression, upper right, UR, corner is in tension. On the contrary, when the lower left, LL, corner is in tension, the lower right corner, LR, is in compression as illustrated in Figure 3.45. Figure 3.46 and Figure 3.47 gives the dynamic pressure time histories recorded at the corners for illustration of phase difference. This result can be interpreted by the cross-coupling forces which compel the culvert model to make racking deformation. Besides, it should again be noted that the "tension" forces do not represent the negative or suction forces. It is an indication of the reduction in the static soil pressures acting on the sidewalls of the culvert.
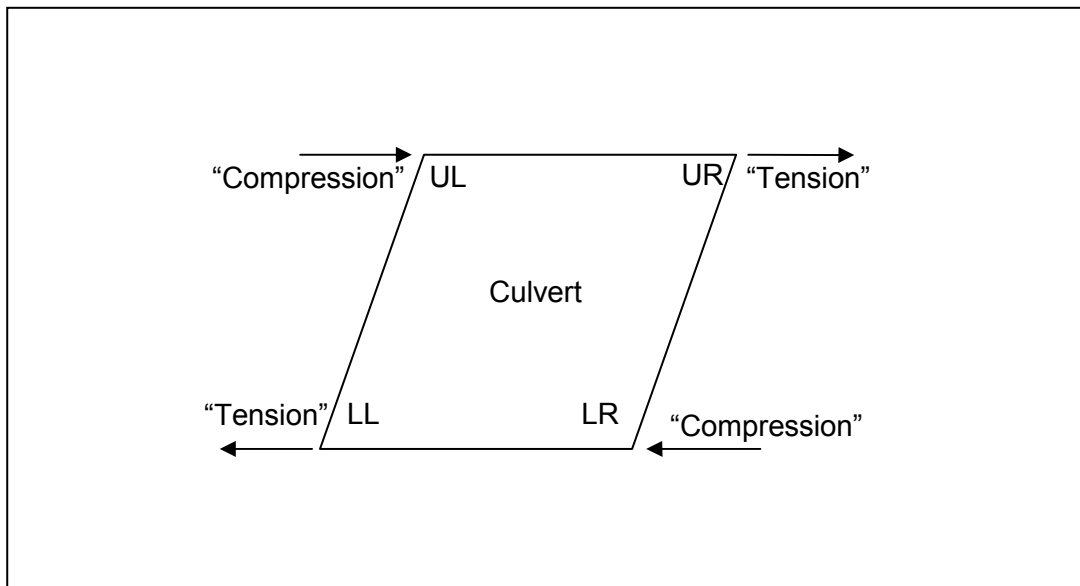
Figure 3.45. Schmetical illustration of dynamic couple forces acting on culvert box
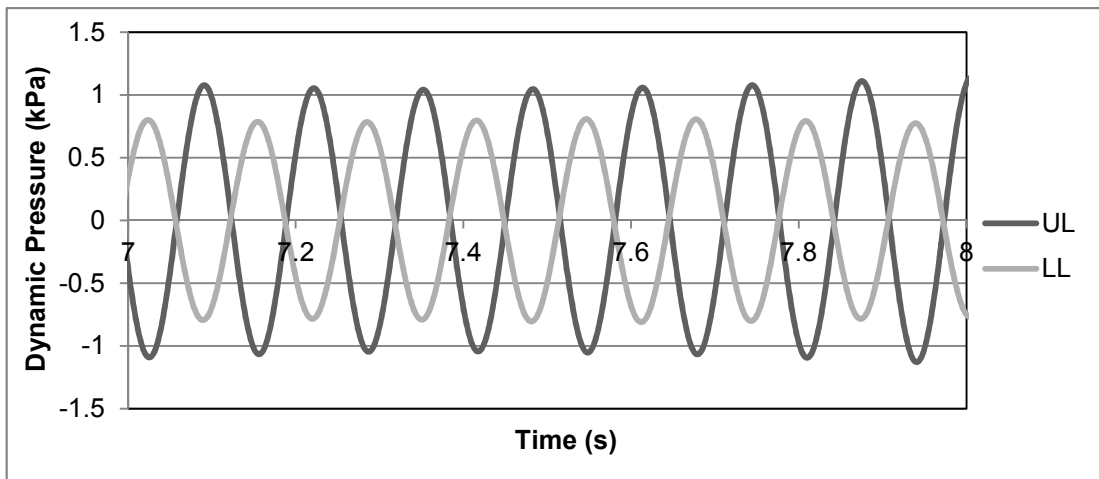
Figure 3.46. Comparison of dynamic pressure time histories recorded at upper left corner (UL) and lower left corner (LL).
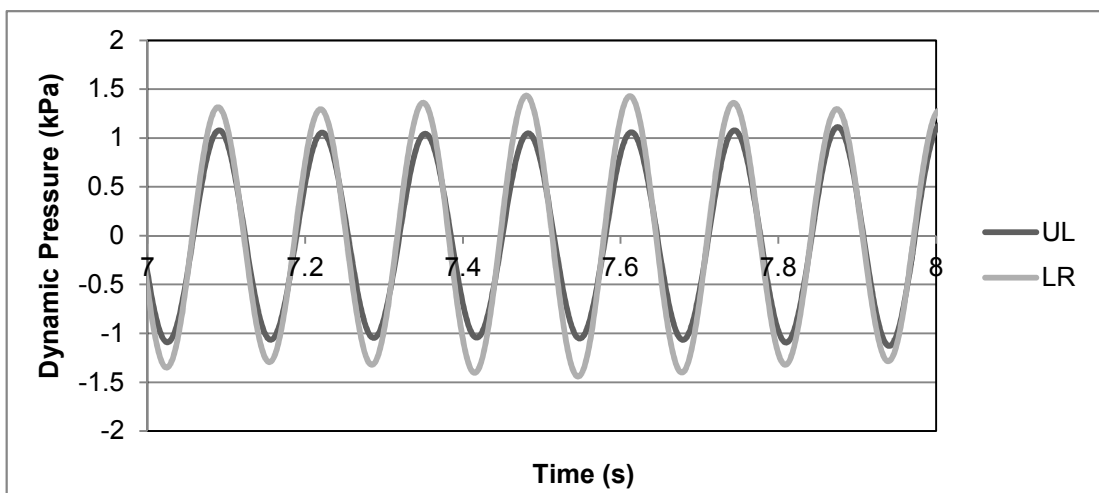
Figure 3.47. Comparison of dynamic pressure time histories recorded at upper left (UL) and lower right (LR) corner.

Figure 3.48 shows an example dynamic pressure distribution acting on the sidewalls of the culvert tested in shaking table tests. A piecewise linear interpolation was assumed and the data points were connected by straight lines. Besides, measurement points near the upper and lower parts of the culvert were extended linearly to the edges of culvert.
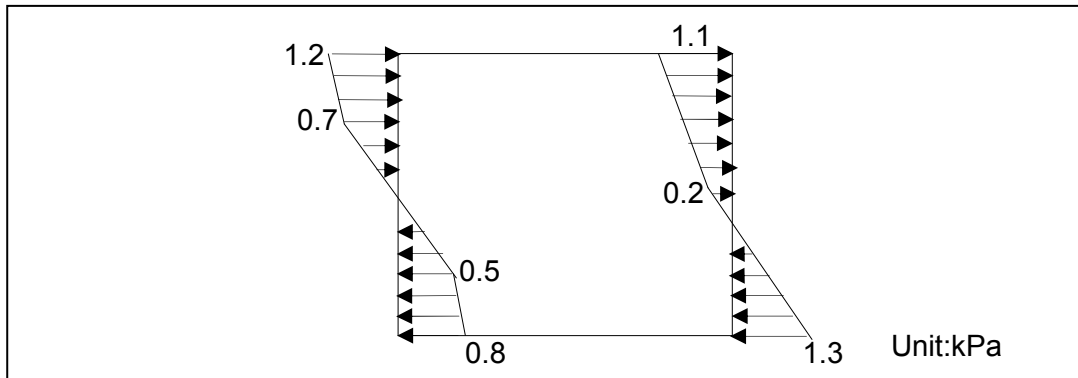
Figure 3.48. An example of lateral dynamic pressure distribution acting on sidewalls of the culvert model

3.5.8 Simplified pressure distribution

For the preliminary assessment of box-type culverts buried in dry sand, the most critical pressure distributions obtained from the shaking table measurements was simplified as given in Figure 3.49. Peak value of the triangular dynamic pressure distribution is denoted as P_d. P_d value was taken as the maximum pressure value measured at the upper corner of culvert in the shaking table tests. It was normalized with the geostatic vertical stress, $\sigma_{v,mid}$, at mid-depth of the culvert. The resulting factor was defined as dynamic lateral pressure coefficient, k_d:

$$k_d = \frac{P_d}{\sigma_{v,mid}} \tag{3.12}$$

Figure 3.50 and Figure 3.51 shows the variation of k_d with respect to free-field shear strain (at mid-depth of the structure) and maximum input acceleration for different culvert models. As mentioned in section 3.5.5, flexibility ratio of a culvert varies with the intensity of dynamic motion. It is strongly dependent on the degraded soil shear modulus and accordingly shear strain. For this reason, the culvert models are represented by initial flexibility ratio, IFR, values as given in Figure 3.50 and Figure

3.51. IFR value is defined as the ratio of maximum soil shear modulus to structural racking stiffness.
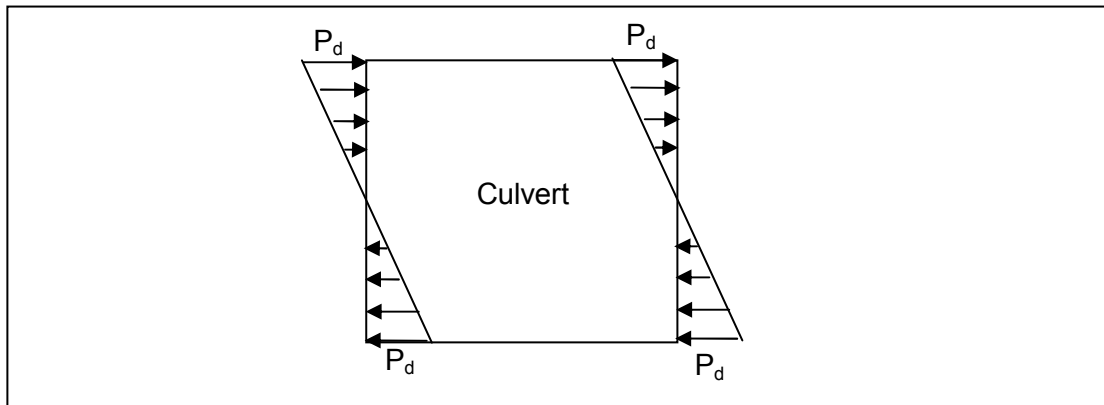
Figure 3.49. Simplified dynamic pressure distribution acting on the sidewalls of culvert
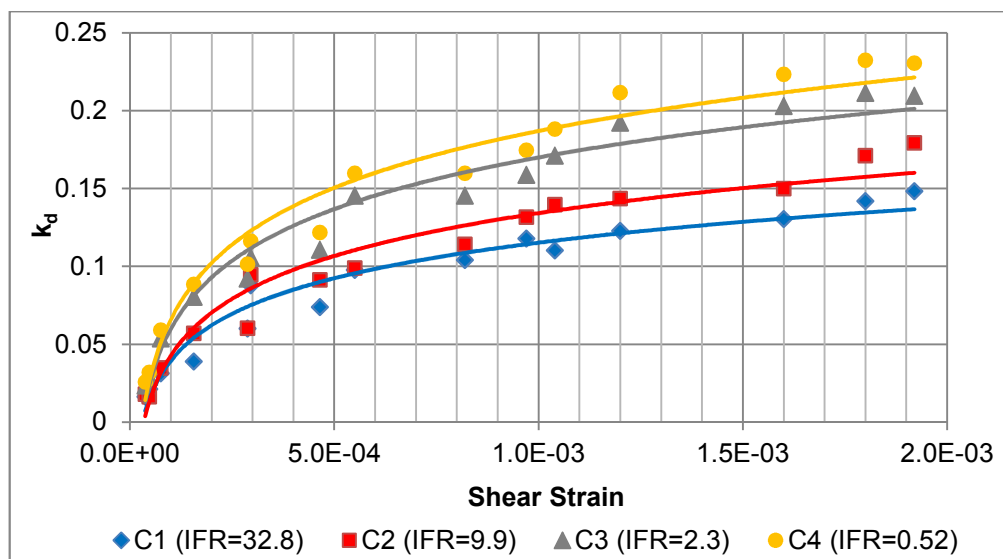
Figure 3.50. Variation of k_d (dynamic lateral pressure coefficient) with respect to free-field shear strain and IFR (initial flexibility ratio)
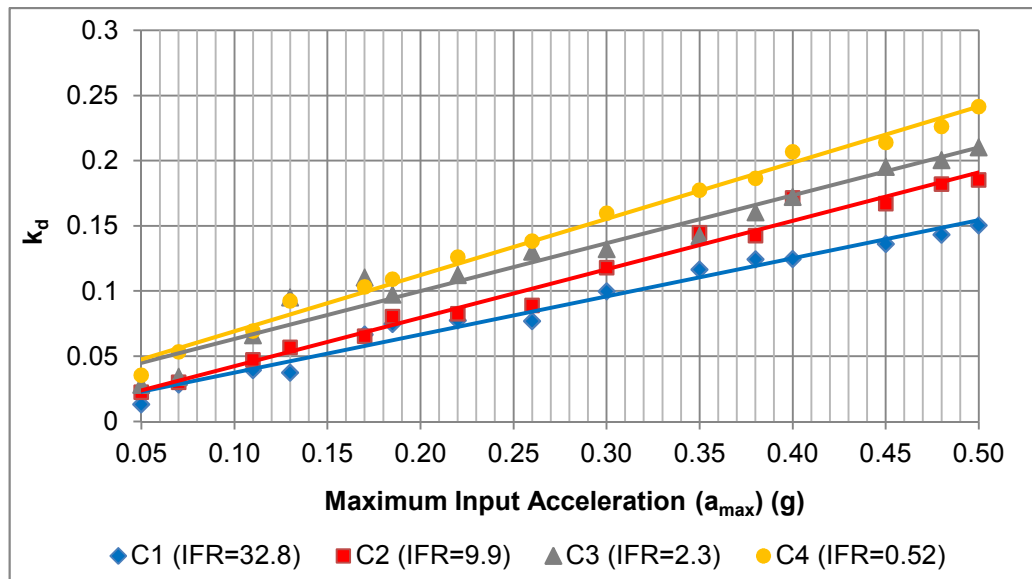
Figure 3.51. Variation of k_d (dynamic lateral pressure coefficient) with respect to maximum input acceleration and IFR (initial flexibility ratio)

The variation of k_d with respect to shear strain and maximum input acceleration were approximated by logarithmic and linear curves respectively. Approximated equations of the curves for different IFR values are given as follows:

For IFR=32.8:

$$k_d = 0.0329 \ln(\gamma_s) + 0.5005 \quad (R^2 = 0.9659) \tag{3.13}$$

$$k_d = 0.2921 \, a_{max} + 0.0082 \quad (R^2 = 0.978) \tag{3.14}$$

For IFR=9.9:

$$k_d = 0.0397 \ln(\gamma_s) + 0.4084 \quad (R^2 = 0.9518) \tag{3.15}$$

$$k_d = 0.3717 \, a_{max} + 0.0051 \quad (R^2 = 0.9938) \tag{3.16}$$

For IFR=2.3:

$$k_d = 0.0479 \ln(\gamma_s) + 0.5005 \quad (R^2\text{=0.9659}) \tag{3.17}$$

$$k_d = 0.3676\, a_{max} + 0.0264 \quad (R^2\text{=0.9718}) \tag{3.18}$$

For IFR=0.52:

$$k_d = 0.0526 \ln(\gamma_s) + 0.5505 \quad (R^2\text{=0.9659}) \tag{3.19}$$

$$k_d = 0.4307\, a_{max} + 0.0261 \quad (R^2\text{=0.9914}) \tag{3.20}$$

where, a_{max} maximum input acceleration in g and γ_s is the free-field strain at mid-depth of culvert.

The intensity of shaking is better represented by shear strain as compared to maximum input acceleration. Hence, it is recommended to estimate the dynamic lateral pressure coefficient by using the k_d versus shear strain curves shown in Figure 3.50 or corresponding approximated equations given for different IFR values. It should be noted that the given curves are valid in the range of shear strain between 0.00 and 0.002. Experimental validation is required for higher strains.

3.5.9 Effect of embedment depth

1-g shake table tests were conducted on the most flexible and rigid culvert models, (C1, C4) to investigate the variation of dynamic lateral pressure coefficient (k_d) at a different embedment depth. Culverts were buried in the model ground at a depth of 60cm. The same procedure and testing program applied previously was repeated in these tests. The embedment ratio, h/H, in the previous experiments was 2, while in the present tests was taken as 3. Figure 3.52 shows the variation of k_d with maximum input acceleration and embedment depth ratio for the culvert models C1 and C4. It was observed that k_d values were very close to each other for both

embedment depth ratios 2 and 3. This result indicate that the embedment ratio has little influence on the dynamic lateral pressure coefficient when the embedment depth ratios 2 and 3.
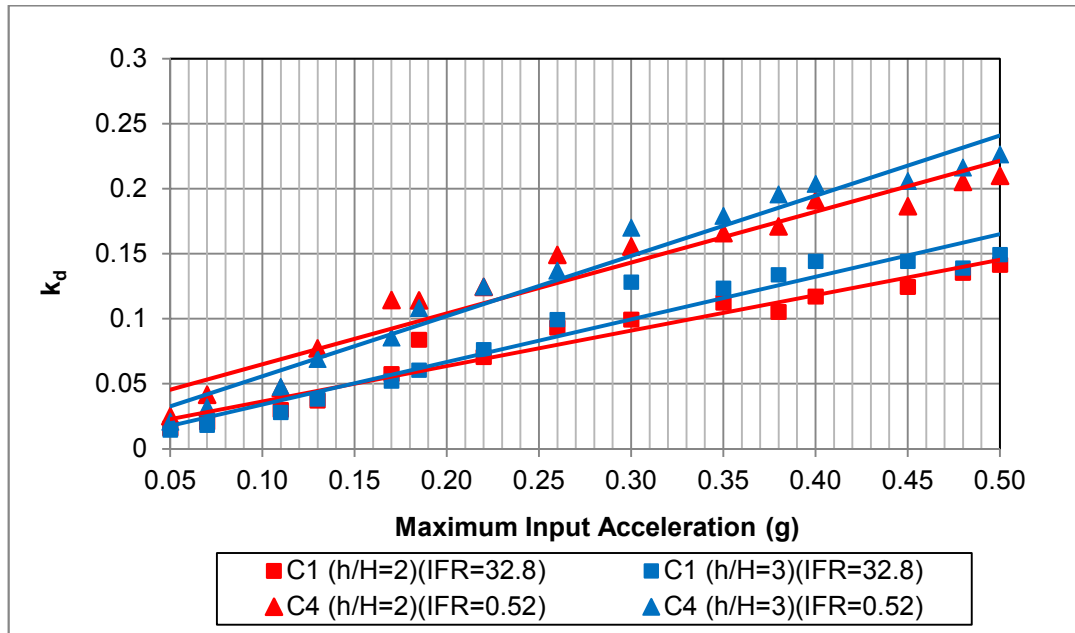
Figure 3.52. Comparison of dynamic pressure lateral coefficients at embedment depth ratios of h/H=2 and h/H=3.

3.5.10 Proposed simplified approach for the preliminary assessment of box-shaped culverts buried in dry sand

Based on the results obtained in shaking table tests, a simplified procedure was developed for the preliminary design of the box-shaped underground culverts. Considering the form of dynamic pressure distribution acting on the sidewalls of a culvert, a simplified frame model was proposed as shown in Figure 3.53. As seen from the figure, culvert model is assumed to be fixed at the bottom. Total lateral

pressure is divided into static pressure (σ_s) and dynamic pressure (σ_d). Maximum absolute values of the dynamic pressure are denoted as P_d. Additionally, there exists shear stress (τ) acting on the upper face of the culvert model.
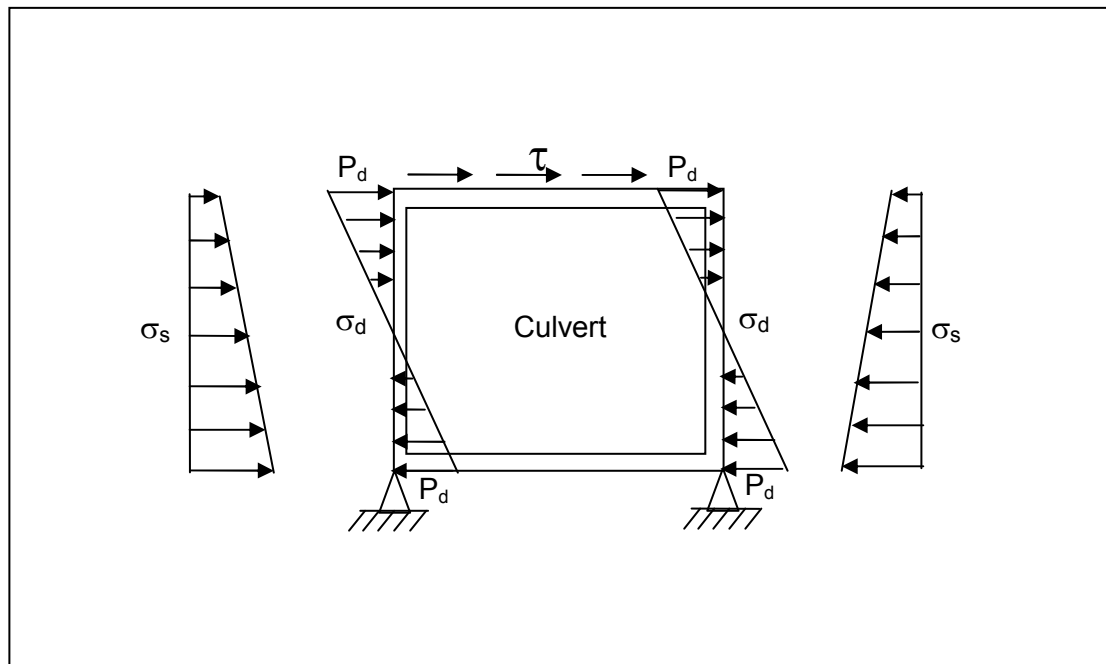
Figure 3.53. Simplified frame analysis model

All these stresses can be determined by the following ways:

i) Static Pressures

The lateral static pressure acting on the sidewalls of the underground culvert can simply be calculated by the following equation:

$$\sigma_s = K\gamma h \qquad (3.21)$$

where, γ is the unit weight of the soil, h is the soil depth and K is the lateral earth pressure coefficient. Recalling that the culvert is restrained by the soil at both sides,

the lateral earth pressure coefficient K can be taken as K_0 (at rest earth pressure coefficient). K_o can be calculated by Jaky's (1948) equation:

$$K_0 = 1 - \sin\phi'$$
(3.22)

ii) Dynamic Pressures

In order to estimate the maximum absolute value (P_d) of dynamic pressure distribution, a step by step procedure is given as follows:

1) Estimate the free-field strains around the culvert model by applying one dimensional ground response analysis.

2) Calculate the structural stiffness for a unit racking deflection using a structural analysis program. Find the initial flexibility ratio by dividing maximum soil shear modulus by the racking stiffness. For single barrel frames Equation 3.8 suggested by Wang(1993) can be used to determine the flexibility ratio.

3) Determine the lateral dynamic pressure coefficient (k_d) based on the free-field shear strain and flexibility ratio obtained in Step 1 and Step 2 by using Figure 3.50 or approximated equations (Equation 3.13, 3.15, 3.17, 3.19).

4) Calculate the maximum absolute value (P_d) of the dynamic pressure distribution by multiplying the $\sigma_{v,mid}$ by the lateral dynamic pressure coefficient, k_d.

. **iii) Shear Stresses**

The cyclic shear stresses acting on the interface between soil and culvert upper face can be estimated from one dimensional ground response analysis. An alternative way for the prediction of the cyclic shear stress is using the simplified procedure developed by Seed and Idriss (1971). In this approach, first, it was assumed that a soil column moves as a rigid body with a surface peak acceleration (a_{max})

(Figure 3.54). Based on this assumption maximum shear stress on a soil element at depth h, is given by:

$$(\tau_{max})_r = \gamma h \frac{a_{max}}{g}$$

(3.23)

where $(\tau_{max})_r$ is the maximum shear stress, γ is the unit weight of the soil and g is gravitational acceleration.
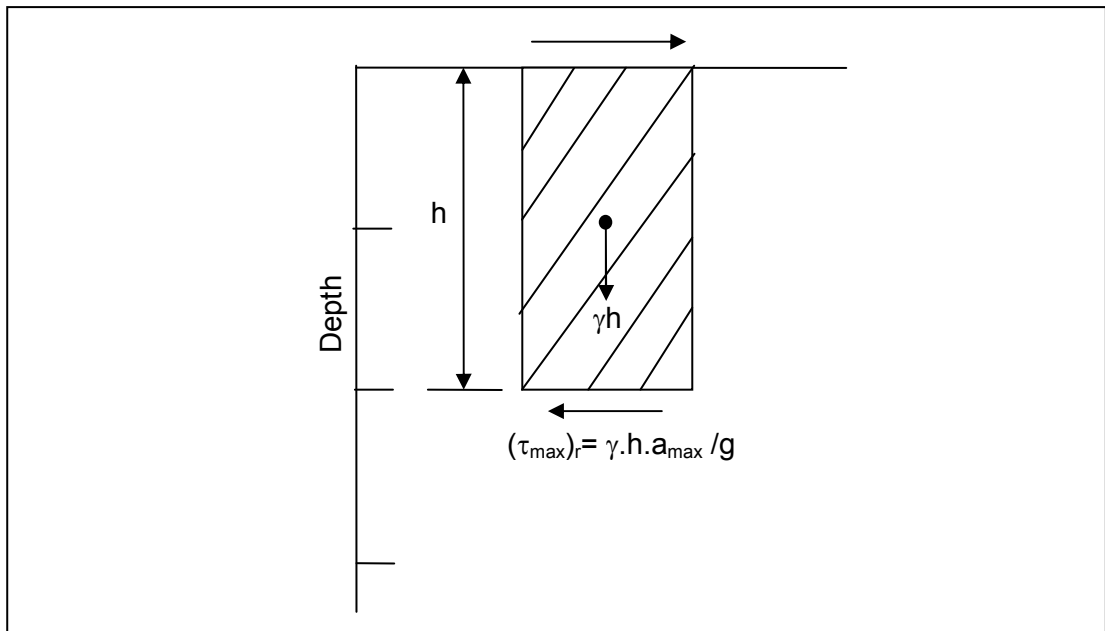
Figure 3.54. Maximum shear stress at depth h when the soil behaves as a rigid block

Next, considering that the soil is a deformable body, a stress reduction coefficient (r_d) was introduced and maximum shear stress was modified as:

$$(\tau_{max})_d = r_d (\tau_{max})_r$$

(3.24)

where $(\tau_{max})_d$ is the maximum shear stress at depth h when the soil behaves as a deformable body.

117

Finally, the maximum shear stress $(\tau_{max})_d$ is reduced by a factor of 0.65 so as to obtain the equivalent uniform cyclic shear stress. Thus, equivalent cyclic shear stress at any depth h, becomes:

$$\tau_{eq} = 0.65\gamma h \frac{a_{max}}{g} r_d \qquad (3.25)$$

Stress reduction coefficient (r_d) values can be estimated by applying the procedure of Çetin and Seed (2004). In this procedure, several response analyses were employed by statistically processing the results of the analyses. The closed form solutions for predicting the r_d values are given as follows:

If d<20 m (~65 ft) Then,

$$r_d(d, M_w, a_{max}, V^*_{s,12m}) = \frac{1 + \dfrac{-23.013 - 2.949 \times a_{max} + 0.9999 \times M_w + 0.0525 \times V^*_{s,12m}}{16.258 + 0.201 \times \exp^{0.341 \times (-d + 0.0785 \times V^*_{s,12m} + 7.586)}}}{1 + \dfrac{-23.013 - 2.949 \times a_{max} + 0.9999 \times M_w + 0.0525 \times V^*_{s,12m}}{16.258 + 0.201 \times \exp^{0.341 \times (0.0785 \times V^*_{s,12m} + 7.586)}}} \mp \sigma_{\varepsilon_{r_d}}$$

$$(3.26)$$

Else,

$$r_d(d, M_w, a_{max}, V^*_{s,12m}) = \frac{1 + \dfrac{-23.013 - 2.949 \times a_{max} + 0.9999 \times M_w + 0.0525 \times V^*_{s,12m}}{16.258 + 0.201 \times \exp^{0.341 \times (-d + 0.0785 \times V^*_{s,12m} + 7.586)}}}{1 + \dfrac{-23.013 - 2.949 \times a_{max} + 0.9999 \times M_w + 0.0525 \times V^*_{s,12m}}{16.258 + 0.201 \times \exp^{0.341 \times (0.0785 \times V^*_{s,12m} + 7.586)}}} - 0.046 \times (d - 20) \mp \sigma_{\varepsilon_{r_d}}$$

$$(3.27)$$

where, d is the depth of soil block, M_w is the moment magnitude, a_{max} is the peak ground acceleration and $V_{s,12m}^*$ is the equivalent shear wave velocity of top 12m. Standard error terms for the above equations are as follows:

If d < 12m (~40ft) Then,

$$\sigma_{\varepsilon_{r_d}} = d^{0.850} \times 0.0198 \qquad (3.28)$$

If d ≥ 12m (~40ft) Then,

$$\sigma_{\varepsilon_{r_d}} = 12^{0.850} \times 0.0198 \qquad (3.29)$$

Estimated shear stresses must be smaller than the friction between the soil and culvert. Therefore, it is suggested that the calculated shear stresses should be checked by comparing with the maximum friction. Maximum frictional stress, σ_f, can be simply calculated by using the following equation:

$$\sigma_f = \sigma_v \tan\delta \qquad (3.30)$$

where, σ_v is the overburden stress at culvert upper surface and δ is the interface friction angle between the culvert and soil.

The proposed simplified approach for the preliminary assessment of box-type culverts can be summarized as follows:

1) Calculate the static stresses acting on the sidewalls of the culvert using the at rest lateral earth-pressure coefficient.

2) Compute the free-field strains by applying one dimensional ground response analysis and estimate the lateral dynamic pressure absolute value (P_d) by using the chart (Figure 3.50) or approximated equations.

3) Estimate the shear stress acting on the interface between soil and culvert roof either from one dimensional ground response analysis or simplified procedure developed for the determination of cyclic shear stress.

4) Compare the estimated shear stress with frictional stress between the culvert and soil and use smaller one in the analysis.

5) Apply the obtained shear and lateral normal stresses on the simplified frame model as shown in Figure 3.53.

3.5.11 Comparison of Proposed Simplified Approach with Closed-Form Solutions

As described in Chapter 2, Penzien (2000) and Huo et al. (2006) proposed analytical models for the assessment of rectangular underground structures subjected to dynamic loading. In these approaches, a racking coefficient, R, was estimated by considering the relative stiffness between the soil and structure. R was defined as the ratio of structure deformation to free-field deformation.

Racking ratios of culvert models tested with 1-g shake table were estimated by using the closed-form solutions. Results were compared with the predictions of suggested simplified procedure. Figure 3.55 indicates the variation of estimated racking ratio values with respect to flexibility ratio, FR. For FR values greater than 5, proposed simplified approach gives higher racking ratios as compared to Penzien (2000) and Huo et al. (2006) closed-form solutions. On the other hand, for FR values less than 5, the closed-form solutions predict higher racking ratios. It should be noted that the below chart is very sensitive to maximum and degraded shear modulus. Therfore, determination of shear modulus is the most important step when calculating the racking ratios.
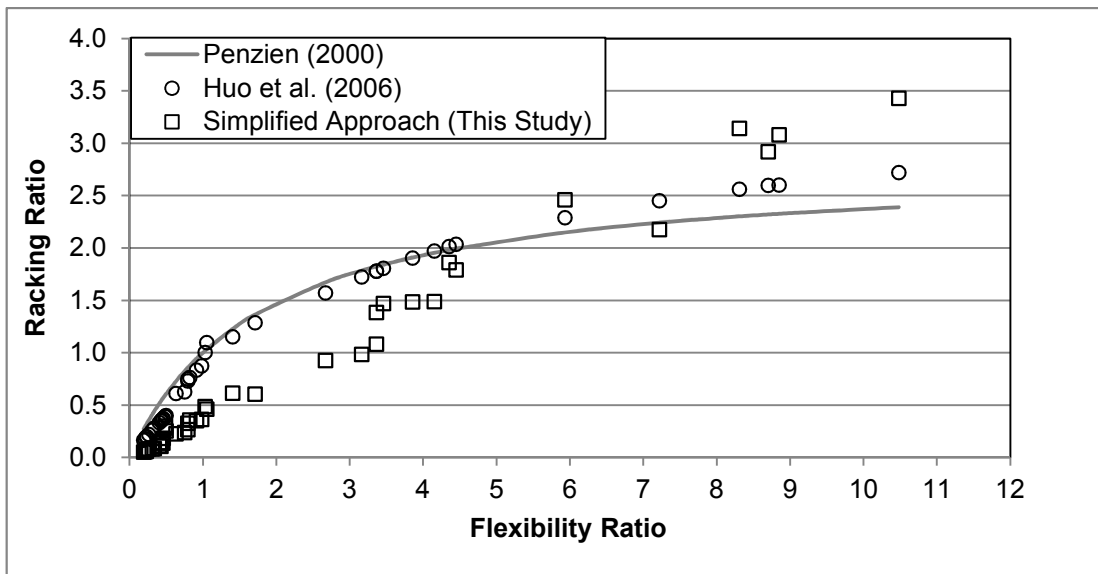
Figure 3.55. Comparison of simplified approach's results with analytical solutions

CHAPTER 4

DYNAMIC CENTRIFUGE TESTS ON A FLEXIBLE BOX CULVERT AND COMPARISON OF RESULTS WITH SIMPLIFIED APPROACH

4.1 Introduction

In the 7th Framework Programme of the European Community, selected research teams can access the seismic engineering infrastructures in Europe under the SERIES (Seismic Engineering Research Infrastructures for European Synergies) project. A transnational access (TA) project with Grant Agreement No. 227887,led by Middle East Technical University (Turkey) in conjunction with University of Kaiserslautern (Germany) was accepted and committed to IFSTTAR (Institut français des sciences et technologies des transports, de l'aménagement et des réseaux)-France for using the centrifuge facility. The TA project is called as DRESBUS which is the shortened title of "Centrifuge modeling of dynamic behavior of box-shaped underground structures in sand".

The aim of the TA research is to investigate the dynamic response of box-shaped underground structures experimentally under harmonic motions. The major variables considered in this research are the relative stiffness between the structure and soil and intensity of shaking. TA project has just started in 2011 and the centrifuge tests were conducted only for free-field condition and flexible underground structure. The centrifuge system, the methodology and the results of the tests for the flexible underground structures are discussed in detail in the following sections.

4.2 Centrifuge test system

Centrifuge tests were carried out in the LCPC-IFSTTAR geotechnical centrifuge laboratory in Nantes-France. The geotechnical centrifuge is a beam type centrifuge with a swinging basket platform. The radius of the centrifuge is 5.5m and the dimensions of swinging platform are approximately 1.4m x 1.2m. The centrifuge is capable of carrying a maximum payload capacity of 2 tones model at a centrifugal acceleration of 100g. General view of the geotechnical centrifuge at LCPC-IFSTTAR is illustrated in Figure 4.1.

Figure 4.1. General view of the beam centrifuge at IFSTTAR

In order to make dynamic tests in geotechnical centrifuge, an earthquake simulator system is placed into the basket. The system includes a flexible equivalent shear box model container, shaker and counter weights. Base excitation is given by the shaker only in horizontal direction. The shaker can simulate harmonic motions and real earthquake motions.

4.2.1 Earthquake simulator

An electrohydraulic shaker was used in the centrifuge tests. The shaker can generate multiple successive shakings without stopping the centrifuge during the flight. It is capable of generating 1-dimensional harmonic or real earthquake motions. In this study, centrifuge test were performed by using only harmonic motions. The motions are produced by a linear hydraulic actuator to drive the 400kg payload capacity shake table mounted on hydraulic bearings. The displacement of the actuator and oil flow can be controlled by a servo-valve. For harmonic motions, the actuator has a peak displacement of 5mm in model scale. Frequency range changes between 20-200Hz (model scale) and maximum duration of the sinusoidal input signal is 1 second (model scale). Peak acceleration that can be produced by the shaker is 0.5g (prototype scale). The cross section of the shaker system is depicted schematically in Figure 4.2.
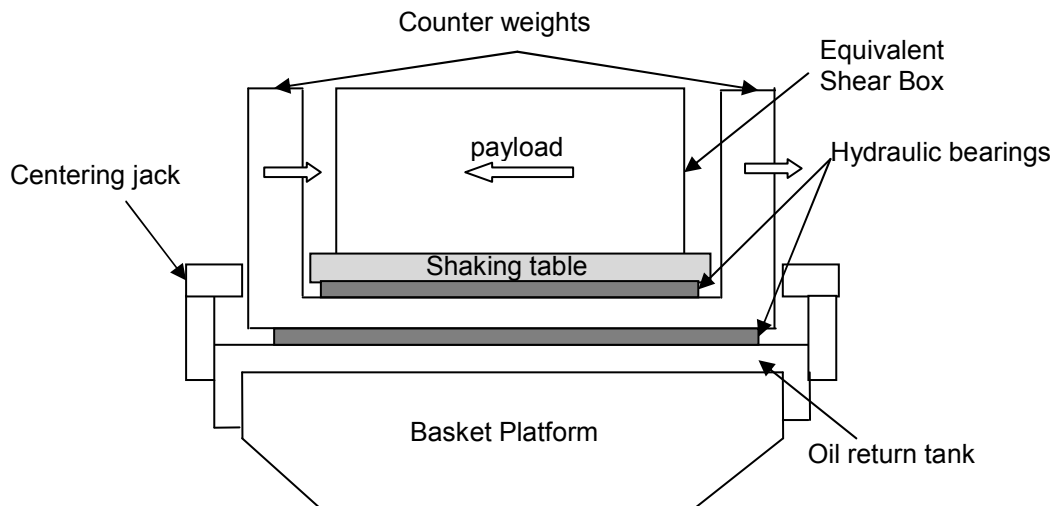
Figure 4.2. Schematic view of the shaker system

4.2.2 Soil container

The flexible soil containers such as laminar box or equivalent shear beam (ESB) box are commonly preferred by the researchers in the dynamic model tests. Thus, free-field boundary conditions are approximated and the soil can deform in a shear mode. Within the scope of this study, an ESB container was used in the dynamic centrifuge model tests. The soil container has internal dimensions of 0.80m (length) x 0.35m (width) x 0.41m (height). For a 40g centrifugal acceleration, the prototype dimensions of the container is 32m in length, 14m in width and 16.4m in height. The ESB box consists of 15 aluminum alloy frames separated by rubber sheets. The box is restrained in transverse direction and allowed to move in longitudinal direction during shaking. General view of the equivalent shear beam box is shown in Figure 4.3.
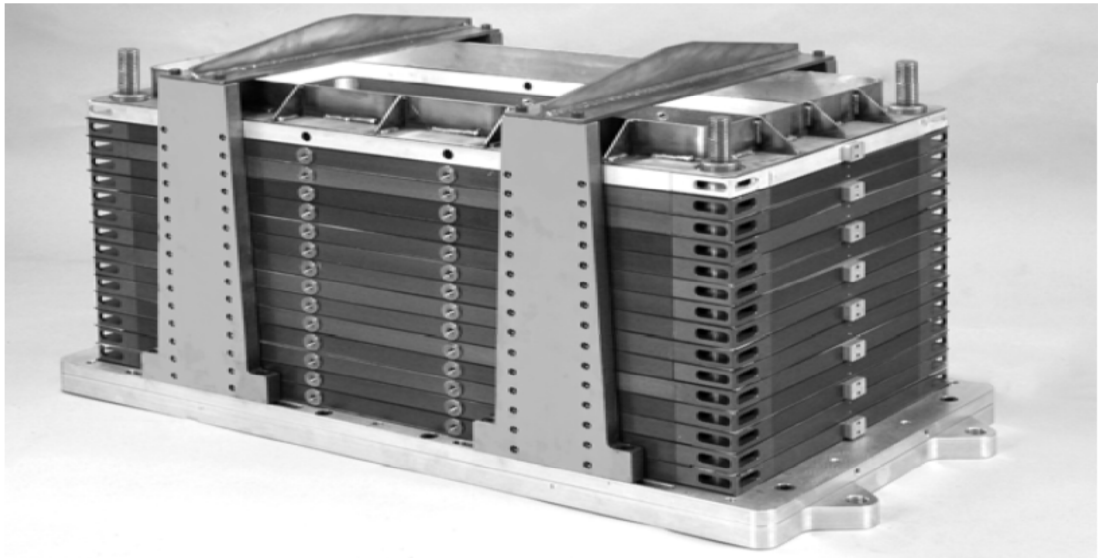
Figure 4.3. General view of the equivalent shear beam box designed by IFSTTAR

4.2.3 Data acquisition system

An onboard computer was installed on the centrifuge arm so that data acquisition system placed in the swinging basket is controlled by the computer, remotely. LMS Scadas data acquisition system was used during the centrifuge tests. It is a high flexible card with various signal conditioning modules. There are 72 channels for voltage, ICP accelerometers and 48 channels for strain gauge, voltage and ICP accelerometers. The card incorporates 24bits Analog to Digital Converter with a maximum sampling rate of 25kHz. Data are collected by LMS data acquisition system and sent to control room over the wireless network.

4.2.3.1 ICP accelerometers

Bruel Kjaer model piezo-electric accelerometers were used in the tests. They are lightweight and sufficiently small to be used in centrifuge model tests. There are totally twenty six accelerometers buried in sand and placed on the culvert model.

4.2.3.2 Strain gauges (Extensometers)

Two systems of extensometers were developed by IFSTTAR and GAROS for measuring the deformations of buried culvert model. The first system (Figure 4.4) was designed to determine the displacement profile of the side walls of culvert model due to soil pressure under dynamic loading. In this system, there are 5 pairs of independent extensometers (thin metal rods) located on the left and right side of the box model at different levels (Figure 4.5). Strain gauges were placed on the rods to measure the deformation of the walls at each level. In order to satisfy the stability of the system, the extensometers were attached to a rigid body fixed to the bottom slab of the box. The displacements of the side walls were determined by measuring the change in voltage proportional to the deformations of the extensometer.
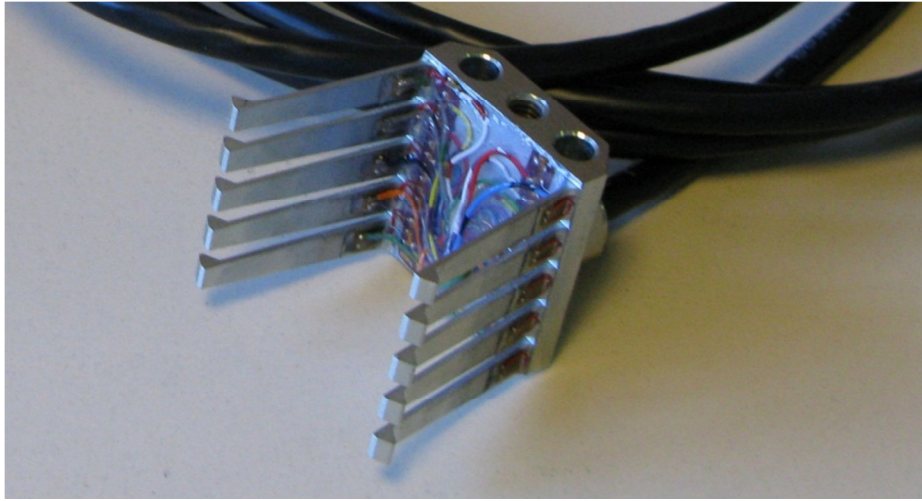
Figure 4.4. General view of the extensometer system measuring the lateral displacement of the side walls.
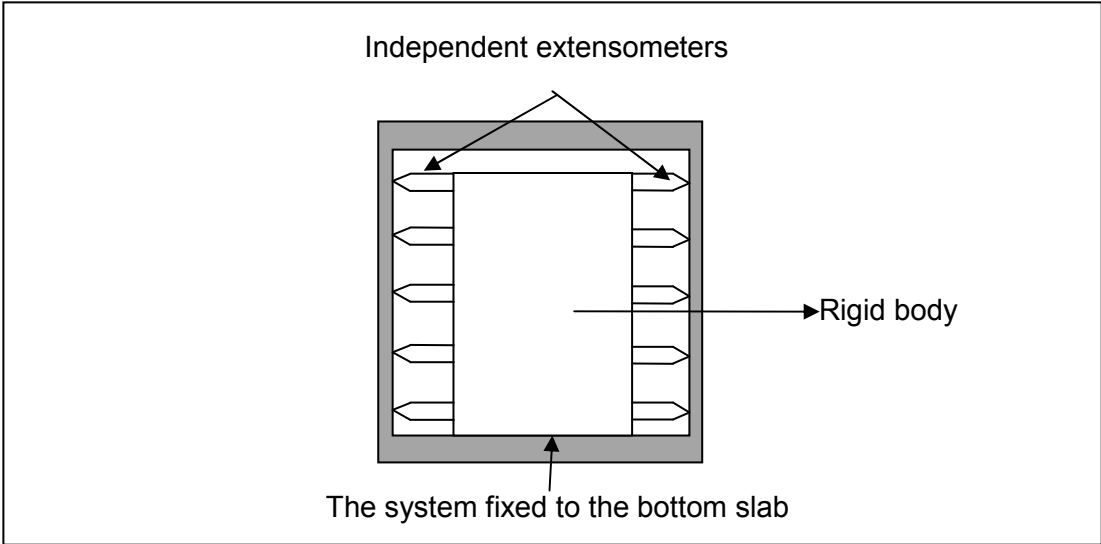
Figure 4.5. Cross section view of the extensometer system measuring the lateral displacement of the side walls.

The second system (Figure 4.6) was developed for measuring the racking deformation of the buried culvert model. For this purpose, a strain gage type extensometer was placed diagonally inside the box. It was designed as stiff as possible so as to avoid its resonance frequency under dynamic loading. The measuring principle of the system is based on the change in chord length of the extensometer. The diagonal extensometer was placed into the culvert model with an arch form (Figure 4.7). As the model deforms the strain gages located at mid-span of the extensometer measure the deformation of arch. There were totally four diagonal extensometers used in the centrifuge tests. Two of them were located near the central section and the others were located near the both extremities of the culvert model.
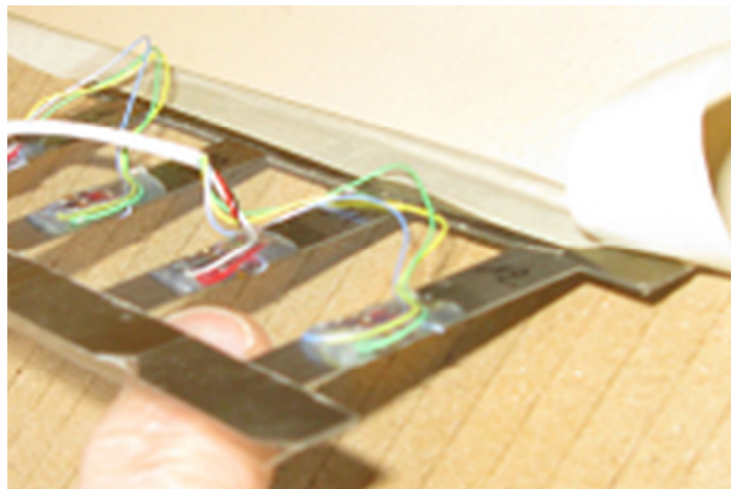
Figure 4.6. General view of the diagonal extensometer system measuring the racking deformation
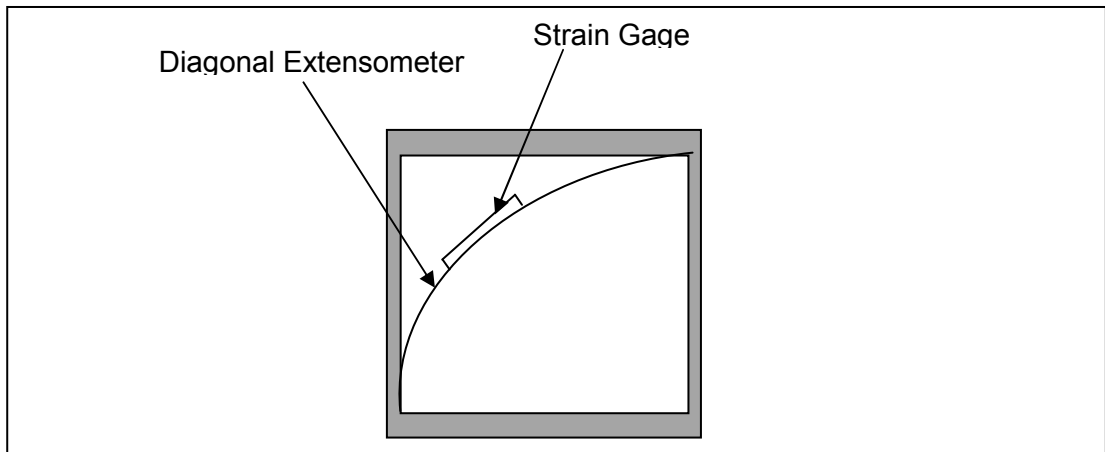
Figure 4.7. Schematical drawing of the diagonal extensometer placed in the culvert model

4.2.4 Physical properties of the sand

Dry Fontainebleau sand was used in the dynamic centrifuge tests. It is uniform silica fine sand with rounded particles. Average particle size diameter (D_{50}) of the Fontainebleau Sand is 0.20mm. The sand was placed into the equivalent shear beam box at a relative density of 70%. Physical properties of the sand are presented in Table 4.1.

Table 4.1. Physical properties of the dry Fontainebleau Sand determined by IFSTTAR

	Fontainebleau Sand
Minimum void ratio	0.55
Maximum void ratio	0.86
Minimum unit weight (kN/m^3)	13.93
Maximum unit weight (kN/m^3)	16.78
Mean diameter (D_{50}) (mm)	0.20
Specific gravity	2.64
Friction Angle	38°

Maximum shear modulus of the Fontainebleau sand was estimated by using the following relationship proposed by Hardin and Drnevich (1970):

$$G_{\max} = 3230.\frac{(2.973-e)^2}{(1+e)}.OCR^k.(\sigma'_m)^{1/2} \tag{4.1}$$

where $G_{\max}$ is the maximum shear modulus in kPa, e is the void ratio, OCR is the overconsolidation ratio, k is a parameter depending on the plasticity of soil and σ'_m is the mean effective stress in kPa. For a relative density of 70%, the maximum shear modulus at mid-depth of the culvert was estimated as 56500kPa.

4.2.5 Preparation of model ground

Sand pluviation method was used to obtain a consistent and uniform soil density for the dynamic centrifuge tests. Dry Fontainebleau sand was pluviated into the ESB box by means of IFSTTAR automatic hopper. Falling height of the hopper was tried to be kept at 60cm during sand filling operation. A sketch and a photo of the pluviation system are depicted in Figure 4.9. Density control boxes were placed in the box to measure the relative density of the soil. Besides, Cone Penetration Tests (CPT) were conducted in centrifuge to check the uniformity and repeatability of the sand specimen filled by pluviation. The tests were performed without measuring the side friction, before and after shake. The CPT device (Figure 4.8) was equipped with a force sensor having 12mm diameter at the rod tip for measuring the cone resistance (q_c). It is on board and can be loaded remotely during the flight. CPT test procedure can be summarized as follows:

1) The device is installed in the swinging basket before starting the centrifuge.
2) The centrifuge is started and the model is then spun up to 40g.
3) At 40-g level CPT test is performed and data are taken remotely.
4) The centrifuge is then switched off and CPT device is taken out.
5) Laser displacement sensors were placed above the sand surface to measure the settlements after shaking.

6) After shaking the centrifuge, same procedure (1-4) is repeated.

Measurements showed that a homogeneous model ground was attained at a relative density of 70%.
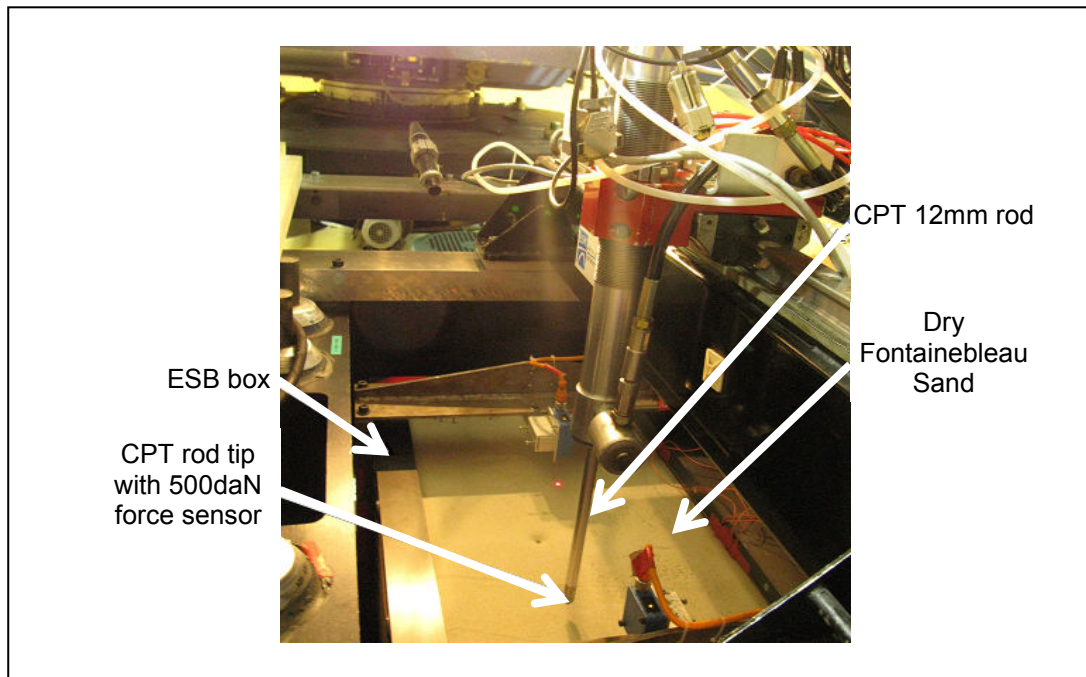
Figure 4.8. General view of CPT device in IFFSTAR

4.2.6 Reduction scaling and scale effects

The equivalent shear beam (ESB) box used in the centrifuge experiments was designed for 40g centrifugal acceleration. Considering the performance of the ESB box, the centrifuge tests were performed under the 40g gravitational field to simulate the prototype. Table 4.2 presents the scaling rules for a 40g centrifugal acceleration.
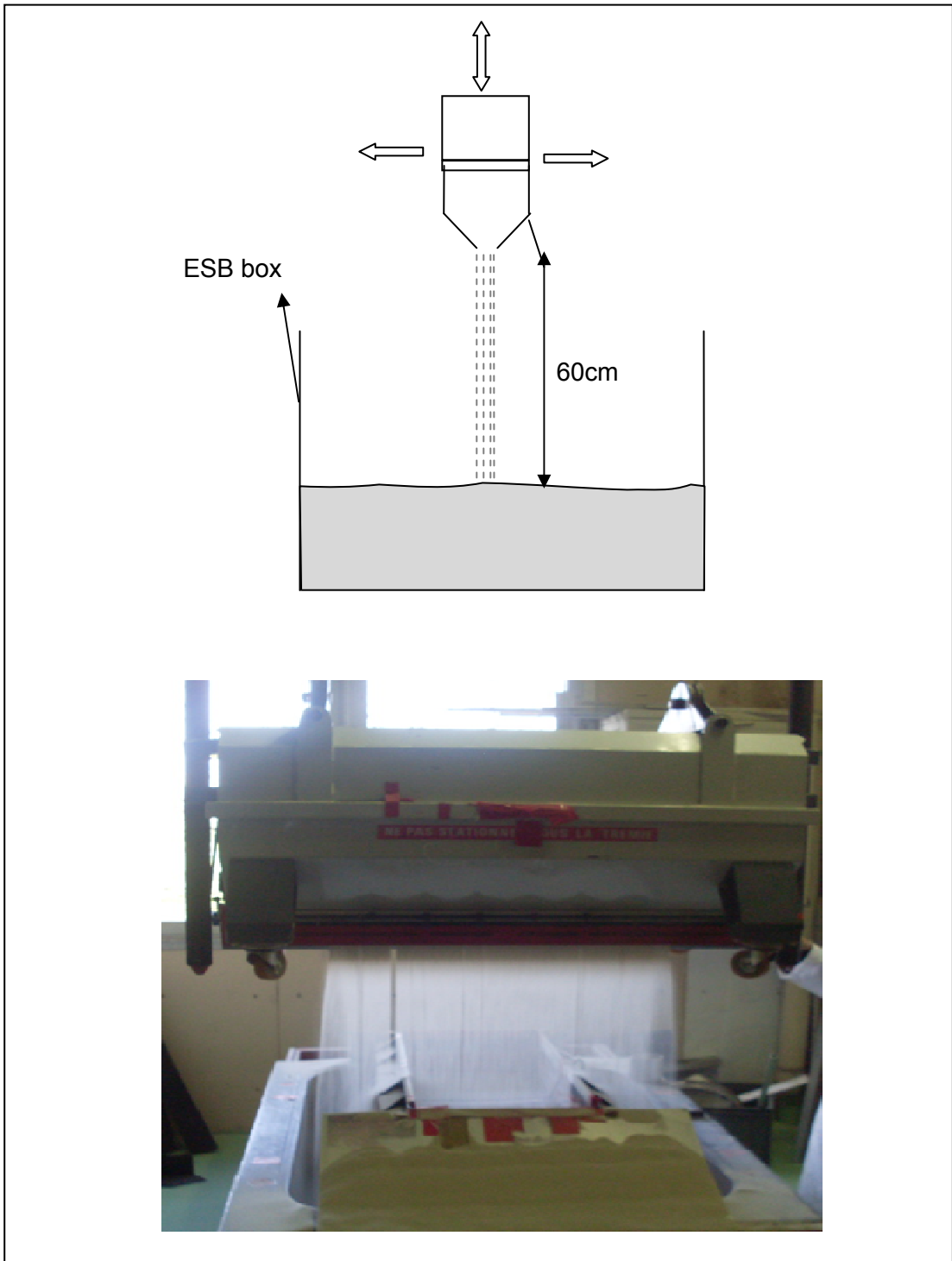
Figure 4.9. Schematic drawing and photo of sand pluviation in IFSTTAR

Table 4.2. Scaling rules for a 40g centrifugal acceleration.

Parameter	Prototype	Model
Gravity	1	40
Length	40	1
Area	40^2	1
Volume	40^3	1
Mass	40^3	1
Force	40^2	1
Energy	40^3	1
Stress	1	1
Strain	1	1
Mass density	1	1
Energy density	1	1
Acceleration	1	40
Time (dynamic)	40	1
Time (diffusion)	40^2	1
Velocity	1	1
Frequency	1	40

Acceleration within the model increases from surface to the bottom of the model due to the increase in radius. In the present study, the region around the culvert model is of interest for evaluating the dynamic response of the box culverts. For this reason, at the mid-depth of the culvert model z_{Ng}=7.5cm, R_{Ng}=4.794 was taken as the reference radius. For a scale factor of N, the centrifugal acceleration $A(z_{Ng})$ is given as follows (Taylor, 1995):

$$A(z_{Ng}) = \omega^2 R_{Ng} = Ng \qquad (4.2)$$

Similarly, the centrifuge acceleration *A(z)* at any depth z in the model can be expressed as:

$$A(z) = \omega^2 R_z \qquad (4.3)$$

where ω is the natural circular frequency and the radius at depth z R_z:

$$R_z = R_{Ng} + (z - z_{Ng})$$ (4.4)

The vertical stress σ_z at any point in the model at depth z can be given by:

$$\sigma_z = \int_0^z \rho A(z) d(z)$$ (4.5)

Then, following equation is obtained by substituting Equation 4-3 and 4-4 into Equation 4-5,

$$\sigma_z = \int_0^z \rho \omega^2 \left[R_{Ng} + (z - z_{Ng}) \right] d(z)$$ (4.6)

Solution of Equation 4-6 is given by:

$$\sigma_z = \rho Ng \left[z + \frac{z^2}{2R_{Ng}} - \frac{z_{Ng} z}{R_{Ng}} \right]$$ (4.7)

Equation 4-7 gives the stress at depth z in the model under a gravitational field of Ng. At the prototype scale the stress can be defined as:

$$\sigma_z = \rho g z_p$$ (4.8)

where z_p is the depth in the prototype. If the stresses are to be the same in model and prototype, then z_p is computed as follows:

$$z_p = N \left[z + \frac{z^2}{2R_{Ng}} - \frac{z_{Ng} z}{R_{Ng}} \right]$$ (4.9)

where N=40, z_{Ng}=0.075m and R_{Ng}=4.794m

The average grain size (D_{50}) of the Fontainebleau Sand used in the centrifuge tests is 0.2mm. Minimum dimension of the culvert model is 4.7cm. Thus, the ratio of model size to average grain size is calculated as 235. This ratio is high enough to avoid grain size effects.

4.2.7 Design and manufacturing of the culvert model

The underground culvert model was manufactured by IFSTTAR. It was made of Aluminum 2017. In order to avoid fabrication stresses and strains, it was preferred to be manufactured by extrusion instead of welding. Dimensions of the culvert model were determined by considering the following features:

1) Ratio of length to the cross section dimensions of the culvert model should be as high as possible to satisfy the plain strain condition.

2) Boundary effect: The culvert model should be placed in the middle of the boundary so as to eliminate the boundary effects. Distance between the model and side boundaries should be kept as much as possible.

3) Relative stiffness between the culvert model and soil: Thickness of the walls and slabs were determined by computing the relative stiffness.

4) Structural deformations due to dynamic loading: Slabs should be thick enough to prevent the bending deformation due to dynamic loading.

5) Prototype dimensions: Scaling ratio and the model dimensions should be optimized together to represent the prototype dimensions.

6) Instrumentation: Sensor size should not be too big as compared to culvert model dimensions.

Based on the features given above, the culvert model dimensions were specified as 4.7cm (width) x 5cm (height) in cross section and 35cm in length. Thickness of the slabs and side walls were determined as 6mm and 1.5mm, respectively. Based on

the scaling rules, corresponding prototype dimensions of the culvert are 1.88m (width), 2.00m (height) and 14m (length).

Extremities of the tunnel section were closed with thin teflon plates. Thus, sand did not enter the culvert and friction between the culvert and equivalent shear beam box was reduced. In order to provide free movement at culvert ends under dynamic loading, two pieces of foam was placed between the culvert and teflon plate at both extremities. Due to the small stiffness of the foam material, culvert model can easily move during the dynamic centrifuge tests. Cross section and longitudinal section of the culvert are given in Figure 4.10.
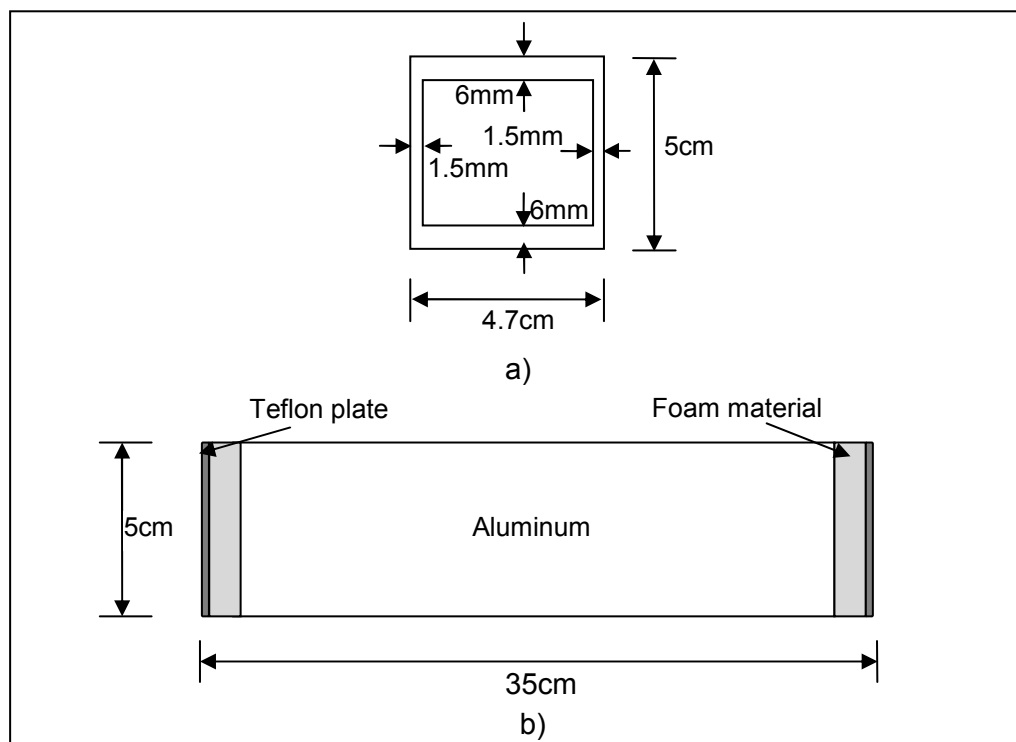
Figure 4.10. a) Cross section of the culvert model b) Longitudinal section of the culvert model

136

4.2.8 Test instrumentation

There are totally twenty six accelerometers used in the centrifuge tests. Two accelerometers were set on the upper and lower parts of culvert model for assessing the racking deformation while others were buried in the soil and placed on the ESB box. Layout of the accelerometers is indicated in Figure 4.11.
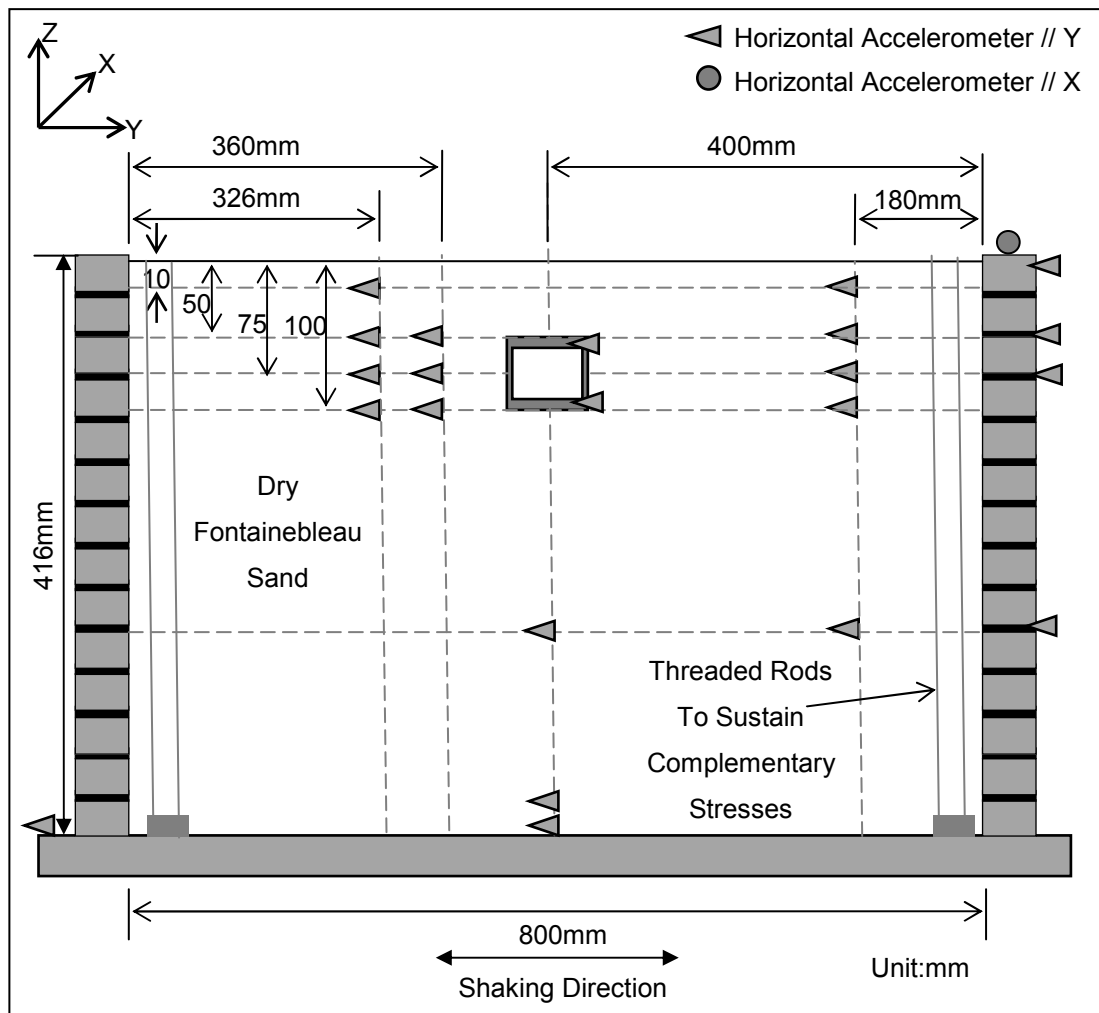
Figure 4.11. Layout of the accelerometers used in the centrifuge tests.

The box culvert was buried in Fontainebleau sand at a depth of 7.5cm. Five pairs of horizontal extensometers were mounted on side walls at different heights to measure the lateral deformations (Figure 4.12). They were located in the central section of the culvert. Four pairs of diagonal extensometers were placed diagonally for evaluating the racking deformations (Figure 4.12). Two of them were near the central section and others near the ends of the culvert.

Figure 4.12. Layout of the extensometers inside the culvert model

4.2.9 Test procedure

The centrifuge tests were performed on the flexibility culvert model under harmonic motions. Inertial dimensions of the culvert are 44mm (width), 38 mm (height) and 350mm (length). Thickness of the roof and invert slabs are 6mm and thickness of the side walls 1.5mm. Two centrifuge tests were conducted at different frequencies and acceleration amplitudes. The testing program is summarized in Table 4.3.

Table 4.3. Centrifuge testing program

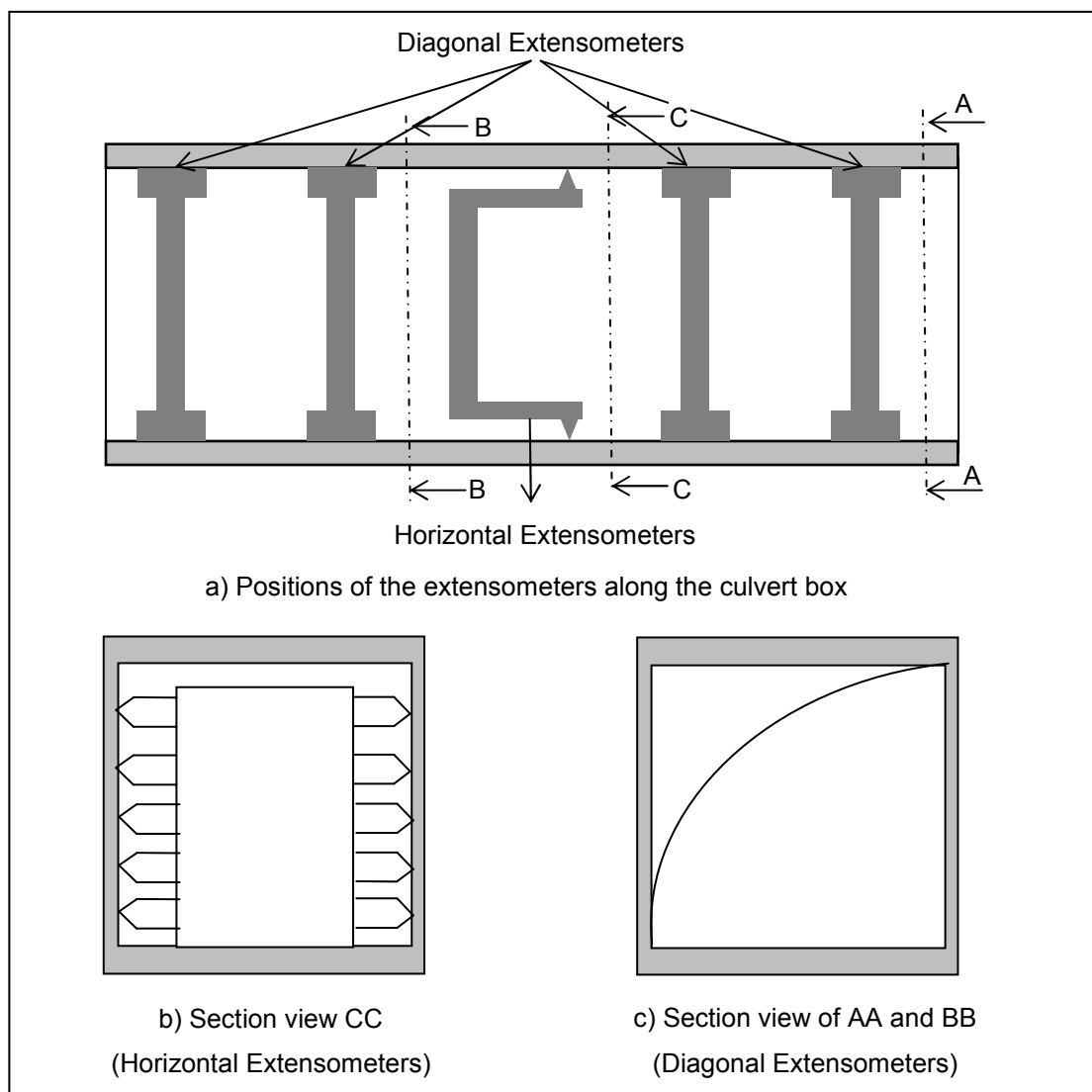| Test #	Model	Acceleration (g) (Prototype scale)	Frequency (Hz) (Prototype scale)	Duration (s) (Prototype scale)
1	Free-Field	0.4	3.5	15
2	Flexible Culvert	0.4	3.5	15
3	Flexible Culvert	0.25	3.5	15

As can be seen from Table 4.3, one test was performed for free-field condition and the others were conducted at presence of the culvert model under 40g centrifugal acceleration. The detailed procedure for the centrifuge tests can be described as follows:

1) Dry sand was filled into the ESB container by pluviation method to obtain a consistent and uniform soil density. Falling height was kept constant at 60cm and tuned at every 2 round trips.

2) Accelerometers were buried into the soil during filling operation. When the sand level was at a depth of 100 mm, the culvert model was placed into the box (Figure 4.13). Extensometers were mounted into the box before the placement. After that, accelerometers were set up on the culvert model and the dry sand was pluviated into the box until it was full.

3) ESB box was placed on the swinging basket platform of the centrifuge facility. The CPT device was set on the ESB and centrifuge was switched

on and the ESB box was spun up to 40g. When the centrifuge beam rotated at 40g, the CPT test was carried out for checking the soil uniformity. The CPT tests were conducted at two points in the model ground. Then the centrifuge was switched off and the CPT device was taken out.

4) The centrifuge was switched on and spun up to 40g again. During its flight with an acceleration of 40g, the model was shaken by applying harmonic motions in horizontal direction.

5) After the shaking, CPT test was repeated as explained in step 3. Settlements after shaking were recorded by laser displacement sensors. The same procedure from step 1 to 5 was repeated for various harmonic motions having different accelerations.
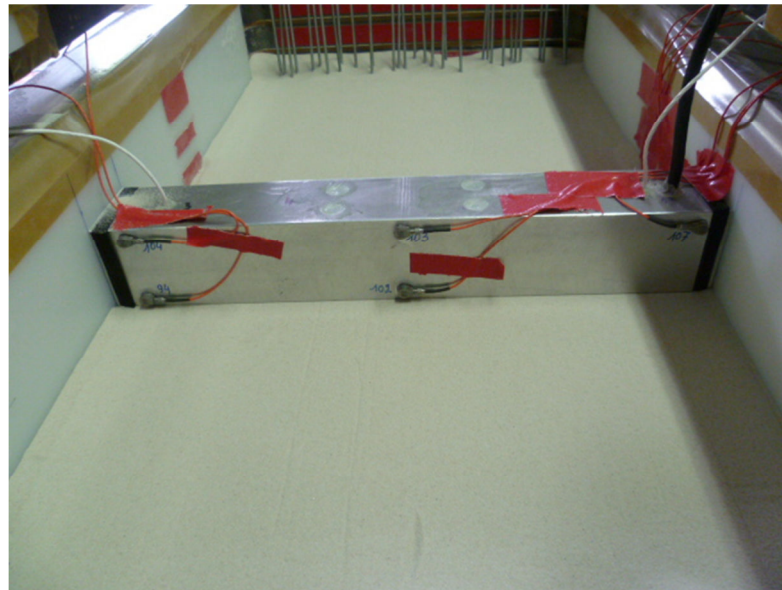
Figure 4.13. General view of the culvert during preparation of centrifuge model

4.3 Results and discussions

4.3.1 CPT test results

Variation of the cone penetration tip resistance along the depth of sand specimen was recorded at four different boreholes (Figure 4.14). The depths are corrected by using the Equation 4-9 and then plotted against the tip resistance values before shaking. Figure 4.15 shows a uniform ground model obtained by pluviation. Average settlement of the sand after shaking is about 6.5mm in the model which corresponds to 26cm in the prototype.
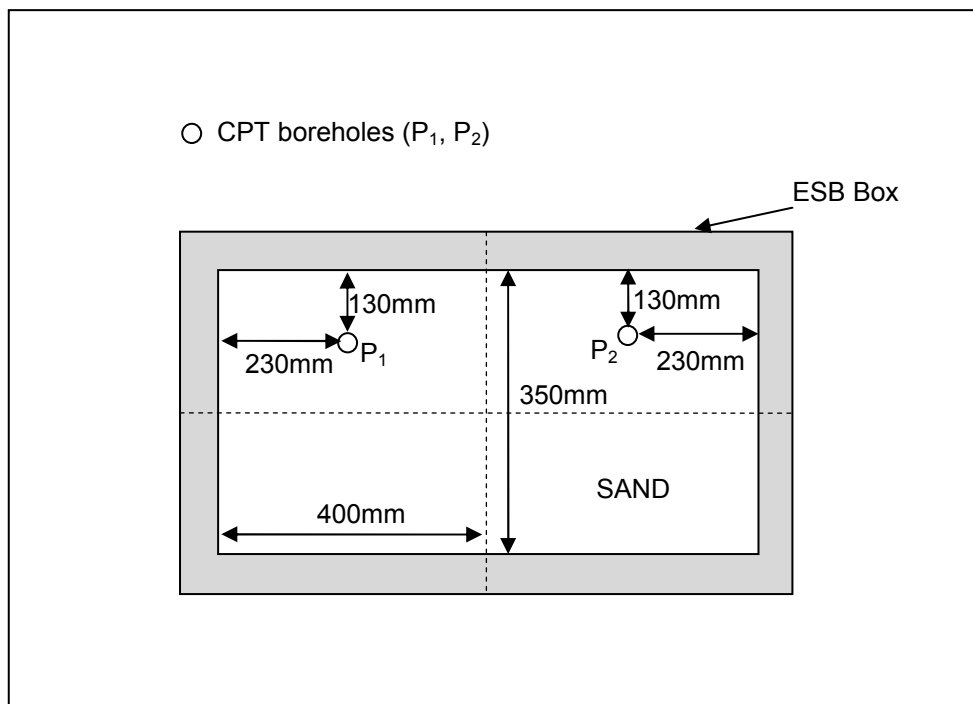
Figure 4.14. Location of the CPT boreholes
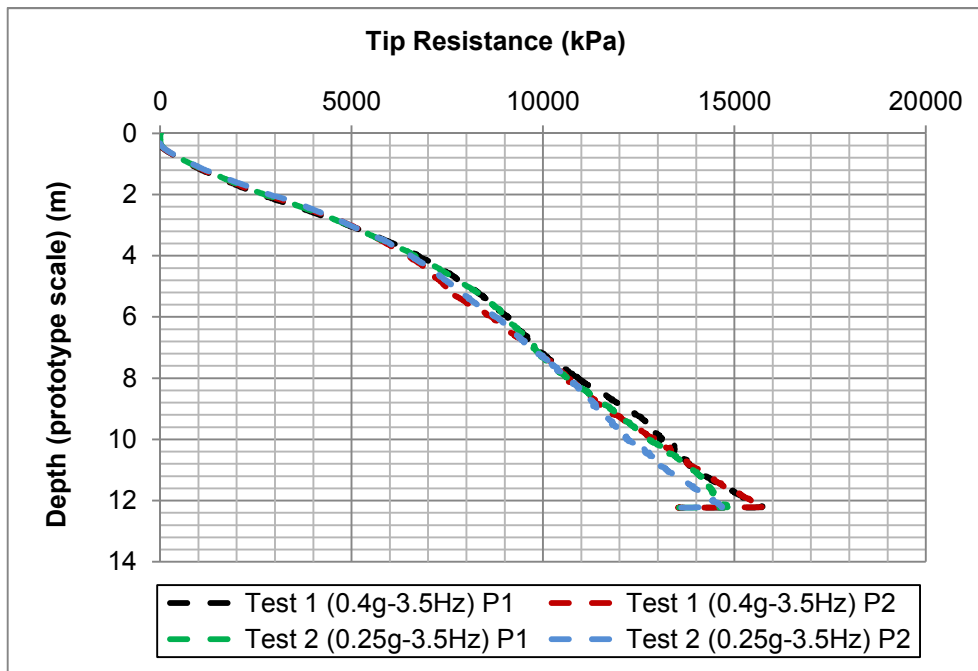
Figure 4.15. Variation of CPT tip resistance along the depth of soil

4.3.2 Free-field test results

Free-field test was performed under a 40g centrifugal field, with a prototype acceleration of 0.40g and frequency of 3.5Hz. The results of the test were used for evaluating the acceleration response, displacements and shear strain of model ground.

4.3.2.1 Maximum accelerations along the soil profile

The accelerations in the dry sand were recorded at different heights as shown in Figure 4.11. Recorded maximum accelerations at those heights were normalized with the maximum input acceleration measured on the shaking table and plotted against the soil depth (Figure 4.16). As can be seen from Figure 4.16 acceleration

amplification increases gradually from 16m to 4m and from that point increases sharply near the surface.
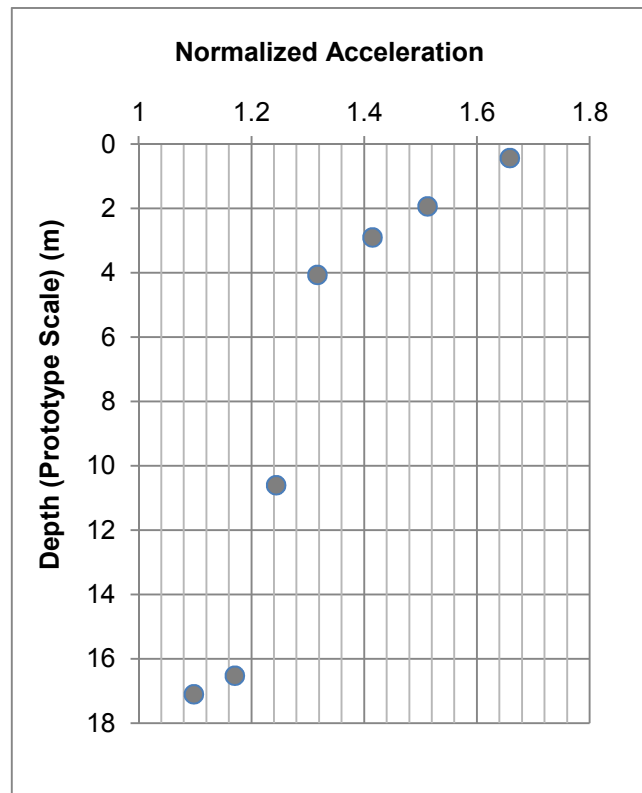
Figure 4.16. Variation of maximum acceleration along the soil profile

Figure 4.17 shows the fourier spectra of the acceleration records at different levels in the model ground. As seen in the figure, fourier amplitude increases from base to surface at low frequencies. On the other hand, soil damps the high frequency components of the motion.
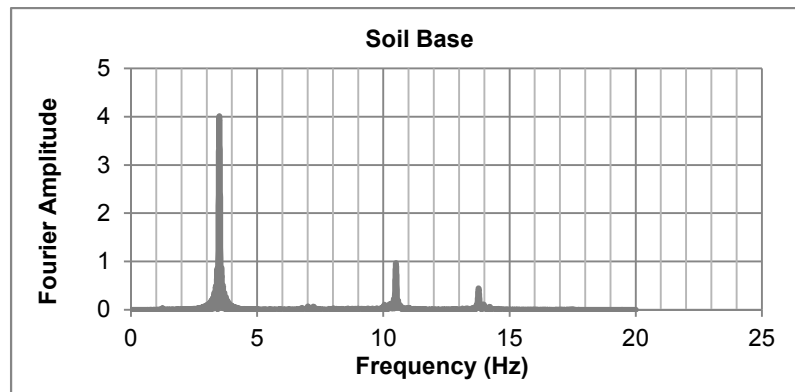
a)
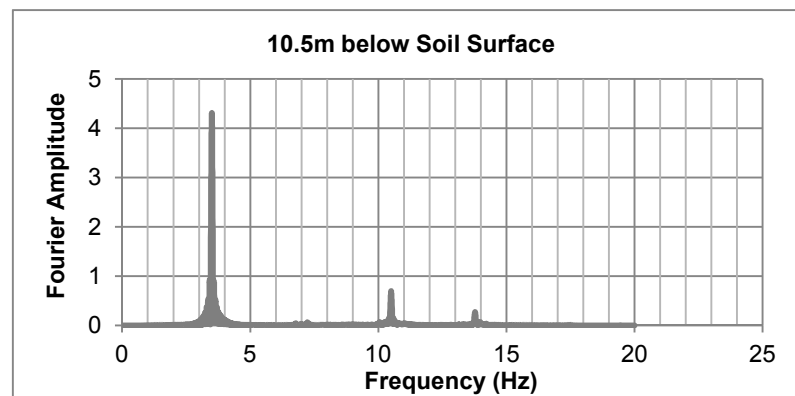
b)
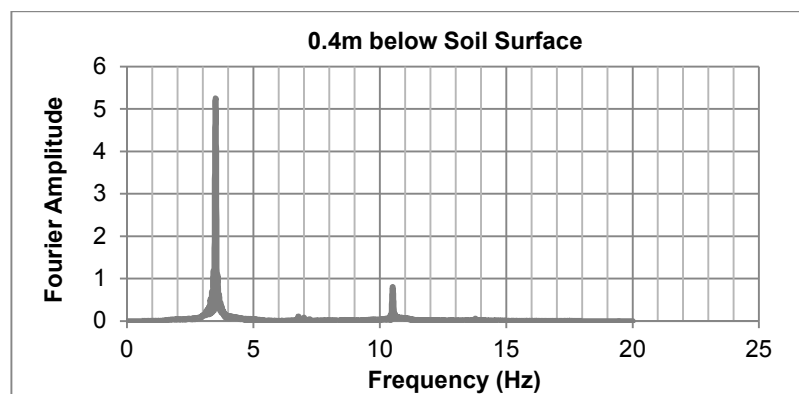
c)

Figure 4.17. Fourier spectra of the acceleration records along the soil profile
a)Soil base b)10.5m below surface c)40cm below surface

4.3.2.2 Evaluation of displacements and shear strains

Displacement and shear strains were calculated from the acceleration measurements. For this purpose, the acceleration records were integrated twice and displacement time histories were obtained. Before the integration process, accelerometers were filtered with a bandpass filter from 20Hz to 600Hz (0.5Hz to 15Hz corresponding to the prototype) to prevent the undesired errors and misleading results.

Layout and location of the acceleration transducers are given in Figure 4.18. There were totally twenty three accelerometers numbered from 1 to 23. Most of the accelerometers were placed between 100mm depth and soil surface in the model for evaluating the shear strains near the culvert. Average shear strain between the two accelerometers can be calculated by:

$$\gamma = \frac{d_2 - d_1}{z_2 - z_1}$$

(4.10)

where γ is the shear strain, d_1, d_2 are the integrated displacements at points 1, 2 and z_1, z_2 are the heights at points 1, 2, respectively. If there are three consecutive accelerometers in a soil column, the shear strain at depth z_i can be given by a second order approximation (Zeghal & Elgamal, 1994) :

$$\gamma(z_i) = \frac{\left[(d_{i+1} - d_i)\frac{(z_i - z_{i-1})}{(z_{i+1} - z_i)} + (d_i - d_{i-1})\frac{(z_{i+1} - z_i)}{(z_i - z_{i-1})} \right]}{(z_{i+1} - z_{i-1})}$$

(4.11)

Free-field shear strain at the mid-depth of culvert was calculated from the results of accelerometers no. 7,8,9,11,12,13 (See Figure 4.18). Resulting average shear strain was found to be 3.6×10^{-3}. Integration of the acceleration records obtained from accelerometers no. 15,16,17 gives higher displacements. The corresponding strain obtained from those displacements is 4.5×10^{-3}. This may be due to the sidewall

effect of the equivalent shear box. For this reason, the culvert model was placed in the middle of the equivalent shear beam box.
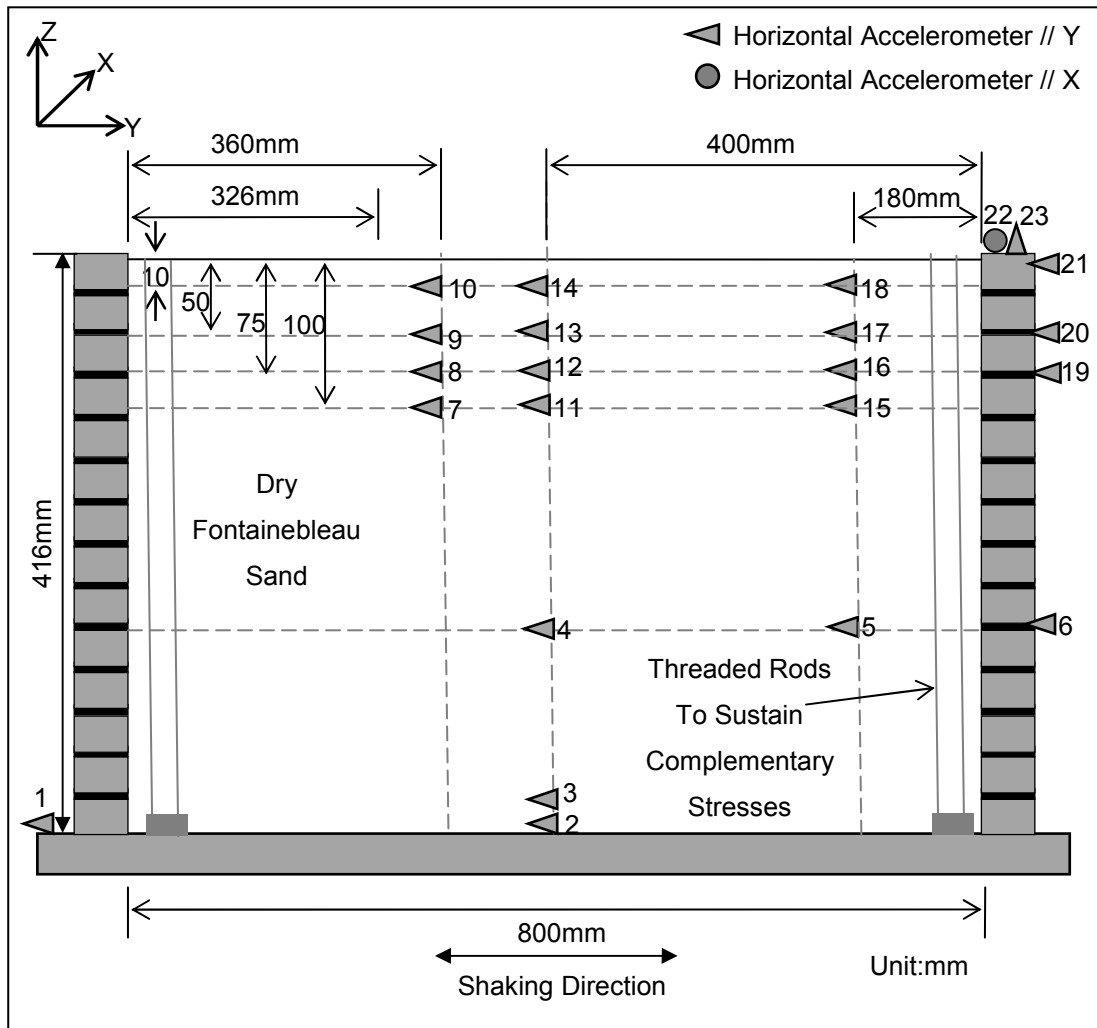

Figure 4.18. Layout and numbering of accelerometers used in free-field test

4.3.3 Results of culvert model tests

4.3.3.1 Shear strain

Displacement and shear strains obtained from Test 2 (3.5Hz-0.40g) were almost the same as the free-field test results (Test 1). In Test 2, The average shear strain at the mid-depth of the culvert model was calculated as 3.4×10^{-3} which was 3.6×10^{-3} in free-field tests. This result can be interpreted as that the culvert model conforms to ground motions during the dynamic loading. For Test 3 (3.5Hz-0.25g) the average shear strain at the mid-depth of culvert was found to be 2.2×10^{-3}.

4.3.3.2 Culvert deformations

Accelerometers and extensometers were used to measure the culvert deformations. Acceleration transducers were placed at the upper and lower parts of the culvert to estimate the racking deformations. Racking deformations were also determined by diagonal extensometers located in the culvert model. Sidewall deformations were determined by using horizontal extensometers.

There are 5 pairs of horizontal extensometers at the sidewalls of culvert model. They are labeled from HE1 to HE10 as given in Figure 4.19. These extensometers measure the cyclic horizontal deformations during the centrifuge test. Figure 4.19 to Figure 4.22 show the deformation time histories at the sidewalls of culvert model for Test 2 (3.5Hz–0.40g) and Test 3 (3.5Hz-0.25g), respectively. Although cyclic deformations at the left and right sidewalls are not perfectly equal to each other, records are reasonably consistent. Slight differences may arise from the calibration and sensitivity of extensometers. Deformations increase with a decreasing rate from bottom slab to upper slab of culvert and the measurement of displacement mode on the culvert sidewalls show the expected opposite phase between the reciprocal extensometers (Figure 4.23, Figure 4.24).
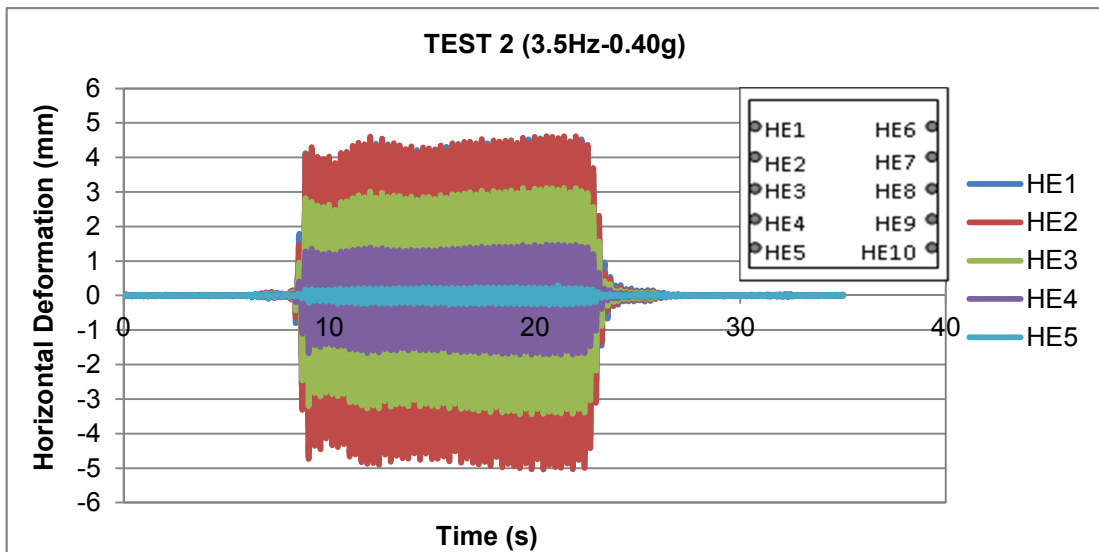
(a)
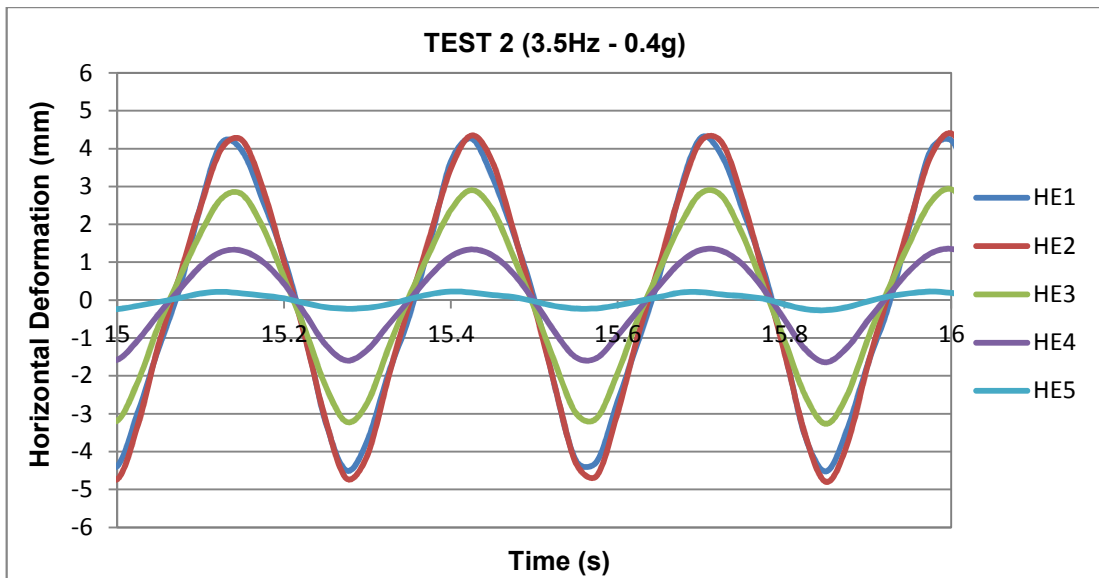
(b)

Figure 4.19. a) Cyclic horizontal deformations measured at the left sidewall (Test 2)
b) Closer view of deformations measured at the left sidewall (Test 2)
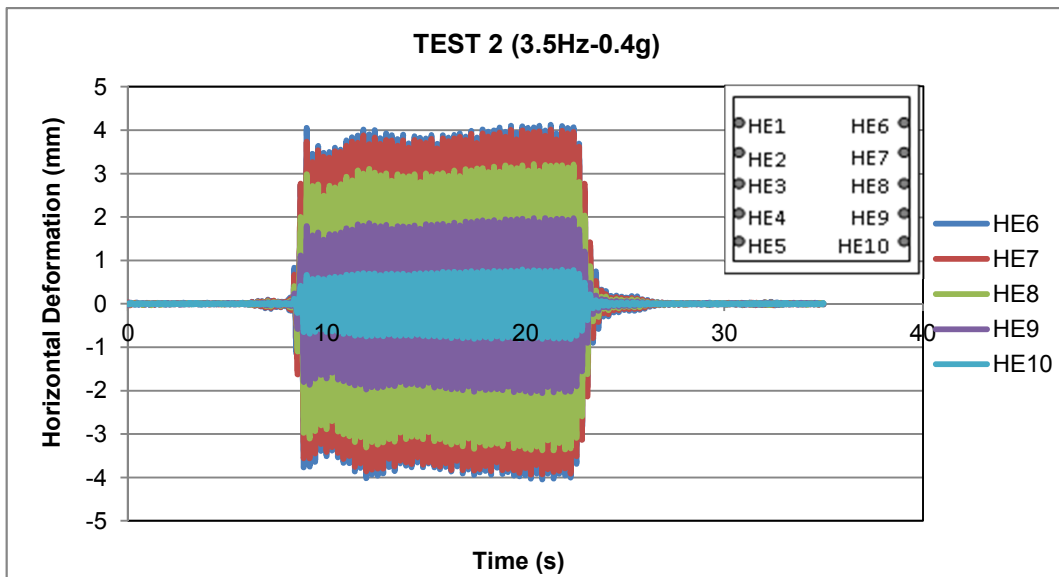
(a)
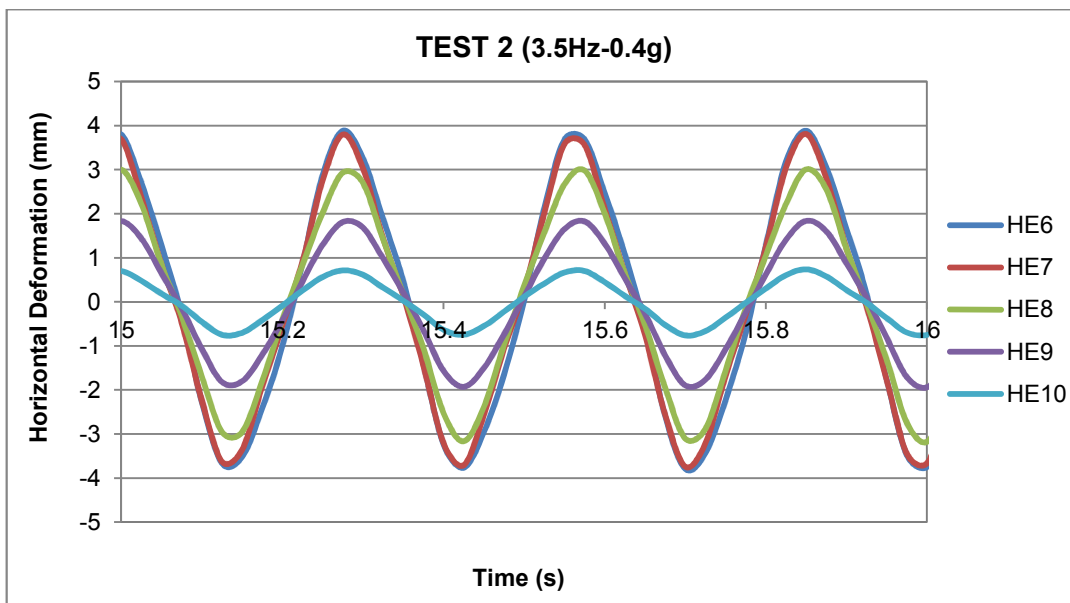
(b)

Figure 4.20. a) Cyclic horizontal deformations measured at the right sidewall (Test 2)
b) Closer view of deformations measured at the right sidewall (Test 2)
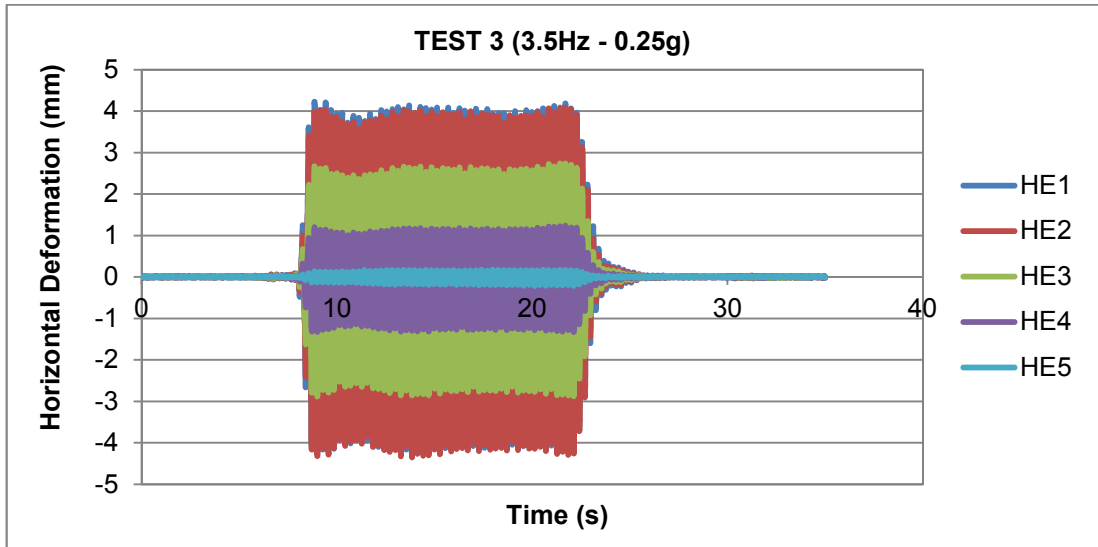
(a)
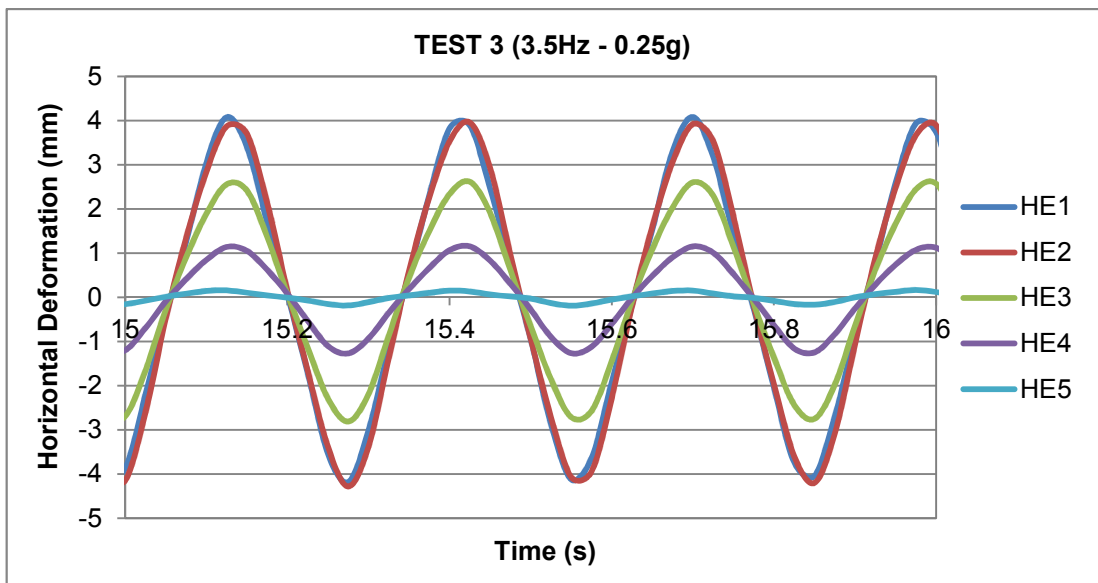
(b)

Figure 4.21 a) Cyclic horizontal deformations measured at the left sidewall (Test 3)
b) Closer view of deformations measured at the left sidewall (Test 3)
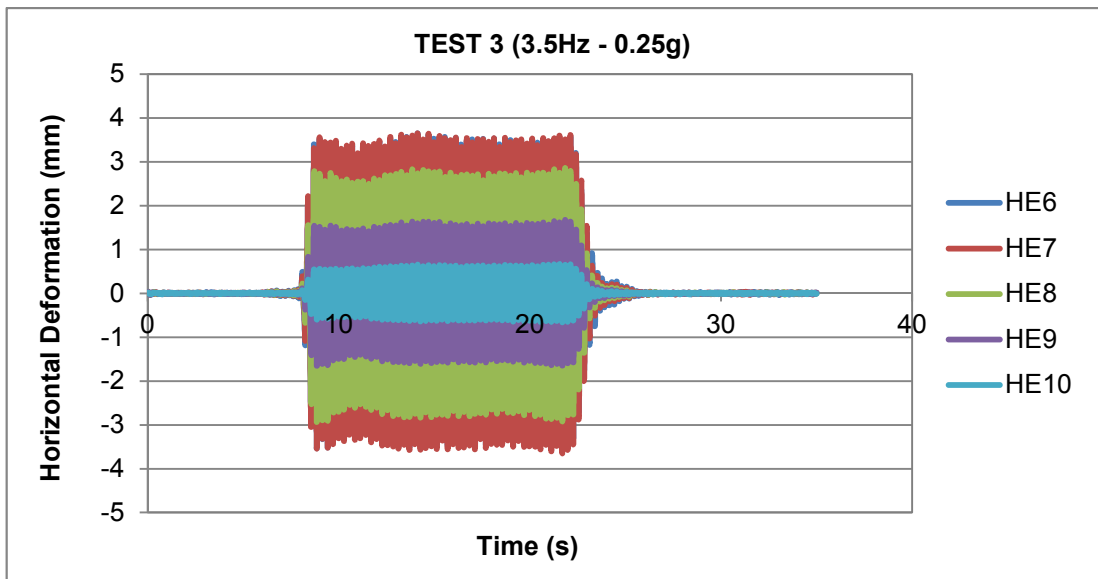
(a)
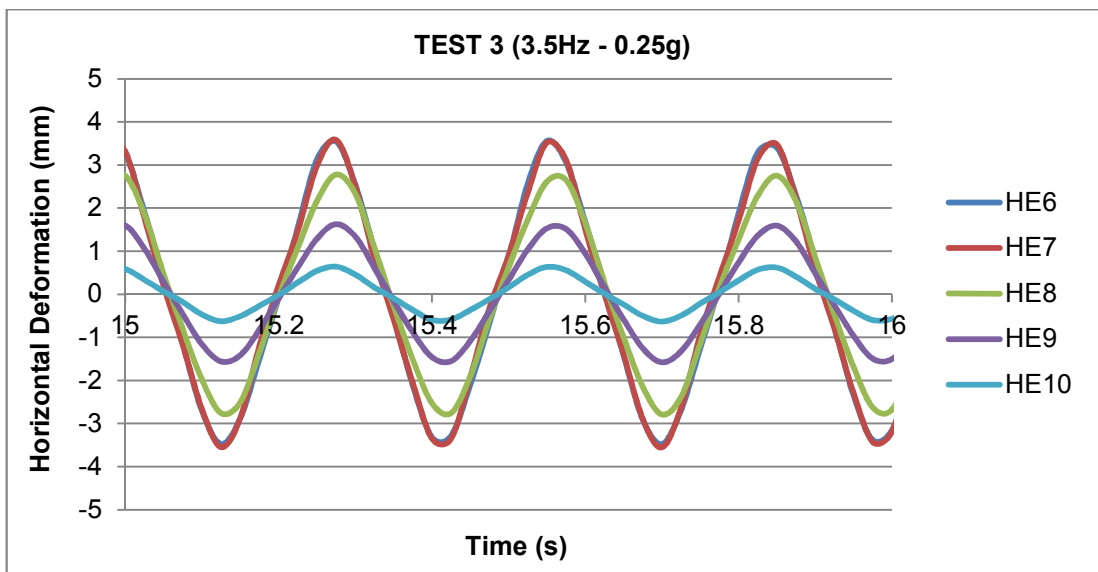
(b)

Figure 4.22. a) Cyclic horizontal deformations measured at the right sidewall (Test 3)
b) Closer view of deformations measured at the right sidewall (Test 3)

151
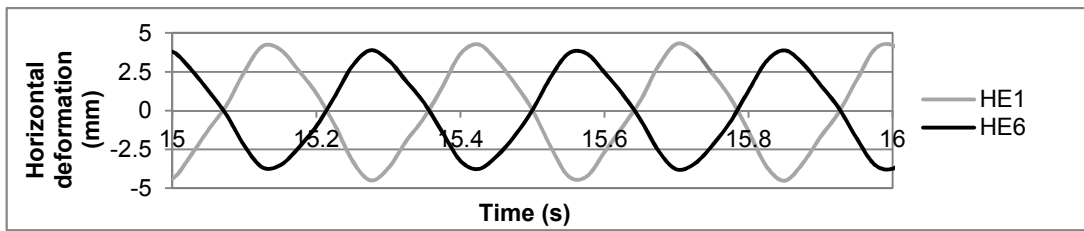
(a)
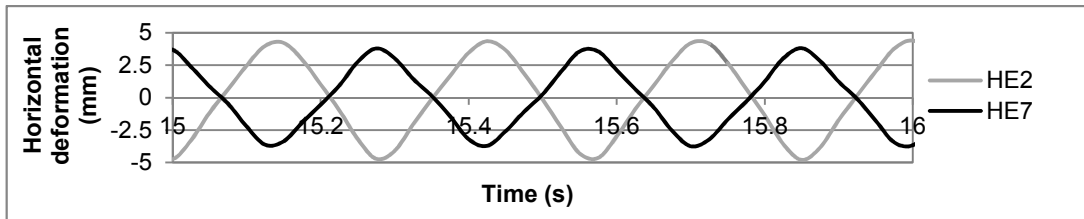
(b)
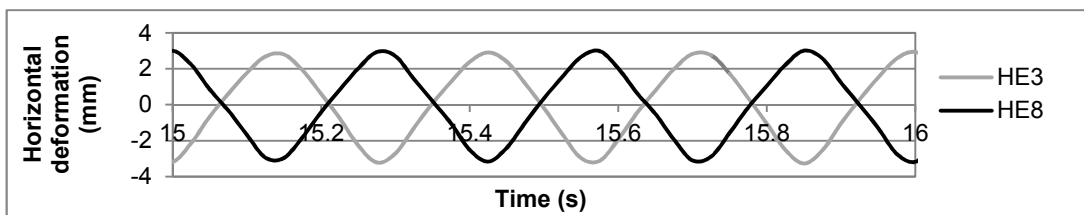
(c)
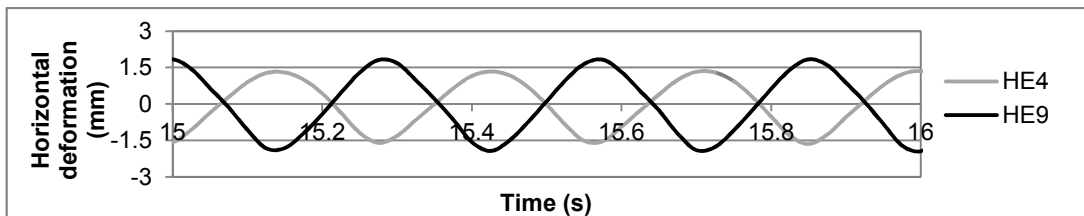
(d)
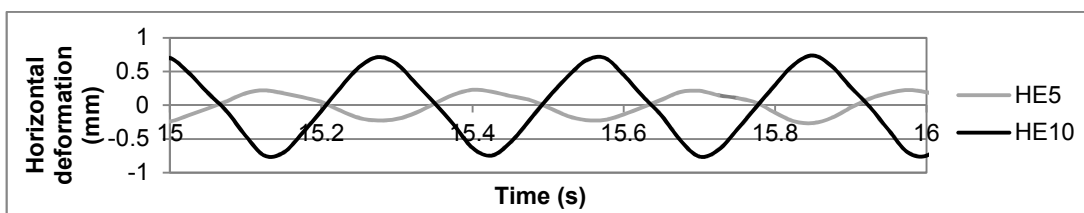
(e)

Figure 4.23. Comparison of deformations between reciprocal extensometers located on sidewalls (Test 2 - 3.5Hz - 0.40g)
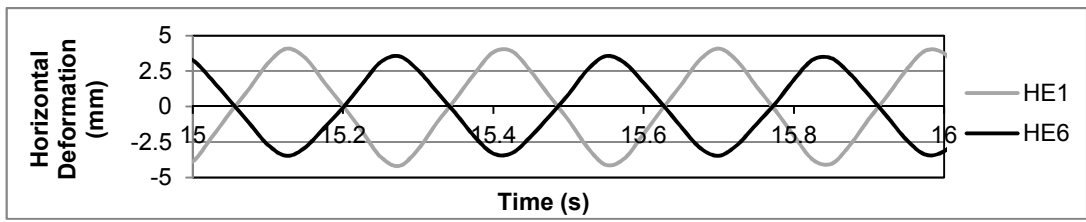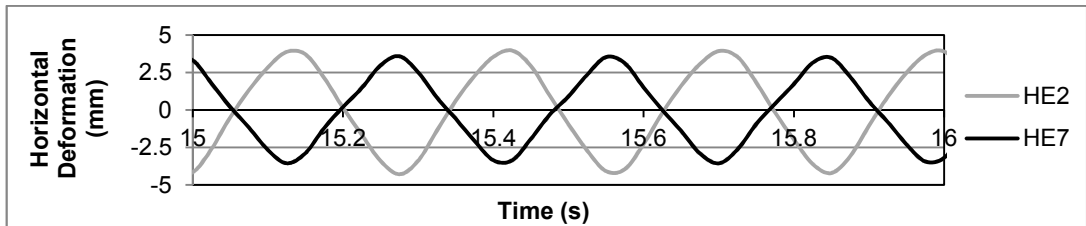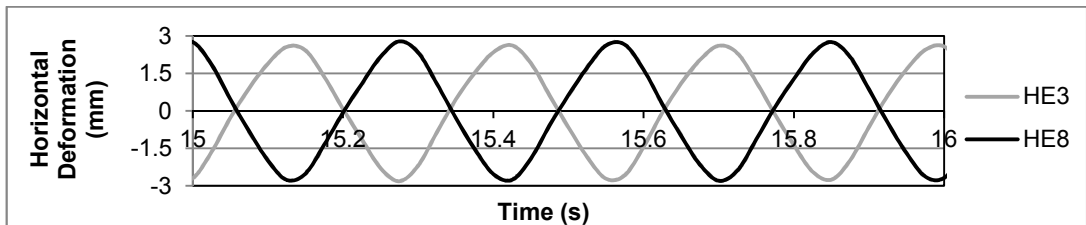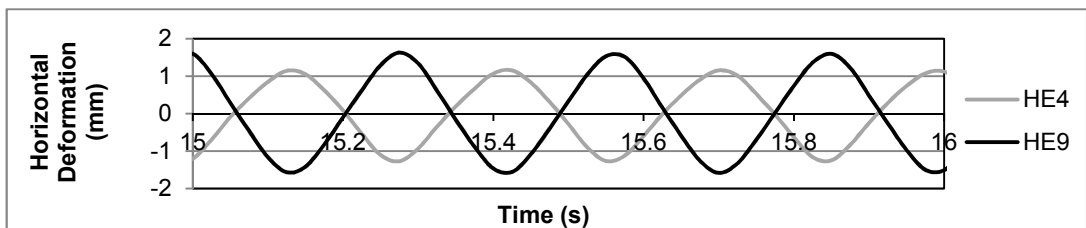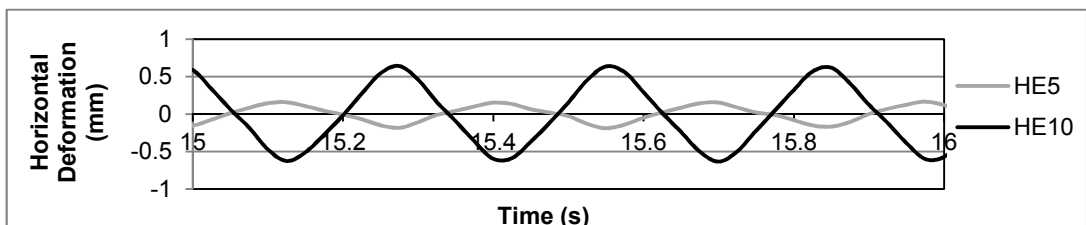
Figure 4.24. Comparison of deformations between reciprocal extensometers located on sidewalls (Test 3 - 3.5Hz - 0.25g)

Table 4.4 presents the measured horizontal deformations at sidewalls of the culvert for Test 2 and Test 3.

Table 4.4. Deformations measured by horizontal extensometers for Test 2 and Test 3.

| Elevation from Culvert Bottom (m) | Horizontal Deformations (mm) | | | |
| | TEST 2 (3.5Hz-0.40g) | | TEST 3 (3.5Hz-0.25g) | |
	Left Sidewall	Right Sidewall	Left Sidewall	Right Sidewall
1.6	4.7	4.1	4.2	3.6
1.3	4.8	4.0	4.2	3.6
1	3.3	3.3	2.8	2.9
0.7	1.6	2.0	1.3	1.7
0.4	0.3	0.8	0.2	0.7

There are 4 diagonal extensometers along the longitudinal section of the culvert model. The relative displacement between the lower and upper slabs was determined by measuring the variations in diagonal deformation of culvert. Figure 4.25 and Figure 4.26 show the variation of average relative horizontal deformation obtained from 4 diagonal extensometers for Test 2 and Test 3, respectively. In Test 2 (3.5Hz-0.4g) the maximum racking deformation at the inner side of the upper slab was measured as 3.6mm and in the third test racking deformation reduced to 2.8mm.
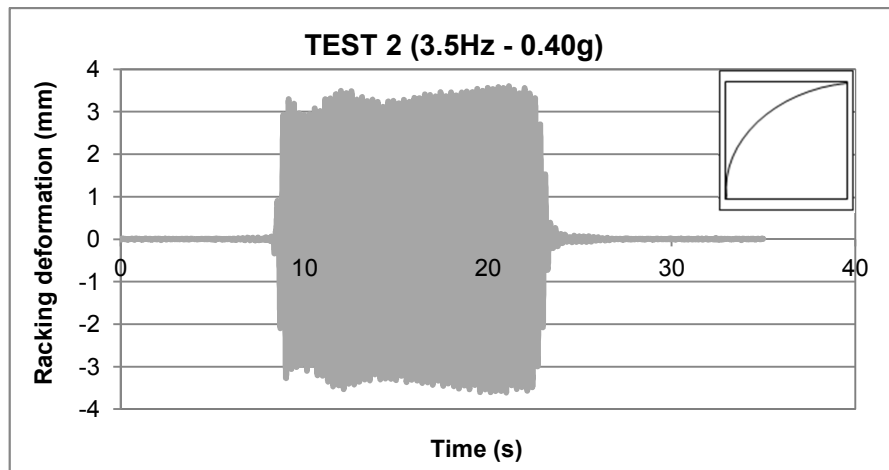
Figure 4.25. Racking deformation time history measured inside of culvert
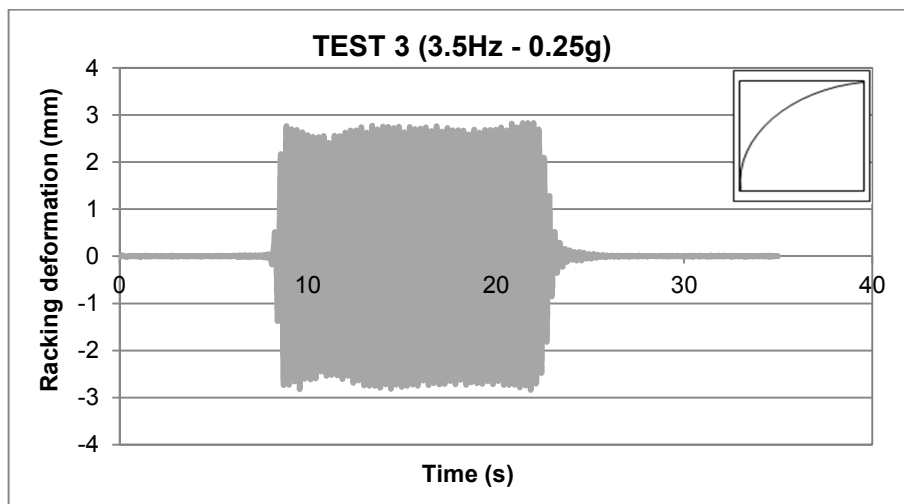
Figure 4.26. Racking deformation time history measured inside of culvert

Two accelerometers were placed at the upper and lower parts of the culvert model to obtain the relative deformation, indirectly. Displacements were calculated by double integration of the acceleration time histories. Figure 4.27 presents the variation of racking deformation (relative deformation between lower and upper slab) with respect to time. The maximum racking deformation in Test 2 was computed as 6mm. This value was consistently higher than the deformation values measured by extensometers. Spurious accelerations created by the centrifuge shaker may have

caused misleading results by increasing the actual accelerations. For this reason, in Test 2, deformations were evaluated only by using extensometer measurements.
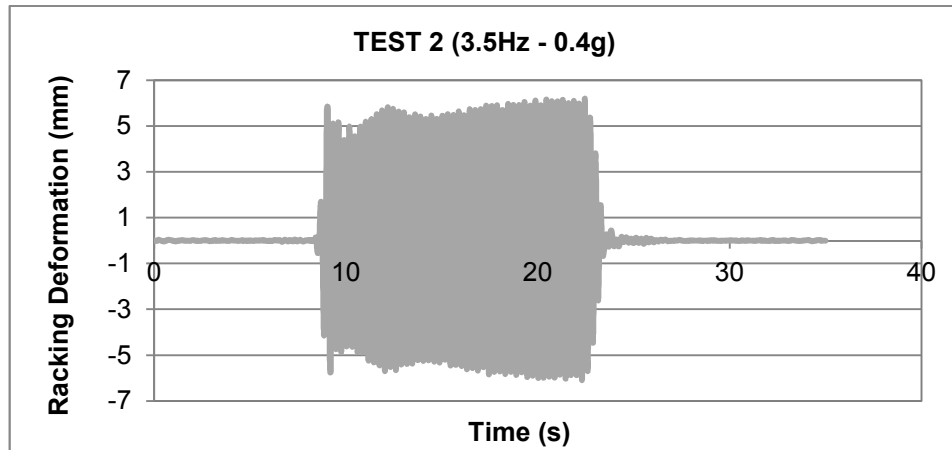
Figure 4.27. Racking deformations obtained from accelerometer records

In Test 3, racking deformation obtained from the accelerometers is consistent with the deformation measured from diagonal extensometers. Maximum racking deformation was found to be 3.4mm.
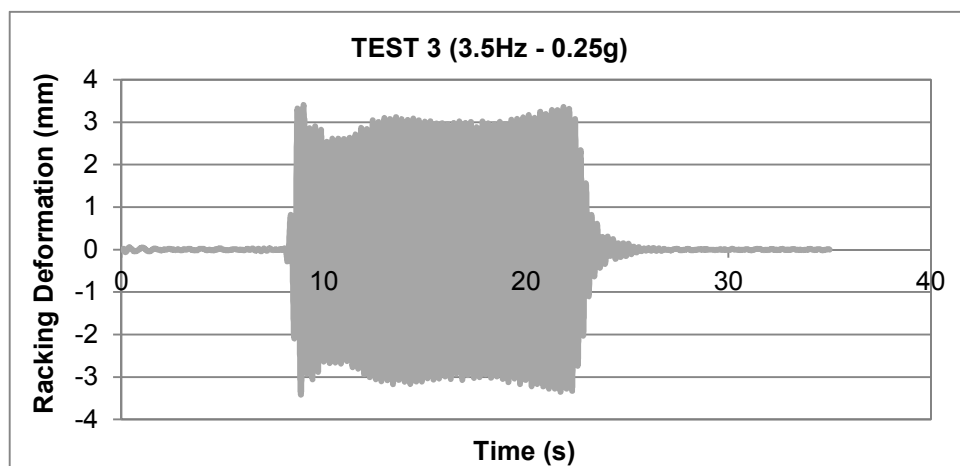
Figure 4.28. Racking deformations obtained from accelerometer records

Based on the deformation measurements, average values of sidewall horizontal deformations in prototype scale for Test 2 and Test 3 are summarized in Table 4.5. It was assumed that deformation measured inside of the top slab is equal to extreme top of culvert model.

Table 4.5. Average Deformation Along the Sidewalls of the Culvert in Prototype Scale

Elevation from Culvert Bottom (m)	TEST 2 (3.5Hz-0.40g) Average Sidewall Deformation (mm)	TEST 3 (3.5Hz-0.25g) Average Sidewall Deformation (mm)
2.0	3.6	2.8
1.76	3.6	2.8
1.6	4.4	3.9
1.3	4.4	3.9
1	3.3	2.85
0.7	1.8	1.5
0.4	0.55	0.45
0	0	0

4.3.4 Verification of simplified approach by centrifuge tests

In chapter 3, the simplified approach was proposed for the preliminary assessment of box type culverts buried in dry sand. This approach is applied to the centrifuge data in order to compare the measured deformations of a flexible culvert model tested in centrifuge under dynamic loading. The steps followed for Test 2 and Test 3 are given below:

For Test 2 (0.4g-3.5Hz)

1) Initial flexibility ratio (IFR) of the culvert model tested in centrifuge can be calculated by using the following equation (for single barrel frames) proposed by Wang (1993):

$$IFR = \frac{G_{\max}}{24}\left(\frac{H^2W}{EI_W} + \frac{HW^2}{EI_R}\right)$$

(4.12)

where,

G_s= 56500kPa (Maximum shear modulus)

H= 2m (Height of the culvert)

W=1.88m (Width of the culvert)

E=7.1 x 10^7kPa (Elastic modulus of the culvert)

I_W= 1.80 x 10^{-5} m^4 (Moment of Inertia of Sidewall)

I_R= 1.15 x 10^{-3} m^4 (Moment of Inertia of Slab)

Solution of Equation 4.12 gives:

IFR=14.1

2) Free-field strain measured at the mid-depth of the culvert is 0.0036. The maximum shear strain is 0.00192 in the proposed curves, but it is not unreasonable to use those curves for a strain value of 0.0036. To be on the safe side, the equation for an initial flexibility ratio of 9.9 was used for estimation of dynamic lateral pressure coefficient (k_d). Approximated equation was given as follows:

k_d=0.0397ln(γ_s)+0.4084

(4.13)

γ_s=0.0036 (free-field shear strain at mid-depth level of culvert)

k_d=0.185

3) The maximum dynamic pressure absolute value (P_d) was calculated by multiplying the vertical stress at the mid-depth of culvert by dynamic lateral pressure coefficient (k_d). P_d was given by:

$$P_d = \gamma.h.k_d \tag{4.14}$$

γ=15.81kN/m^3 (unit weight of the sand)
h=3m (culvert mid-depth)
k_d=0.185
P_d=15.81*3*0.185=8.78kPa

4) The shear stress acting on the interface was estimated by using the following equation:

$$\tau_{eq} = 0.65 \gamma h \frac{a_{\max}}{g} r_d \tag{4.15}$$

γ=15.81kN/m^3 (unit weight of sand)
h=2m
a_{max}=0.9g (maximum ground acceleration near the surface)
r_d=0.97 (estimated by the equation proposed by Çetin and Seed (2004))
τ_{eq}=17.94kPa

Maximum shear stress between the aluminum and sand is given by:

$$\tau_{max} = \sigma_v.\tan\delta \tag{4.16}$$

σ_v=15.81*2=31.62kPa (vertical stress culvert top sand interface)
δ = 20° (Porcino et al. 2003)
τ_{max}=11.51kPa

The maximum shear stress is smaller than the estimated shear stress. Thus, shear stress acting on the culvert top was taken as 11.51kPa.

5) Static stresses were simply calculated by using at rest horizontal earth pressure coefficient.

$$K_0 = 1 - \sin\phi'$$ (4.17)

ϕ'=38° (friction angle of sand)
K_0=0.384

The lateral static earth pressure at the upper corner of the culvert is 12.15kPa and at lower corner of culvert is 24.31kPa.

6) Shear stresses, static and dynamic pressures acting on the culvert model are illustrated in Figure 4.29. The frame was analyzed using structural analysis program Sap2000. The maximum deformation at the top of culvert was estimated as 7.6mm. 1.9mm of the total racking deformation (7.6mm) is developed by total lateral pressure and the rest (5.7mm) by shear stress acting on the top culvert interface. Sidewall deformations predicted from simplified frame analysis is plotted against the actual deformations measured in centrifuge tests as shown in Figure 4.30.

Figure 4.29. Simplified frame and calculated stresses
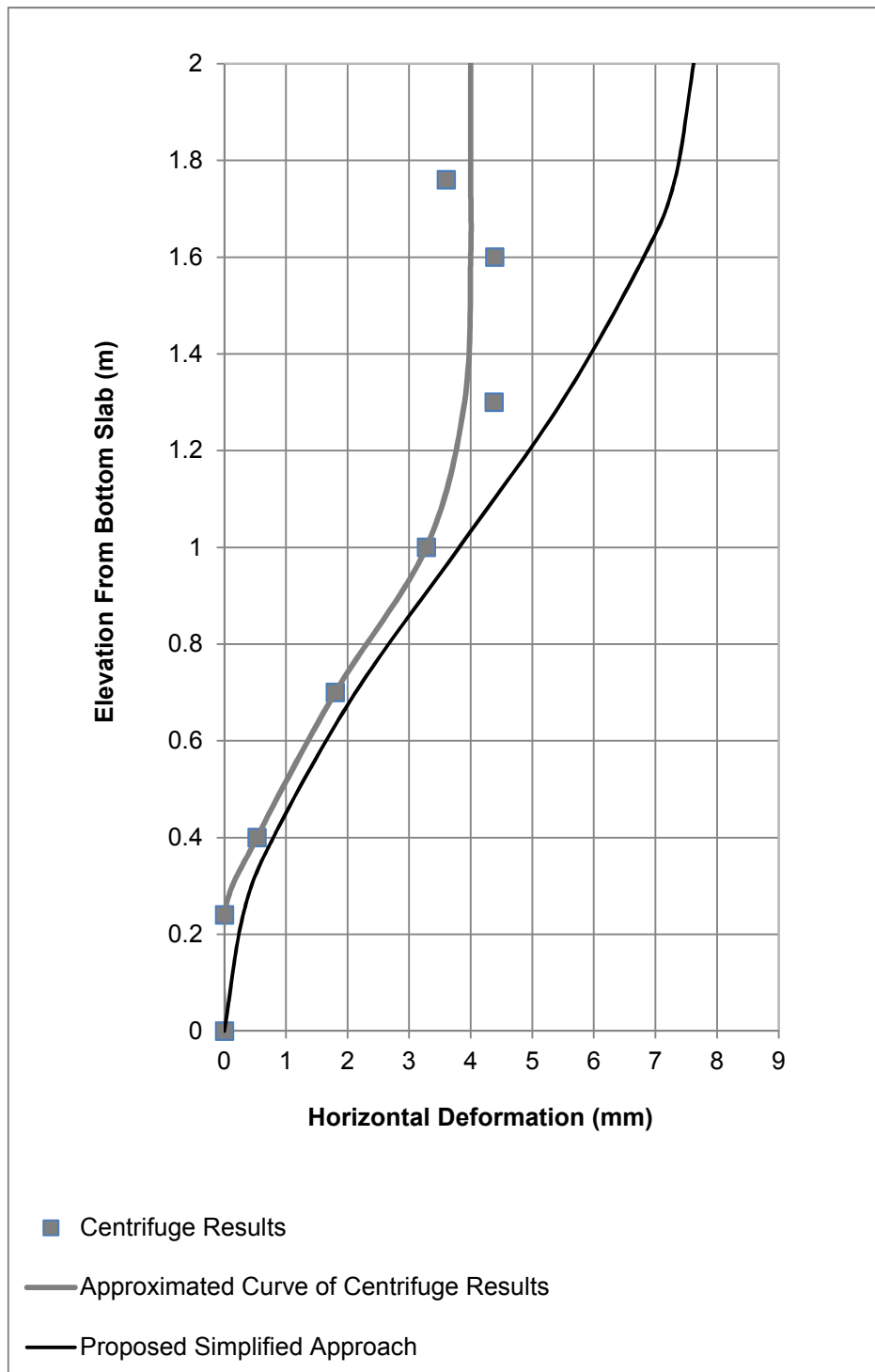
Figure 4.30. Sidewall deformation comparison of centrifuge test (Test 2) results with proposed simplified estimation

For Test 3 (0.25g – 3.5hz)

1) This step is same with the step 1 of Test 2 (0.40g – 3.5Hz).

2) Free-field strain measured at the mid-depth of the culvert is 0.0021. To be on the safe side, the equation given for a initial flexibility ratio of 9.9 was used for estimation of dynamic lateral pressure coefficient (k_d). Using equation 4.13:

γ_s=0.0021 (free-field shear strain at mid-depth level of culvert)
k_d=0.164

3) Maximum dynamic pressure absolute value (P_d) was calculated by multiplying the vertical stress at the mid-depth of culvert by dynamic lateral pressure coefficient (k_d). P_d is given by Equation 4.13.

γ=15.81kN/m^3 (unit weight of the sand)
h=3m (culvert mid-depth)
k_d=0.164

P_d=15.81*3*0.164=7.78kPa

4) The shear stress acting on the interface was estimated by using Equation 4.11.

γ=15.81kN/m^3 (unit weight of sand)
h=2m
a_{max}=0.6g (maximum ground acceleration near the surface)
r_d=0.97 (estimated by Equation 3.24 proposed by Çetin and Seed (2004))
τ_{eq}=11.96kPa

τ_{max}=11.51kPa (Calculated by equation 4.15)

Maximum shear stress is smaller than the estimated shear stress. Thus, shear stress acting on the culvert top was taken as 11.51kPa.

5) Same with the step 5 of Test 2 (0.40g – 3.5Hz).

6) Shear stresses, static and dynamic pressures acting on the culvert model are illustrated in Figure 4.31. The maximum deformation at the upper corner of culvert was estimated as 7.4mm. 1.7mm of the total racking deformation (7.4mm) was developed by total lateral pressure and the rest (5.7mm) by shear stress acting on the upper face of culvert. Sidewall deformations predicted from simplified frame analysis is plotted against the actual deformations measured in centrifuge tests as shown in Figure 4.32.
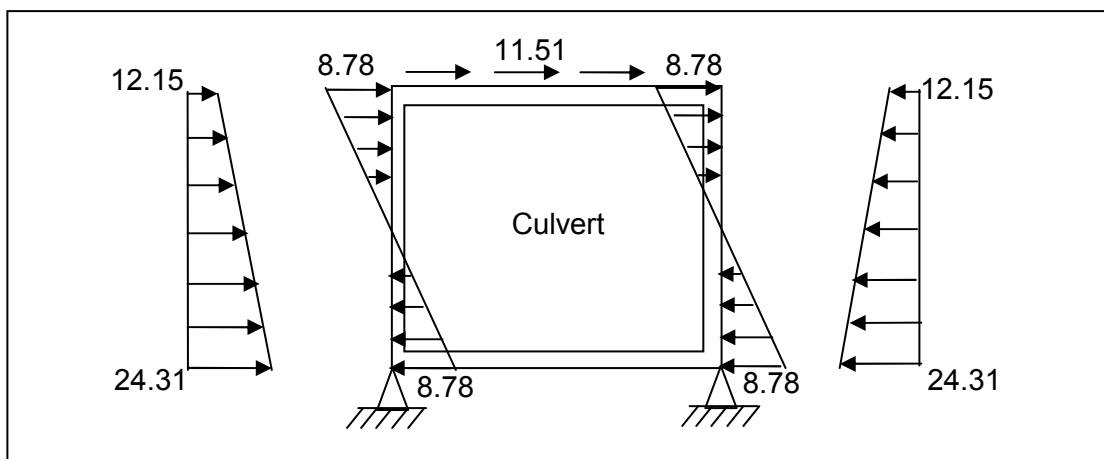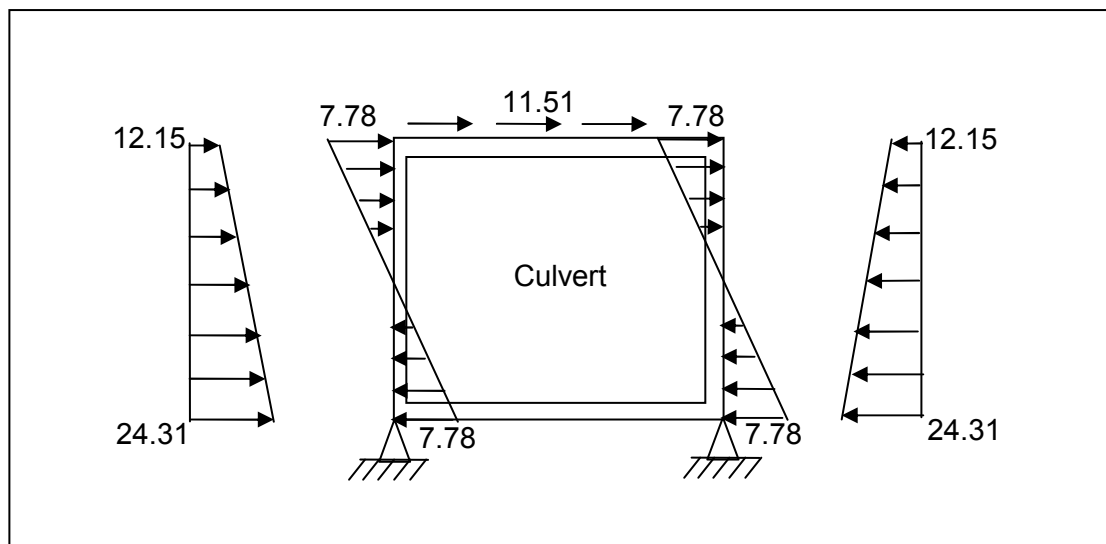

**Figure 4.31.** Simplified frame and calculated stresses
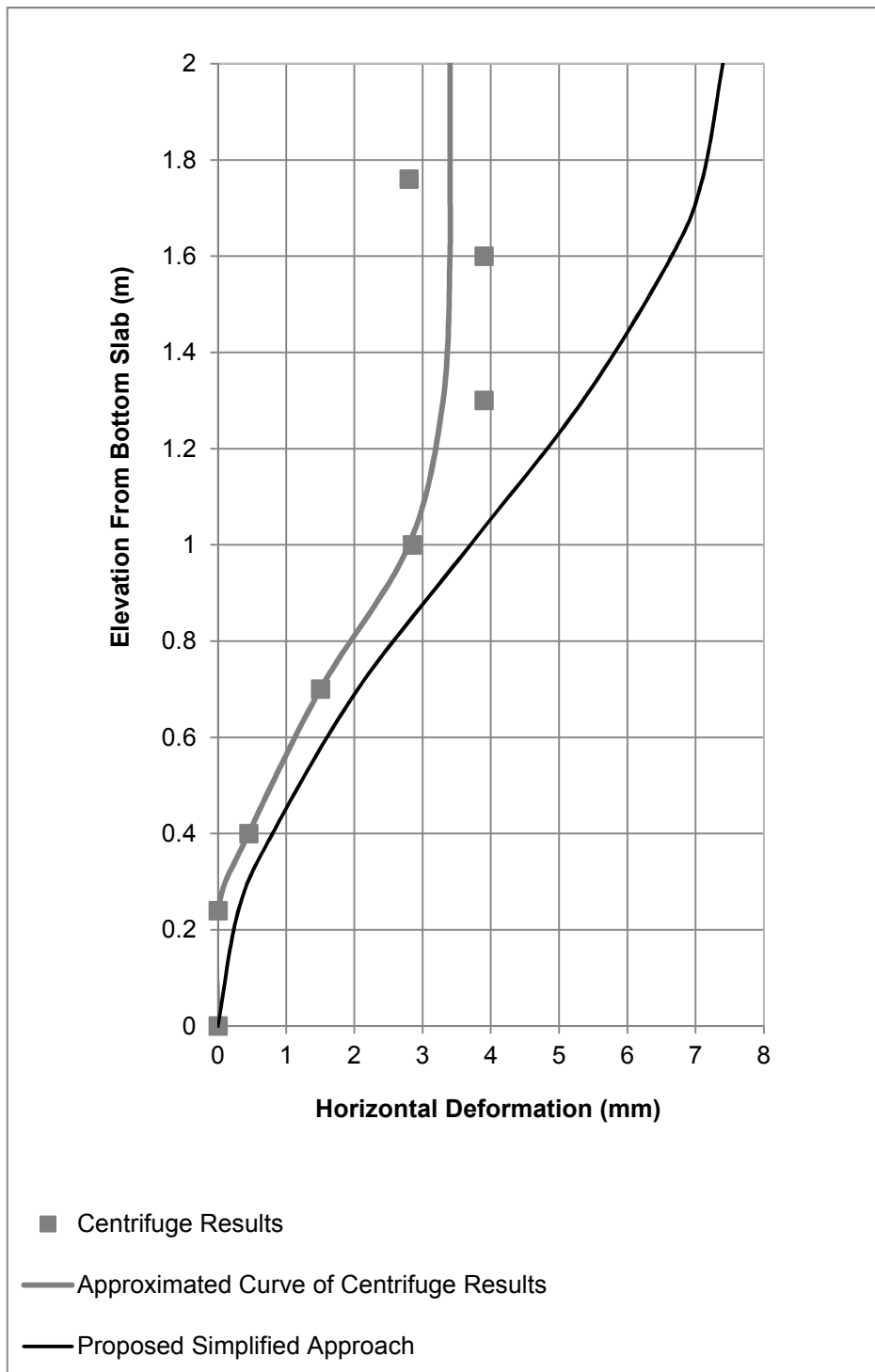
Figure 4.32. Sidewall deformation comparison of centrifuge test (Test 3) results with predictions of proposed simplified approach

As can be seen from Figure 4.30 and Figure 4.32, proposed simplified approach gives higher deformations as compared to actual deformations measured in Test 2 and Test 3. From lower to middle part of culvert, the deformation form is close to actual deformation shape while after that part it deviates and overestimates the racking deformation by a factor of 2 at the top of culvert. This overestimation may arise from the predicted shear stresses acting on upper soil-culvert interface. For both tests, shear stress values were estimated as the frictional stress which corresponds to maximum shear stress value. However, mobilized shear stresses during the dynamic excitation may be lower than this value. Therefore, more research is needed to investigate the shear stress mobilization at soil-culvert interface during dynamic excitations.

4.3.5 Comparison of Centrifuge Test Results with Closed-Form Solutions

Closed-form solutions proposed by Penzien (2000) and Huo et al. (2006) were compared with the proposed simplified approach and actual measurements of centrifuge tests in terms of racking deformations. In closed-form solutions, degraded shear modulus at mid-depth of culvert was needed so as to calculate racking distortions. Figure 4.33 shows the normalized modulus reduction curve proposed for clean sands by Darendeli (2001). The curve is valid for a mean effective stress (σ'_m) of 28kPa which corresponds to mean effective stress at mid-depth of culvert. Using the shear strain obtained from centrifuge test, degraded shear modulus, G_s, was estimated by Darendeli's curve.

-In Test 2 (0.40g-3.5Hz), for a shear strain value of 3.6×10^{-3} corresponding G_s is obtained as 6255 and F (flexibility ratio) as 1.15.

-In Test 3 (0.25g-3.5Hz), for a shear strain value of $2.2 \times 10^{*3}$ corresponding G_s is obtained as 9153 and F as 1.71.

Using these values, racking deformations of the culvert were calculated by Penzien (2000) and Huo et al. (2006) closed-form solutions. Comparison of centrifuge test results with closed from solutions and proposed simplified approach are given in Figure 4.34 and Figure 4.35 respectively. In this comparison, it is considered that the centrifuge represents the actual field conditions more realistically and accordingly it gives better results as compared to other approaches.
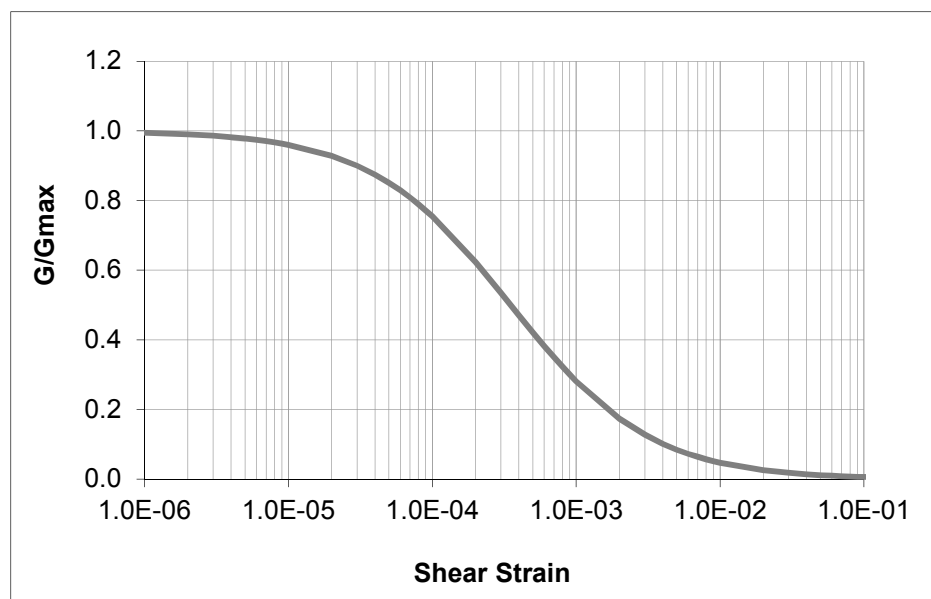
Figure 4.33. Normalized shear modulus reduction curve for clean sand, σ'_m=28kPa

As seen from Figure 4.34 proposed simplified approach and Penzien's (2000) solution give closer estimates for Test 2. Besides, both approaches yield conservative results as compared to Huo's et al. (2006) solution. In Test 3, simplified approach gives higher deformation values than the analytical solutions. As mentioned previously, the reason may be the overestimation of shear stress acting on upper soil-culvert interface.
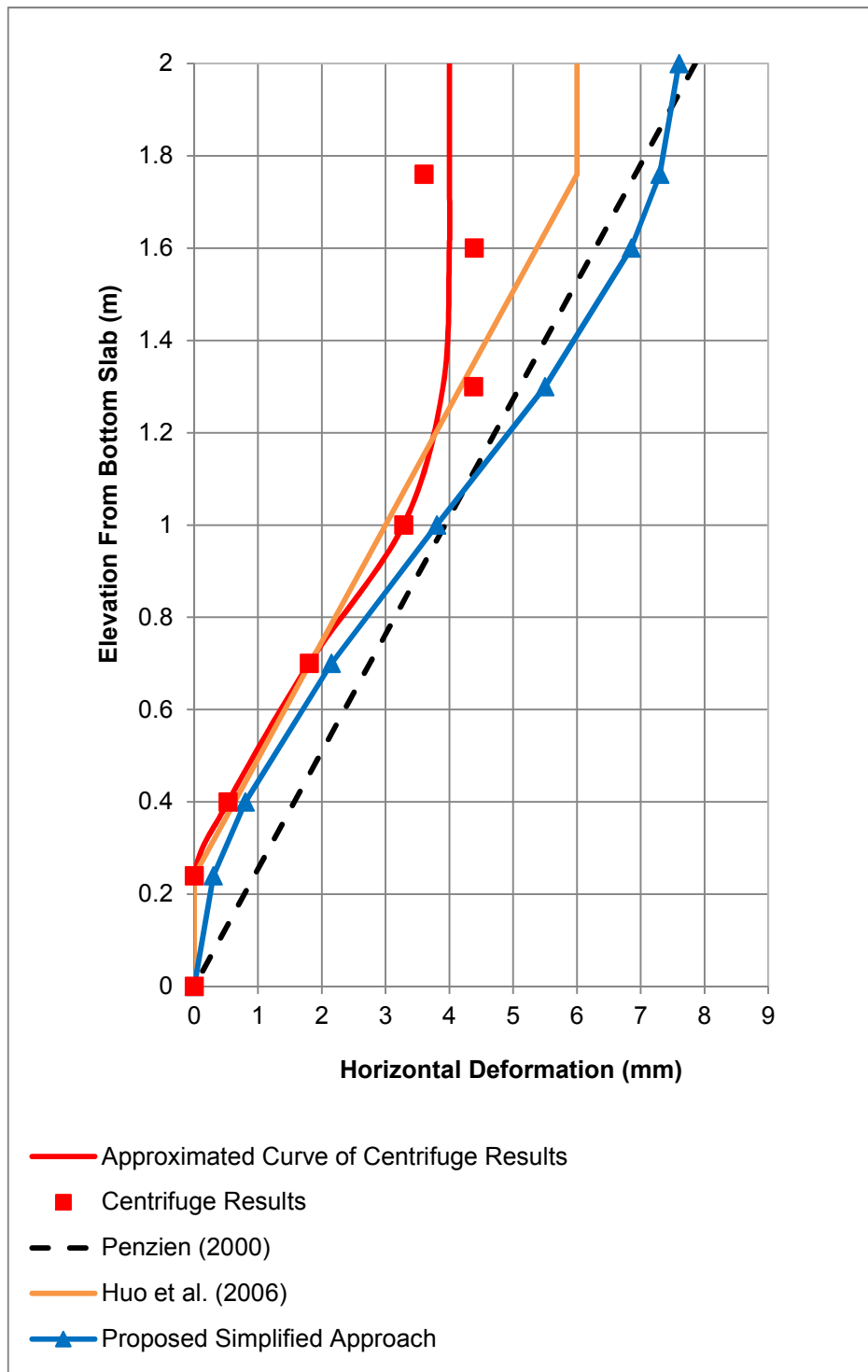
Figure 4.34. Comparison of analytical solutions and proposed simplified approach with centrifuge test results for Test 2
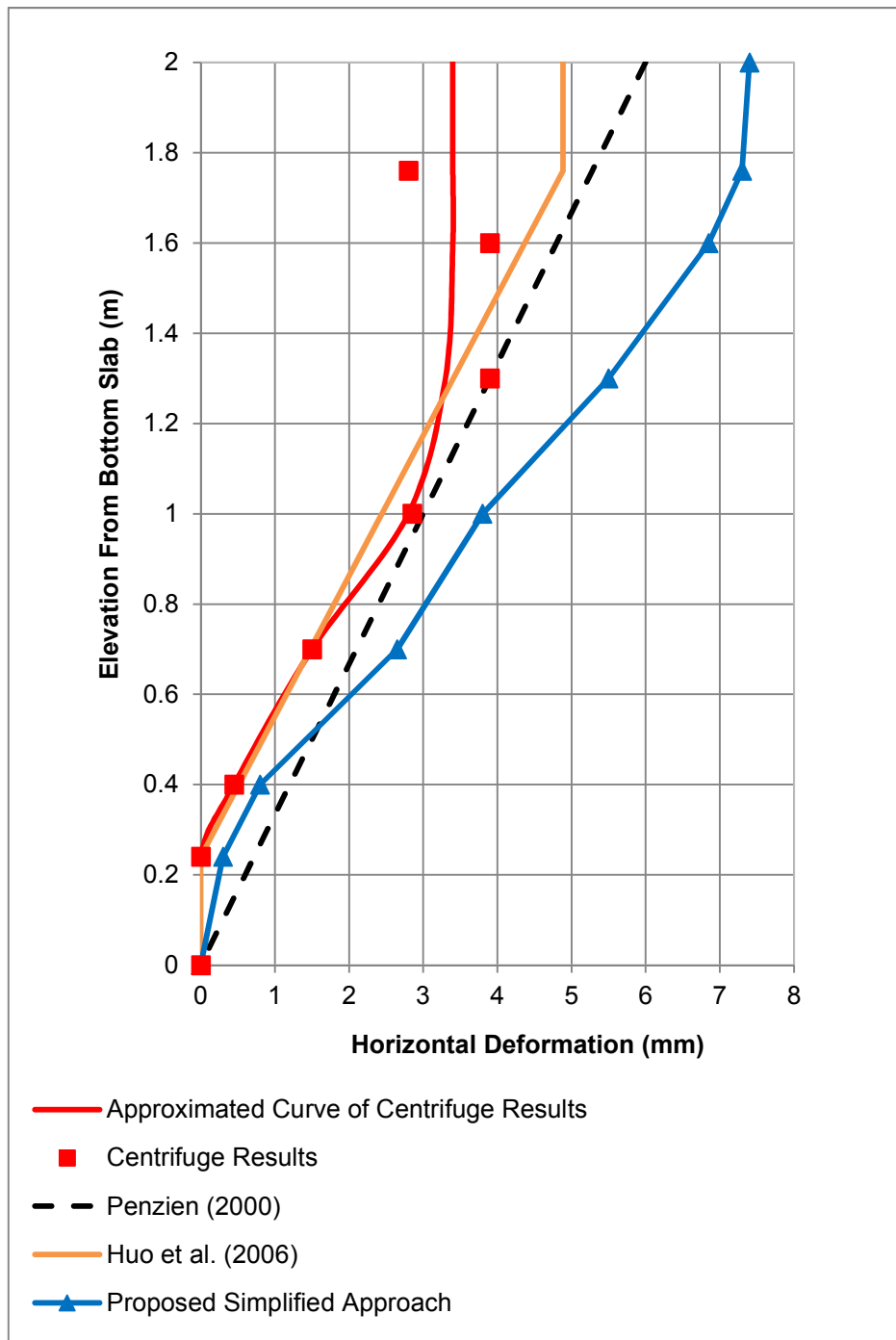
Figure 4.35. Comparison of analytical solutions and proposed simplified approach with centrifuge test results for Test 3

Deformations estimated by Huo et al. (2006) are slightly smaller than that predicted by Penzien's (2000) solution. There may be two causes for that difference between two closed-form solutions. First, as Huo (2005) stated, the deformation of rectangular opening may not be well represented by a circular opening. Second, thicker slabs may cause more conservative results in Penzien's solution which gives the racking deformations at extreme top and bottom while Huo's et al. (2006) solution predict the racking deformations by considering the inside dimensions of culvert.

In brief, the proposed simplified procedure gives conservative results and maximum deformation at the top a flexible culvert is overestimated by a factor of 2-2.5. Thus, it can be used in reasonable accuracy as a practical approach for the preliminary assessment of underground box-type culverts buried in dry sand under seismic action.

CHAPTER 5

SUMMARY AND CONCLUSIONS

The aim of this study is to investigate the dynamic response of underground culverts by considering the soil-structure interaction. For this purpose, shaking table tests and centrifuge tests were conducted on box-type models under harmonic motions. Results of the experiments were analyzed in order to make an assessment on dynamic lateral pressures acting on underground culverts.

To minimize the boundary effects, a laminar box was designed and manufactured for the shaking table tests. Four culvert models having different aspect ratios were buried at a certain depth in a laminar container and subjected to harmonic excitations. Top and bottom thickness of the box models was kept thicker than the sidewalls of the box. In order to have different relative stiffness values for the box with respect to the surrounding soil, the effect of relative stiffness on the soil dynamic pressures was examined without considering bending of the slabs. Pressure transducers were mounted on the right and left side of culvert model to measure the dynamic earth pressures. Acceleration transducers were buried in the surrounding soil to evaluate the shear strain and acceleration response of soil. Burial depth of the box was changed for two extreme cases, i.e., for the most flexible and least flexible models. This arrangement made it possible to observe the effect of embedment on the dynamic earth pressures. Based on the results of the shaking table tests, a simplified procedure was proposed to estimate dynamic soil pressure distribution acting on culvert sidewalls.

In centrifuge tests, dynamic response of a flexible culvert model was examined under harmonic base excitations applied in horizontal direction. To simulate field boundary conditions, an equivalent shear beam box was utilized throughout the experiments. Due to the small dimensions of the centrifuge model pressure transducers could not have been utilized, instead, strain gauges were installed. Dynamic strains of the buried culverts were measured by means of these strain

gauges and deformation scheme of the flexible culvert model was evaluated. Racking deformations of the culvert measured in the centrifuge tests were compared with the deformed shape obtained by the simplified approach suggested.

Major conclusions upon an evaluation of data obtained from the shake table and centrifuge tests are summarized as given below:

1) Static pressure values recorded at the sidewalls of 1-g culvert models and lateral pressure coefficient, K, calculated from these measurements were compared with well-known at-rest pressure coefficient K_0 and active pressure coefficient, K_a. It was observed that K values decrease with increasing relative stiffness. For most rigid culverts, K values approach to K_0 value obtained by Jaky's equation. For relatively flexible culverts, although K decreases, nevertheless, it is still larger than the K_A value.

2) Amplification of the acceleration depends on the shear strain level which in turn, is dependent upon the input motion acceleration amplitude and frequency. At low strains almost no amplification was observed in the model ground. At relatively higher strains and higher frequencies, amplification values were between 1.2 and 1.4.

3) Dynamic pressure values recorded at upper left corner of culvert model indicate an opposite phase with the lower left and upper right corner. In other words, when a pair of cross corners of culvert is under dynamic compression other pair is under dynamic tension. This behavior indicates that the culvert model is compelled to make racking deformation by the cross-coupling forces.

4) Static and dynamic soil pressures acting on sidewalls of culvert were measured separately in the shaking table tests. Based on the measurements, a dynamic pressure distribution along the sidewalls was approximated. The magnitude of the dynamic pressure distribution was normalized with the overburden pressure at the mid-depth of box-type culvert and accordingly a dynamic lateral pressure coefficient (k_d) was obtained. It

171

was observed that k_d value increases with decreasing flexibility ratio and vice versa. Additionally, k_d increases logarithmically with increasing shear strain.

5) 1-g shake table tests were conducted on the most flexible and rigid culverts with two different embedment depths (h/H=2, h/H=3) in order to investigate the variation of dynamic lateral pressure coefficient (k_d) with depth. It was observed that k_d values are very close to each other for both embedment depth.

6) Lateral deformations occured at the sidewalls of a flexible underground culvert subjected to dynamic loading was determined by performing centrifuge test. Results show that a clear racking deformation scheme was actualized with the theoretical predictions.

7) Deformations of the flexible culvert model tested in the centrifuge were compared with the predictions obtained by proposed simplified approach. Results show that this approach conservatively estimate the deformations of flexible culvert model. The possible reason for conservative result is the overestimation of shear stress acting on the culvert's exterior surface. Therefore, more research is needed to investigate the shear stress mobilization at soil-culvert interface during dynamic excitations.

8) Centrifuge tests results were also compared with the analytical solutions proposed by Penzien (2000) and Huo et al. (2006). Huo's et al. (2006) predictions are close to deformations measured in centrifuge tests while Penzien's approach gives higher deformations as compared to Huo's et al. (2006) solution.

9) As a consequence, comparisons of the proposed simplified procedure with closed-form solutions adn centrifuge measurements show that simplified approach can be used as a practical approach for the preliminary assessment of underground culverts under seismic action. Additionally, it should be noted that the given approach is valid for box-type culverts buried in dry sand.

Limitations

1) Resonance frequencies of the ground model can not be captured due to the limitations of motion generating system.

2) Mean stresses are low due to small scale of the box. Thus, friction angle is higher and soil exhibits more dilative behavior.

Recommendations for further studies

1) The proposed simplified approach is given for the preliminary assessment of box-type culverts buried in dry sand. It is necessary to perform further 1-g shake table tests or centrifuge tests for exploring the effects of structural dimensions and type of soil.

2) In this study, the range of shear strain levels at the mid-depth of culvert varies between 0.001% and 0.2%. Further laboratory tests are needed to investigate variation of dynamic pressure at higher strain levels. For this purpose, tests can be conducted on saturated soils or soils having lower relative densities.

3) Cyclic shear stresses acting on the top culvert-soil interface should be investigated by further studies for a better estimation of mobilized shear stresses acting on the top culvert-soil interface under dynamic loading. This can be achieved by laboratory tests by measuring shear stresses at the culvert-soil interface.

4) For the confirmation of proposed simplified approach, additional centrifuge tests should be performed for different geometries and soil type.

REFERENCES

American Society of Civil Engineers (1984) "Guidelines for the seismic design of oil and gas pipeline systems," Committee on Gas and Liquid Fuel Lifelines Technical Council on Lifeline Earthquake Engineering, ASCE , New York.

Bagherzadeh, A., and Ferdowsi, B., (2009). "Dynamic analysis of Esfahan metro tunnels." Journal of applied sciences. Vol.9, No.4, pp. 671-679

Bobet, A. (2003). "Effect of pore water pressure on tunnel support during static and seismic loading." Tunnelling and Underground Space Technology 18, pp. 377-393.

Bobet, A., Fernández, G., Huo, H., and Ramírez, J., (2008). "A Practical Iterative Procedure to Estimate Seismic-Induced Deformations of Shallow Rectangular Structures." Canadian Geotechnical Journal. 45, pp. 923-938.

Che, A., and Iwatate, T., (2002). "Shaking table test and numerical simulation of seismic response of subway structures." Structures under shock and impact VII, pp. 367-376.

Che, A., Iwatate, T., and Ge, X. (2006). "Study on dynamic response of embedded long span corrugated steel culverts using scaled model shaking table tests and numerical analyses." Journal of Zhejiang University-Science A, Vol. 7, No. 3, pp. 430–435.

Che, A., Iwatate, T., and Ge, X. (2006). "Evaluation of dynamic soil-structure interaction and dynamic seismic soil pressures acting on it subjected to strong earthquake motions. " Journal of Shangai Jiaotong University, Vol. 4, No. 21.

Crosariol, V. A. (2010). "Scale model shake table testing of underground structures in soft clay." M. Sc. Thesis, Faculty of California Polytechnic State University, San Luis Obispo,CA,USA.

Çalısan, O. (1999). "A Model Study On The Seismic Behavior of Gravity Retaining Walls." Ph.D Dissertation, Middle East Technical University, Ankara, Turkey.

Çetin K. Ö. and Seed R. B., (2004). "Nonlinear shear mass participation factor (rd) for cyclic shear stress ratio evaluation." Soil Dynamics and Earthquake Engineering, Volume 24, Issue 2, February 2004, Pages 103-113.

Çilingir, U., (2005). "A model study on the effects of wall stiffness and surcharge on dynamic lateral earth pressures." M. Sc. Thesis, Middle East Technical University, Ankara, Turkey.

Darendeli, M. (2001). "Development of a new family of normalized modulus reduction and material damping curves." Ph.D. Thesis, Dept. of Civil Eng., Univ. of Texas, Austin.

Davis, A. C. (2003). "Lateral seismic pressures for design of rigid underground lifeline structures." Earthquake Engineering, ASCE, pp. 1001-1010.

Dowding, C.H., Rozen, A., (1978)." Damage to rock tunnels from earthquake shaking." J. Geotech. Eng. Div., ASCE, Vol. 104, No. GT2, pp. 175-191.

Duke, C.M., Leeds, D.J., (1959). "Effects of Earthquakes on Tunnels." RAND Second Protective Construction Symposium.

Ferguson, K. A., and Ovesen, N. K. (1988), "The Application of the Theory of Modelling to Centrifuge Studies," Centrifuges in Soil Mechanics, edited by W. H. Craig, R. G. James, and A. N. Schofield, A. A. Balkema, Rotterdam, pp. 119-138.

Gomez-Masso, A., Attalla, I. (1984). "Finite element vs. simplified methods in the seismic analysis of underground structures." Earthquake Eng. Struct. Dyn. Vol. 12, pp. 347-367.

Ha, D., Abdoun, T.H., O'Rourke, M.J., Symans, M.D., O'Rourke, T.D., Palmer, M.C., Stewart, H.E. (2010). "Earthquake Faulting Effects on Buried Pipelines - Case History and Centrifuge Study." Journal of earthquake engineering, Vol. 14, No.5, pp. 646-669.

Hardin, B. O. and Drnevich, V. P. (1970). "Shear modulus and damping in soils - ii: Design equations and curves." Technical Report UKY 27-70-CE3, Soil Mechanics Series No. 2, University of Kentucky.

Hashash, Y. M., Hook, J. J., Schmidt, B., and I-Chiang Yao, J. (2001). "Seismic design and analysis of underground structures." Tunnelling and Underground Space Technology., 16, pp. 247–293.

Hoeg, K., (1968). "Stresses against underground structural cylinders." Journal of Soil Mechanics and Foundation Division, ASCE 94 SM4, pp. 833-858.

Huo,H. (2005). "Seismic design and analysis of rectangular underground structures." Ph.D. thesis, Purdue University,West Lafayette, Ind.

Huo, H., Bobet, A., Fernández, G., and Ramirez, J. (2005). "Load Transfer Mechanisms between Underground Structure and Surrounding Ground: Evaluation of the Failure of the Daikai Station." Journal of Geotechnical and Geoenvironmental Engineering, Vol. 131, No. 12, pp. 1522-1533.

Huo, H., Bobet, A., Ferna´ndez, G., and Ramı´rez, J. (2006). "Analytical solution for deep rectangular underground structures sub-jected to far-field shear stresses." Tunnelling and Underground Space Technology, 21: 613–625.

Iida, H., Hiroto, T., Yoshida, N., and Iwafuji, M. (1996). "Damage to Daikai Subway Station." Soils and Foundations Special Issue on Geotechnical Aspects of the January 17, 1995 Hyogoken-Nambu Earthquake, Japanese Geotechnical Society.

Iglesia, G.R., Einstein, H.H., and Whitman, R.V., (2011). "Validation of centrifuge model scaling for soil systems via trapdoor tests." Journal of Geotechnical and Geoenvironmental Engineering, ASCE.

Jaky J. (1948.) "Pressure in soils". 2nd ICSMFE, London, Vol. 1, pp 103-107.

Kaneshiro, J.Y., Power, M., Rosidi, D., (2000). "Empirical correlations of tunnel performance during earthquakes and aseismic aspects of tunnel design." Proceedings of the Conference on Lessons Learned From Recent Earthquakes-On Earthquakes in Turkey 1999.

Kutter BL (1995). "Recent Advances in Centrifuge Modeling of Seismic Shaking," State-of-the-Art Paper, Proceedings, Third International Conference on Recent Advances in Geotechnical Earthquake Engineering and Soil Dynamics, St. Louis, MO, Vol.2, pp. 927-942.

Ling, H.I., Mohri, Y., Kawabati, T., Liu, H., Burke, C., Sun, L., (2003). Centrifugal modeling of seismic behavior of large-diameter pipe in liquefiable soil. Journal of Geotechnical and Geoenvironmental Engineering, ASCE,Vol. 129, pp. 1092–1101.

Matsui, J., Ohtomo, K., and Kanaya, K. (2004). "Development and Validation of Nonlinear Dynamic Analysis in Seismic Performance Verification of Underground RC Structures." Journal of Advanced Concrete Technology, Vol. 2, No.1,pp. 25–35.

Matsuda T., and Tanaka N. (1996). "Seismic response analysis for a collapsed underground subway structure with intermediate columns." Eleventh World Conference on Earthquake Engineering, No. 1452.

Mononobe, H.A. and Matsuo, H. (1929). "On the determination of earth pressures during earthquakes." Proceedings, World Engineering Congress, 9 p.

Navarro, C., (1992). Effect of adjoining structures on seismic response of tunnels. International Journal for Numerical and Analytical Methods in Geomechanics. Vol. 16, pp. 797-814.

Newmark, N.M., (1968). "Problems in wave propagation in soil and rock." Proceedings of the International Symposium on Wave Propagation and Dynamic Properties of Earth Materials.

Nishiyama, S., Kawawa, I., Muroya, K., Haya, H., Nishimura, A., "Experimental study of seismic behavior of box type tunnel constructed by open cutting method." Twelveth World Conference on Earthquake Engineering.

Okabe, S. (1926). "General theory of earth pressures." Journal of the Japan Society of   Civil Engineering, Vol 12, No. 1.

O'Rourke M, Vikram G, Abdoun T. (2003). "Centrifuge modeling of buried pipelines." Proceedings of the sixth US conference and workshop on lifeline earthquake engineering, Long Beach, CA, USA, pp. 757–68.

Owen, G.N., Scholl, R.E., (1981). "Earthquake engineering of large underground structures." Report no. FHWA_RD-80_195. Federal Highway Administration and National Science Foundation.

Park, K.H., Tantayopin, K., Tontavanich, B. (1996). "Analytical solutions for seismic design of tunnel lining in Bangkok MRT subway." International symposium on underground excavation and tunneling, Bangkok, Thailand.

Parra-Montesinos, G.J., Bobet, A., and Ramirez, J. (2006). "Evaluation of Soil-Structure Interaction And Structural Collapse In Daikai Subway Station During Kobe Earthquake." American Concrete Institute, Structural Journal, Vol. 103, No. 1, pp. 113-122.

Peck, R.B., Hendron, A.J., Mohraz, B., (1972). "State of the art in soft ground tunneling." Proceedings of the Rapid Excavation and Tunneling Conference. American Institute of Mining, Metallurgical and Petroleum Engineers, New York, Vol. 1, pp. 259-285.

Penzien, J., and Wu, C. L. (1998). "Stresses in linings of bored tunnels." Earthquake engineering and structural dynamics, Vol.27, No.3, pp. 283–300.

Penzien, J. (2000). "Seismically induced racking of tunnel linings." Earthquake Engineering & Structural Dynamics, Vol. 29, No.5, pp. 683-691.

Porcino, D., Fioravante, V., Ghionna, V.N. and Pedroni S., (2003). "Interface Behavior of Sands from Constant Normal Stiffness Direct Shear Tests". Geotechnical Testing Journal, Vol. 26, No.3, pp. 289-301.

Power, M.S., Rosidi, D., Kaneshiro, J., (1996). "Vol. III Strawman: screening, evaluation, and retrofit design of tunnels." Report Draft. National Center for Earthquake Engineering Research, Buffalo, New York.

Power, M., Rosidi, D., Kaneshiro, J., (1998). "Seismic vulnerability of tunnels and underground structures revisited." Proceedings of the North American Tunneling Conference. Elsevier, Long Beach, CA, USA.

Prasad, S.K., I. Towhata, G.P. Chandradhara, and P. Nanjundaswamy. 2004. "Shaking Table Tests in Earthquake Geotechnical Engineering." Current Science. 87(10).

Rankine, W. (1857). "On the stability of loose earth." Philosophical Transactions of the Royal Society of London, Vol. 147.

Richards, R., Huang, C. and Fishman, K.L. (1999). "Seismic earth pressure on retaining structures." Journal of Geotechnical and Geoenvironmental Engineering, ASCE, Vol. 125, No.9, pp. 771–778

Schwartz, C.W., Einstein, H.H., (1980). "Improved design of tunnel supports: vol. 1 simplified analysis for groundstructure interaction in tunneling." Report no. UMTA-MA-06-0100-80-4. US DOT, Urban Mass Transportation Administration.

Seed, H.B. and Whitman, R.V., (1970). "Design of Earth Retaining Structures for Dynamic Loads.", Lateral Stresses in the Ground and Design of Earth Retaining Structures, ASCE, pp.103- 147.

Sitar, N. (1995) (editor and co-author with 18 members of the geotechnical reconnaissance team), "Geotechnical Reconnaissance of the Effects of the January 17, 1995, Hyogoken-Nanbu Earthquake, Japan," Earthquake Engineering Research Center, University of California, Report No. 95-01, 143 p.

Sharma, S., Judd, W.R., (1991). "Underground opening damage from earthquakes." Engineering Geology, Vol. 30, pp. 263-276.

St. John, C.M., Zahrah, T.F., (1987). "Aseismic design of underground structures." Tunneling Underground Space Technology. Vol. 22, pp. 165-197.

Stevens, P.R., (1977). "A review of the effects of earthquakes on underground mines." United States Geological Survey Open File Report 77313, 47 p. US Energy Research and Development Administration.

Sweet, J., (1997). "Los Angeles Metro Red Line project: seismic analysis of the Little Tokyo Subway Station." Report no. CAI-097-100. Engineering Management Consultants.

Taylor, R. N. (1995). "Geotechnical Centrifuge Technology." London: Blackie Academic & Professional.

Veletsos A.S., Younan A.H., (1994a). "Dynamic soil pressures on rigid vertical walls." Earthquake engineering and structural dynamics. vol. 23. New York, Wiley; pp. 275–301.

Veletsos A.S., Younan A.H., (1994b). "Dynamic modeling and response of soil-wall systems." ASCE J Geotech Eng, 120 (12), pp. 2155–79.

Wilson, J.M.R. (1988). "A Theoretical and Experimental Investigation into the Dynamic Behaviour of Soils." Ph.D Dissertation, Cambridge University.

Yunatcı, A. A. (2003). "A Model Study on the Seismic Behavior of Laterally Braced Sheet Pile Walls." M.Sc. Thesis, Middle East Technical University, Ankara, Turkey.

Wang, J.-N., (1993). "Seismic Design of Tunnels: A State-of-the-Art Approach." Monograph 7, Parsons, Brinckerhoff, Quade and Douglas Inc., New York.

Wang W.L., Wang T.T., Su J.J., Lin C.H., Seng C.R., Huang T.H. (2001). "Assessment of damage in mountain tunnels due to the Taiwan Chi-Chi Earthquake." Tunnel Underground Space Technology, Vol. 16, No.3, pp.133–150.

Zeghal, M. & Elgamel, A.W. (1994) "Analysis of site liquefaction using earthquake records". Journal of Geotechnical Eng ineering, ASCE. 120(6): 996-1017.

CURRICULUM VITAE

PERSONAL INFORMATION

Surname, Name	: Ülgen, Deniz
Nationality	: Turkish (TC)
Date and Place of Birth	: 20 July 1978, Diyarbakır
Marital Status	: Married
Phone	: +90 312 210 24 16
Fax	: +90 312 210 54 01
Email	: denizulgen@gmail.com

EDUCATION

Degree	Institution	Year of Graduation
M.S.	METU Civil Engineering	2004
B.S.	METU Civil Engineering	2000
High School	Isparta S. Demirel Science High School	1996

WORK EXPERIENCE

Year	Place	Enrollment
2004-Present	METU Department of Civil Engineering	Research Assistant
2001-2002	Günsayıl Construction Company	Civil Engineer
2000-2001	Özkar Construction Company	Civil Engineer

FOREIGN LANGUAGES

English

PUBLICATIONS

Ertuğrul,Ö.L., Ülgen,D.,(2010) "Attenuation of traffic induced ground borne vibrations due to heavy vehicles", Fifth International Conference on Recent Advances in Geotechnical Earthquake Engineering and Soil Dynamics and Symposium in Honor of Professor I. M. Idriss ,San Diego, CA, USA – May 24-29.

Ertugrul, L.Ö., Ülgen, D., Özkan, M. Y., (2009). "Measurements and numerical modeling of ground borne vibrations caused by heavy vehicle traffic", Proceedings of the 2nd International Conference on New Developments in Soil Mechanics and Geotechnical Engineering, 28-10 May, North Cyprus, pp. 274-281.

Ülgen, D., Sağlam, S., (2009). "Seismic Stability Assessment of an Existent Countermeasure Against Landslide in an Urban Area", Proceedings of the 2nd International Conference on New Developments in Soil Mechanics and Geotechnical Engineering, 28-10 May, North Cyprus, pp. 298-305.

Özkan, M.Y., Çiçek, G., Ülgen, D., (2009). "Utilization of gravel drains against liquefaction", Yapı Dünyası, January, No: 154, pp. 11-16 (in Turkish).

Ülgen D., Engin, H.K., (2007). "Predicting Earthquake Displacements of Slopes", Proceedings of the 8th Pacific Conference on Earthquake Engineering, 5-7 December, Singapore.

Özdemir, A., Ülgen D., Özkan, M.Y., (2007). "Traning requirements and suggestions on education of boring machine operators", 2nd National Conference on Geotechnics, November 22-23, TMMOB IMO Adana, pp. 468-472 (in Turkish).

Özdemir, A., Ülgen, D., Özkan, M.Y., (2007)." Evaluations on geotechnical borings carried out in Turkey.", 2nd National Conference on Geotechnics, November 22-23, TMMOB IMO Adana, pp. 473-479 (in Turkish).

Ülgen, D., Engin, H.K., (2007). "A study of CPT Based Liquefaction Assessment Using Artificial Neural Networks", Proceedings of the 4th International Conference on Geotechnical Earthquake Engineering, 25-27 June, Thessaloniki, Greece.

Ülgen, D., Özkan, M.Y., (2004). "Dynamic response and permanent displacement analysis of Akköprü Dam", 10th National Conference of Soil Mechanics and Foundation Engineering, September 16-17, Istanbul Technical University, İstanbul, pp. 527-536 (in Turkish).

Ülgen D., (2004). "Dynamic Response and Permanent Displacement Analysis of Akköprü Dam", MSc. Thesis, METU Graduate School of Natural and Applied Sciences, January 2004, 115 pages.